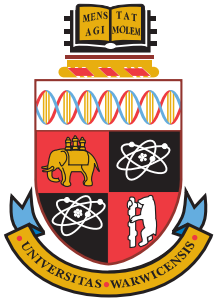

Diffusion of proteins in chloroplast membranes

Elina Vladimirou

Thesis
Submitted to the University of Warwick
for the degree of
Doctor of Philosophy

Supervisors: Professor Colin Robinson and Dr Markus Kirkilionis

MOAC Doctoral Training Centre
September 2010

THE UNIVERSITY OF WARWICK

Abstract

The lateral diffusion of Hcf106, a core subunit of the ΔpH-dependent translocon in higher plants, and chlorophyll-containing complexes is thoroughly investigated by Fluorescent Recovery After Photobleaching (FRAP) and Fluorescent Loss in Photobleaching (FLIP). Simple models of a thylakoid network are derived directly from confocal fluorescence microscopy images by Monte Carlo optimisation. These networks are used as the domain for diffusion simulations using the Particle Strength Exchange method, allowing determination of diffusion coefficients for the thylakoid protein Hcf106 and for chlorophyll-containing complexes. Extending the mobility studies to the chloroplast outer membrane, diffusion coefficients are estimated for Toc159, a component of the chloroplast outer membrane translocon TOC.

Abbreviations

ATP	adenosine-5′-triphosphate
CFP	cyan fluorescent protein
DGDG	digalactosyldiacylglycerol
EGFP	enhanced green fluorescent protein
EM	electron microscopy
ER	endoplasmic reticulum
FLIP	fluorescence loss in photobleaching
FRAP	fluorescence recovery after photobleaching
GFP	green fluorescent protein
GPI	glycosylphosphatidylinositol
GTP	guanosine-5′-triphosphate
kDa	kiloDalton
LHCII	light-harvesting complex II
mA	miliampere
MGDG	monogalactosyldiacylglycerol
NNDF	nearest neighbor distribution function
PCF	pair correlation function
PEG	polyethylene glycol
PG	phosphatidylglycerol
PSE	particle strength exchange
PSI	photosystem I
PSII	photosystem II
RFP	red fluorescent protein
ROI	region of interest
SQDG	sulfoquinovosyldiacylglycerol
TIC	translocon at the inner envelope
TOC	translocon at the outer envelope
TRP	tetratrico-peptide repeat motif
YFP	yellow fluorescent protein

Contents

List of Figures

List of Tables

Acknowledgements

Firstly, I would like to thank my supervisors Prof. Colin Robinson and Dr Markus Kirkilionis for giving me the opportunity to work on this project and for their guidance.

My special thanks go to Nishi Vasisht for her continuous support and valuable friendship. Many thanks go to Mike Li and Cassie Aldridge for their collaboration for part of this project. I would also like to thank all the past and present members of the Robinson lab group.

I wish to thank Prof. Felix Kessler for kindly providing the *Arabidopsis* seeds for the Toc159 study. My special thanks go to Sian Davies for demonstation of the arabidopsis protocols and very useful discussions.

I would like to thank Richard Marshall and Christopher Snowden for useful discussions on transient expression.

I would also like to thank Alison Rodger, Dorothea Mangels and Mónica Lucena for all their help throughout these years.

To my current supervisor Andrew McAinsh, I would like to express my special thanks for encouraging me and being an inspiration.

To my family and my fiancé Jonathan, whose constant support and love kept me going throughtout these years, I am deeply grateful.

This work was funded by the Engineering and Physical Sciences Research Council (EPSRC) through the Molecular Organisation and Assembly in Cells (MOAC) Doctoral Training Centre.

Declaration

The work contained herein is entirely original and my own work, except where acknowledged in the text. I confirm that this thesis has not been submitted for a degree at another university.

Collaborative work has been carried out contributing towards the material presented in this thesis. In summary, collaborative work was carried out with the following:

Mike Li, Department of Biological Sciences, University of Warwick, performed some of the FLIP experiments that I analysed here.

Nishi Vasisht, Department of Biological Sciences, University of Warwick, performed the western blot.

Jonathan Armond, Department of Physics, University of Warwick, provided valuable discussions and ideas for the PSE implementation.

Part of this work has been published in the following journal article:

E. Vladimirou, M. Li, C. P. Aldridge, L. Frigerio, M. Kirkilionis and C. Robinson. Diffusion of a membrane protein, Tat subunit Hcf106, is highly restricted within the chloroplast thylakoid network. *FEBS Letters*, 583:3690-3696, 2009.

This article is reprinted in Appendix F.

1

Introduction

1.1 Overview

This thesis is concerned with the mobility of translocon components in chloroplasts membranes. In this chapter, relevant biological and theoretical background is discussed.

1.2 Biological membranes: Structural organisation and function

Biological membranes are amphipathic lipid bilayer structures that separate cells from their environment and enclose intracellular compartments. The predominant constituents of biological membranes are phospholipids which assemble into large flexible membrane sheets via non-covalent association. Phosphoglycerides, a type of phospholipids, are amphipathic molecules with a hydrophobic tail and a hydrophilic head constructed of fatty acids and glycerol. Two hydroxyl groups of glycerol are linked to fatty acids and the third hydroxyl group is linked to a phosphate group which is also attached to a small polar group such as choline. Sphingolipids, glycolipids and cholesterol are also found in biomembranes.

While lipids provide the basic structure of cell membranes, proteins constitute more than 50% of the membrane mass. Each membrane has its own set of proteins which are responsible for carrying out the membrane's specific function. Membrane proteins can associate with the lipid bilayer in various ways. They can be amphipathic transmembrane proteins, with one or multiple alpha-helices or rolled-up beta-sheet extending across the bilayer. Others are entirely in the cytosol but associate with the cytosolic monolayer of the lipid bilayer either by an amphipathic alpha-helix or via one or more covalently attached lipid chains. Other membrane proteins are bound to the non cytosolic surface of the membrane via an oligosaccharide linker to a glycosylphosphatidylinositol (GPI) anchor. Finally, proteins attach to the membrane by non-covalent interactions with other membrane proteins. Membrane proteins can be classified as peripheral or integral. The former includes proteins that can be released from the membrane by use of gentle extraction procedures such as high or low ionic strength solution or extreme pH to disrupt the protein-protein interactions. The latter refers to transmembrane proteins, tightly bound proteins and proteins that are bound via lipid groups that cannot be released from the membrane in the ways mentioned above.

1.3 Protein lateral diffusion in biological membranes

The lateral motion of membrane proteins is crucial and directly linked to the functional role of the protein within a cell. Free lateral diffusion of proteins is defined as the rate of lateral isotropic diffusion in a fluid lipid bilayer where the protein trajectories can explore all membrane domains [1]. According to the fluid mosaic model developed by S. J. Singer and G. Nicolson, biological membranes are dynamic, fluid structures with most phospholipids and integral proteins diffusing freely and rapidly in the plane of the membrane [2].

1.4 Factors affecting protein lateral diffusion

Ample experimental evidence has shown that proteins diffuse at significantly lower rates in biological membranes rather than in artificial membranes, suggesting the existence of factors hindering the protein movement in cells [1].

Biological membranes are highly crowded environments with the lipid to protein ratio ranging from 0.35 (inner mitochondrial membrane) to 1 (plasma membrane) [3]. Proteins may diffuse slowly due to the entropic phenomenon called the depletion or excluded volume effect which is due to the hierarchy of molecules of different sizes. S. Asakura and F. Oosawa observed that each large molecule is surrounded by a depletion zone of thickness equal to the radius R of the small molecule. The depletion zone reduces the volume available to the small molecules to diffuse within. When two large molecules approach each other to less than the diameter $2R$ of the small particles, their depletion zones merge and lose volume, increasing the entropy of the small molecules because they have less volume to diffuse in, and therefore lowering the free energy. This reduction of free energy of the whole system results in an entropic force keeping the large objects in contact and making them diffuse as one entity [4].

Protein diffusion may be impeded by interaction with peripheral structures. For example, integral membrane proteins of the plasma membrane present a large immobile fraction and diffuse slower when found in intact cells rather than in blebbed membranes where a mechanical disruption of the connections anchoring membrane receptors to the cytoskeleton is assumed [5]. According to the membrane skeleton pickets-and-fences model, the cytoskeleton generates compartmental barriers through filaments and anchored proteins to the diffusion of proteins and lipids. Escapes from the compartments are possible giving rise to a 'hop-diffusion' which is defined as translational motion within a small area, followed by similar restricted motion in an adjacent small area [6, 7].

Lipids and membrane proteins can be organised into localised regions within

a membrane called membrane microdomains. Lipid rafts are sphingolipid-cholesterol rich microdomains in the liquid ordered phase which selectively incorporate or exclude proteins [8]. According to the raft hypothesis membranes are organised in discrete liquid-ordered and liquid-disordered phase domains in the presence of sufficient amounts of sphingolipid and sterol [9]. Lipid rafts appear to be resistant to cold detergent extraction or mechanical disruption [10] and are believed to provide the functional platform to many cellular processes such as protein signalling and signal transduction [8]. It is believed that lipid rafts provide a lateral confinement to the proteins localising in their area. However proteins might still be able to undergo hop-diffusion.

Proteins may exhibit anisotropic diffusion where one direction of motion is more favourable than another when diffusing in membranes of variable corrugation in the different directions [11]. For instance, protein receptors on the surface of mouse fibroblasts were found to exhibit anisotropic two-dimensional diffusion in adherent cells having parallel stress fibers with the rate of diffusion being higher parallel to fibers when compared to the diffusion perpendicular to fibers [12].

Thermal fluctuations of the membrane can also cause reduction of protein lateral diffusion. For example, mobile receptor-ligand bonds in membrane-membrane adhesion zones are slowed down not only because the complex experiences a larger viscous drag but also because of thermal fluctuations of the membrane shape as shown by Monte Carlo computer simulations [13].

Membrane curvature may also affect the lateral diffusion of a membrane protein. Spontaneous curvature of a membrane can be attributed to the shape of the lipid molecules and compositional differences in the two lipid monolayers that make up a bilayer. Lipids whose hydrophilic head and hydrophobic tail span the same area tend to form flat monolayers or bilayers. A positive or negative spontaneous curvature can be a result of a lipid head being larger or smaller than the tail respectively. Spontaneous curvature in a bilayer can also be due to differences in the areas of the two monolayers, due to different numbers of lipids or to the insertion of protein domains into one of the monolayers [14]. Stochastic simulations have demonstrated an enhancement of membrane protein diffusion coefficients coupled to membrane curvature [15].

Proteins have also been reported to induce membrane structures in which protein molecules exhibit slow diffusion. For example, in yeast and mammalian cells the reticulons and DP1/Yop1p proteins oligomerise and form tubular structures in the endoplasmic reticulum (ER). These proteins are found exclusively in the tubular structures and exhibit slower diffusion when compared to the mobility behavior of other membrane proteins of the ER [16].

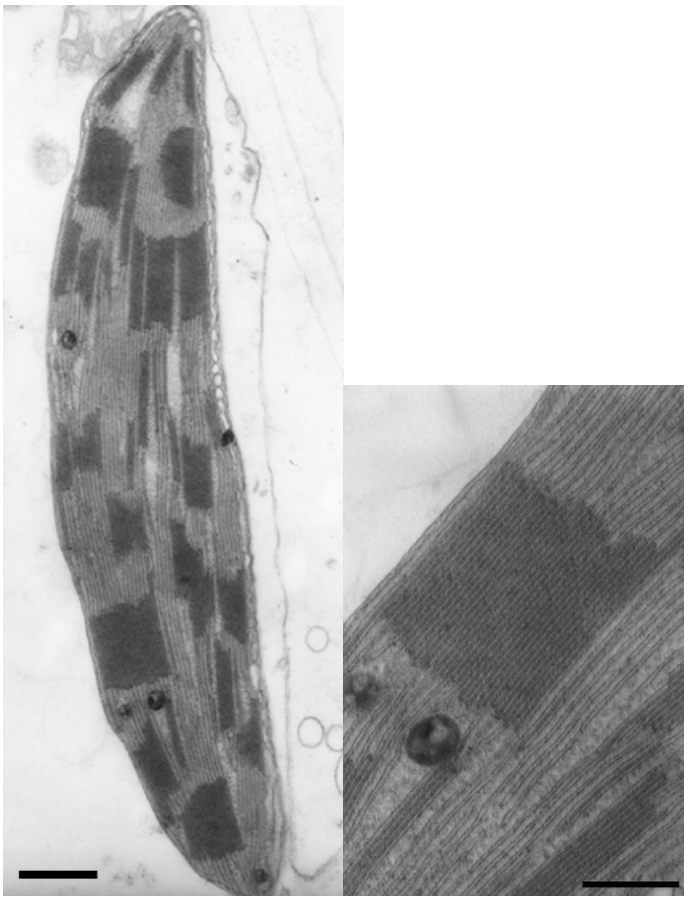

(a) (b)

Figure 1.1: (a) Transmission electron microscopy micrographs of a mesophyll chloroplast. Scale bar 500 nm. (b) An enlarged view of the thylakoid membrane. Stacks of disc-like membrane are connected by elongated stroma-exposed membranes. Scale bar 200 nm. Micrographs were taken from Asakura et al. [20].

1.5 Structure and function of chloroplasts

Chloroplasts are specialised plastids found in all photosynthetic tissues of higher plants. In addition to their core photosynthetic role, they are responsible for fatty acid and amino acid biosynthesis [17]. According to the endosymbiotic theory, chloroplasts are believed to have originated from the engulfment of a photosynthetic bacterium by a primitive eukaryotic cell [18, 19]. Mature chloroplasts have a complex structure which is visible by electron microscopy (EM) revealing a number of distinct compartments (see Figure 1.1). Chloroplasts are bounded by a double-membrane envelope that consists of a highly permeable outer lipid bilayer and a less permeable inner lipid bilayer which are separated by a soluble inter-membrane space. Chloroplasts enclose a highly specialised membrane, the thylakoid. The thylakoid membrane is the site of the light-dependent reactions of photosynthesis and contains photosynthetic light-capturing systems, electron-

transport chains, translocation machinery and ATP synthase. Thylakoids present two distinct structural compartments with each having separate protein complements. Thylakoids fold to form sets of flattened disc-like sacs, the grana, which are joined together by an extended thylakoid membrane, known as the stroma lamellae. The lumen of thylakoids are interconnected defining a second internal compartment called the thylakoid space. The thylakoid membrane and the inner envelope membrane are separated by a large aqueous space called the stroma. This is where many metabolic enzymes, the chloroplasts genome and a special set of ribosomes and RNAs are found.

1.6 Lipid composition of the thylakoid membrane

Thylakoid membranes have a unique lipid composition. They are mainly composed of the two galactolipids, monogalactosyldiacylglycerol (MGDG) and digalactosyldiacylglycerol (DGDG) and also contain a unique sulfolipid, sulfoquinovosyldiacylglycerol (SQDG) and phosphatidylglycerol (PG) [21, 22]. Although MGDG lipids comprise 50% of the total thylakoid acyl lipid they do not spontaneously form lipid bilayers when dispersed in purified form and that could raise potential questions for the actual role of the lipids in thylakoid structure formation [22, 23].

1.7 Structure of the thylakoid membrane in mature chloroplasts

A striking morphological feature of the thylakoid membrane is its differentiation into stacked and non-stacked domains. Mature chloroplasts contain 40 to 60 grana stacks with diameters of 0.3 to 0.6 μm. The number of thylakoids per granum is variable from 10 to as many as 100 thylakoids in the extreme shade plant *Alocasia macrorhiza* [24]. The non-stacked membranes are named stroma thylakoids because of their direct exposure to the stroma. Several models have been proposed for the mechanism by which the thylakoid membrane organises itself into the structural domains of grana and stroma thylakoids (Fig. 1.2). However, it is believed that the entire thylakoid system is a single complex entity [25].

The first 3D model of the thylakoid structure, referred to as the quasi-helical model, is based on EM serial sectioning analysis and suggests that on average eight stroma thylakoids form parallel and evenly spaced right-handed helices around the grana [26–28]. At each intersection, a narrow, neck-like membrane region connects the grana and stroma membrane domains [24].

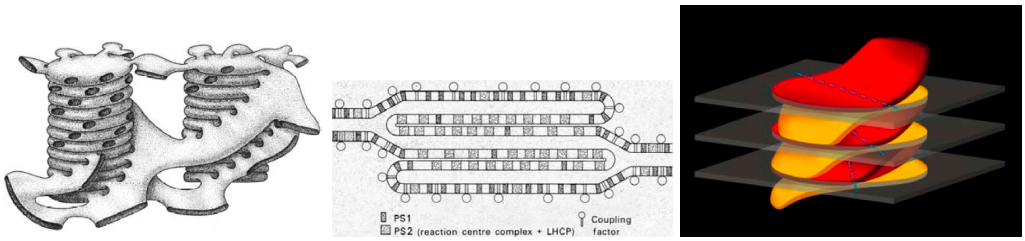

(a) (b) (c)

Figure 1.2: (a) According to the quasi-helical model, stroma thylakoids wind around the granum body in a unidirection right-helix motif. Taken from Staehelin et al. [24]. (b) The folded model suggests that the thylakoid is a continuous bilayer that folds to form stacks of membrane separated from extended membrane exposed to the stroma. Taken from Andersson et. al. [29,35]. (c) The bifurcation model proposes that stroma lamellae overlap and membrane bends upward and downwards to fuse with adjacent layers at the edges. Illustration taken from Shimoni et al. [34].

The second model, known as the folded-membrane model, was originally used to explain the lateral heterogeneity of the two photosystems [29]. It was further extended to suggest that the thylakoid network is constructed by the folding of a single continuous membrane which is stabilised by surface interactions [30] and encloses a single compartment, the thylakoid lumen [24]. This model could explain the complete or partial unstacking and restacking of grana due to variations of ionic strength and light conditions [31,32]. Briefly, fluorescence spectroscopic data in combination with EM micrographs provide good evidence that low salt concentrations induce the reversible unstacking of grana stacks and randomisation of the resident protein complexes [32]. Also, in low intensity light, thylakoids have broader grana stacks, many more thylakoids per granal stack, and more grana stacks relative to chloroplast exposed in high-intensity light [33].

A third model aimed to describe the three-dimensional organization of the thylakoid using dual-axis electron microscope tomography on cryoimmobilised, freeze-substituted, dark-adapted thylakoid membranes. According to this model, each granum layer is formed by bifurcation of stroma thylakoids and subsequent fusion of the membranes. The stroma thylakoids intersect the granum body in a perpendicular manner and not helical. Grana layers are interconnected directly through their edges, with one layer bending upward and fusing with its neighboring grana layer and with the other bending downwards [34].

Although the precise model by which this intricate membrane system is achieved is yet to be elucidated, the quasihelical model appears to be more widely accepted than the competing models [28].

1.8 Protein composition and redistribution during state transitions and PSII repair cycle

Grana and stroma thylakoids demonstrate a lateral heterogeneity with respect to protein composition. Photosystem I (PSI) is exclusively restricted to non-aprressed grana domains such as grana end membranes, grana margins and stroma thylakoids together with ATP-synthase [31, 35]. Photosystem II (PSII) and light-harvesting complex II (LHCII) localise mostly, but not exclusively, in appressed grana membranes. Using statistical analyses such as the nearest neighbour distribution function (NNDF) and the pair correlation function (PCF) on the exact positions of PSII obtained from electron micrographs of freeze-fractured thylakoid membranes and comparing to Monte Carlo simulated purely random distributions, Kirchhoff and colleagues found that the PSII distribution in grana thylakoids does not correspond to a random protein mixture but that ordering forces lead to a structured arrangement on a supramolecular level [36]. However, between 10-20% of PSII and LHCII appears to be found in stroma thylakoids [35] which can be explained by the redistribution of LHCII light-harvesting complexes during state transitions [37], and the migration of photosystem II (PSII) reaction centres as part of the PSII repair cycle [38]. For example, LHCII redistribution occurs due to state transitions, a regulation mechanism that controls light-energy distribution between the two photosystems. Upon increased electron concentration in the electron carier plastoquinone, a protein kinase phosphorylates the apoproteins of the light-harvesting chlorophyll-protein complex, LHCII [39]. Phosphorylation results in increased electrostatic repulsion leading LHCII to migrate away from PSII to act as the light-harvesting antenna for PSI, making the transition to 'state 2'. A decreased electron flow into plastoquinone from PSII and increased electron flow out of plastoquinone to PSI results in a shortage of electrons in the plastoquinone which switches the LHCII kinase off, LHCII becomes dephosphorylated and returns to PSII driving the system to 'state 1' [37]. The cytochrome b6f complex is also an important protein component of the thylakoid membrane. It operates in photosynthetic electron transfer either in linear electron flow from PSII to PSI or in cyclic flow around PSI [40, 41]. A combined immunochemical and freeze-fracture analysis had originally shown that cytochrome b6f complexes were located in both the unstacked and stacked membranes of thylakoids [42]. A more recent study demonstrated that the proportion of cytochrome b6f complexes found in stroma lamellae is significantly higher in 'state 2' conditions than in 'state 1' conditions [40].

1.9 Protein translocation in chloroplasts

A portion of the chloroplast proteome is encoded by the organelle's own genome. During endosymbiosis, most of the original prokaryotic genome was lost or transferred to the nuclear genome [19]. An estimated 95% of the several thousand proteins needed for the organelle's function are encoded on nuclear genes and cytosolically synthesised as precursor proteins with cleavable amino terminal transit peptides [43]. The post-translational import of proteins into chloroplasts is facilitated by protein complexes found in the outer and inner envelope membrane [44]. If required, proteins are further targeted and reach their functional location into and across the thylakoid membrane via alternative translocation protein pathways.

1.9.1 General import pathway across chloroplast envelope

Proteins bearing an N-terminal chloroplast transit peptide are translocated across the envelope via a general import pathway. The translocation of precursor proteins across the envelope membranes depends on proteins in the outer and inner envelope membrane as well as on chaperones, processing peptidases and stromal modulators [45]. TOC (translocase at the outer membrane of chloroplast) and TIC (translocase at the inner membrane of chloroplast) are large multimeric complexes responsible for protein translocation into chloroplasts. TOC and TIC exist as separate protein complexes (Figure 1.3), however, they appear to physically associate at envelope membrane contact sites [43, 46].

1.9.2 TOC complex

The protein components of TOC complex are Toc159, Toc75, Toc64, Toc34 and Toc12. Its core components are Toc75, a beta-barrel membrane protein and two GTPases, Toc159 and Toc34. The transit peptide of Toc75 precursor is believed to be subjected to multiple cleavage until it reaches mature form and there is evidence that type I signal peptidase (SPase I) found in the intermembrane space (IMS) is responsible for its full maturation [47]. The two GTPases act as primary receptors for precursors at the chloroplast surface and form a stable complex with a Toc75 channel [43, 46, 48]. Toc159 has a tripartite structure containing an N-terminal acidic domain (A) of undetermined function, a central GTPase domain (G), and a C-terminal transmembrane domain (M) which is responsible for anchoring the protein to the outer envelope despite the fact that is lacking conventional hydrophobic residues [45, 49, 50]. Toc159 was first identified as an 86 kDa proteolytic fragment lacking the A-domain (Toc86) in pea chloroplasts [50].

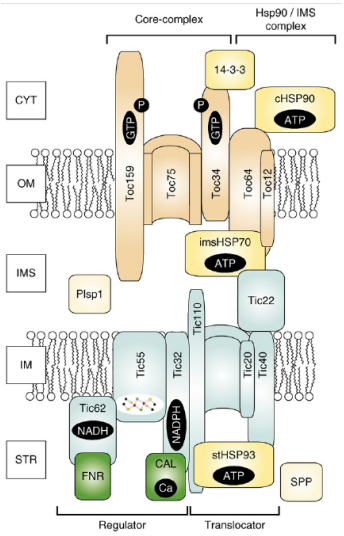

Figure 1.3: A diagram illustrating core and accessory proteins and co-factors involved in the import apparatus residing in the outer and inner membrane of the chloroplast. The model represents a scheme of participating components but does not consider any stoichiometric relations. Illustration taken from Oreb et al. [45].

It was later demonstrated that Toc86 corresponded to a native protein of 159 kDa in pea and *Arabidopsis* chloroplasts [51]. A more efficient import of precursors in chloroplast expressing the intact Toc159 rather than the proteolytic fragment was observed [52] suggesting that the acidic nature of the A-domain could have some role in precursor binding through electrostatic interactions [50]. Toc34 is inserted into the outer membrane by a C-terminal hydrophobic transmembrane domain and also possesses a GTPase domain presenting high similarity to the Toc159 G domain [53]. The TOC core complex, isolated from pea mesophyll cells, was estimated to have molecular mass of 500 kDa and a stoichiometry of 1:4:4 between Toc86 (proteolytic fragment of Toc159), Toc75, and Toc34 [54]. However Blue Native PAGE and size exclusion chromatography of TOC complexes from pea chloroplasts, etioplasts and root plastids have resulted a molecular mass of around 800–1000 kDa and a stoichiometry of 2:6:6 between Toc159, Toc75 and Toc34. Another possibility is that the TOC complex exists as a dynamic protein ensemble [50].

Toc64 and Toc12 do not co-purify with the core TOC complex suggesting that they are transiently associated with the core complex [45,54]. Toc64 has a cytosolically exposed tetratrico-peptide repeat motif (TRP domain) that recognizes Hsp90 chaperones therefore it was proposed that Toc64 acts as an initial docking site for Hsp90 associated precursor proteins [55]. Phosphorylated precursors bind to 14-3-3 proteins which associate with the cytosolic Hsp70 to form a guidance complex

mediating the targeting of precursors to the chloroplast surface [56]. The role of Hsp90 is to maintain the precursor in an import competent unfolded state [57]. Toc12 is associated with Toc64 and is an outer envelope protein exposing a soluble domain into the intermembrane space [58]. It is believed to assist in the precursor translocation across the intermembrane space [58].

1.9.3 TOC function

The function of the TOC complex is still not fully understood. However two competing models have emerged which consider either one of the two GTPases as the initial receptor for newly synthesized precursor proteins [45].

The 'targeting model' takes into account the finding that Toc159 can exist in both soluble and integral membrane form and can switch between the two states [59, 60]. Soluble Toc159 acts as the initial point of contact for the transit peptide which is targeted to the chloroplast surface upon precursor binding. The Toc159-precursor complex associates with Toc34 by dimerisation through their G-domains, the precursor is transferred through the Toc75 channel and Toc159 dissociates from the outer membrane, perhaps due to a conformational change [50, 53, 59, 61]. In the targeting model one cycle of GTP binding and hydrolysis at Toc159 is required to supply Toc34 and Toc75 with a preprotein molecule [61].

The 'motor model' supports that Toc159 and Toc34 remain stably associated with the outer membrane throughout the import mechanism suggesting that the observed Toc159 cytosolic fraction was an experimental artifact [50, 58]. Toc34 molecules act as the initial binding receptors for the transit peptide and Toc159 may be able to rotate about its axis in order to receive precursors and push them through the Toc75 channel [50]. In the motor model, one or more binding and hydrolysis cycles at Toc159 are necessary to drive the preprotein through the Toc75 channel [61].

Both models propose a direct relation between Toc159 GTP-binding and hydrolysis cycles and preprotein translocation events. However, recent experimental evidence suggests that a non-hydrolyzing Toc159, with a mutation in a conserved G1 lysine (at Toc159 K868R), can support protein import into isolated chloroplasts and that Toc159 functions as a molecular switch rather than in generation of the driving force for translocation [61].

1.9.4 TIC complex

TIC is a less well characterised translocase. The three multi-spanning membrane proteins Tic20, Toc21 and Tic110 interact with the inner membrane by hydropho-

bic TMDs and are believed to participate in the TIC channel formation [43,46,62]. Tic22 assembles with imHsp70 for the transfer of the precursor across the intermembrane space (IMS). Tic40 has a binding site for the stromal stHsp93 and associate with the translocation pore to form the translocator. Tic55, the NAD(P)H and ferredoxinNADPoxidoreductase (FNR) binding Tic62 and the NADP(H) and calmodulin (CAL) binding Tic32 form a Tic110 associated complex and may enable regulation of import as a response to redox signals [45,48]. Transit peptides of precursors that enter the stroma are removed by stroma processing peptidase (SPP) [46].

1.9.5 Translocation inside and across the thylakoid membrane

The subset of proteins which are essential for the function of thylakoids are synthesised in the cytosol as preproteins with two N-terminal cleavable signal peptides. Once the precursor has reached the stroma, its chloroplast targeting signal peptide is cleaved off by SPP exposing the thylakoid targeting signal peptide. Proteins insert into the thylakoid membrane via the SRP-like and the spontaneous pathway. Protein translocate across the thylakoid membrane into the thylakoid lumen via the the Sec-dependent and the ΔpH-dependent pathway. Unlike the spontaneous insertion pathway that seems to require no protein complex for membrane integration, all other pathways require specific conditions and make use of specialised translocation contact sites made of unique protein complexes which are believed to localise in the stroma-exposed lamellae [63–65].

1.9.6 The ΔpH-dependent pathway in chloroplasts

The ΔpH-dependent pathway (homologue of the bacterial TAT pathway) is responsible for the transport of fully folded proteins or multimeric protein complexes from the stroma into the thylakoid lumen in the presence of transmembrane proton-motive force. The ΔpH-dependent pathway uses three known membrane proteins: (1) Tha4, a single-span transmembrane protein with an adjacent surface-active amphipathic helix and an unstructured C-terminus region, (2) Hcf106, a single-span transmembrane protein with a predicted amphipathic helix, 260 residues long and molecular weight of ~28 kDa, (3) cpTatC, a protein with six transmembrane helical domains. Substrates of the ΔpH-dependent pathway bear an N-terminal signal peptide with a recognition site of twin-arginine motif which is primarily recognised by a cpTatC site. Quantitative immunoblotting shows that cpTatC is present in thylakoids at about 18 000 copies per chloroplast, similar to the estimated number of ΔpH dependent pathway translocation sites whereas

Hcf106 and Tha4 are present at 5-10-fold the number of translocation sites. This stoichiometry is consistent with the dynamic channel model [66].

Current evidence from Blue-Native PAGE and immunoblotting experiments suggests that, although a small portion of Hcf106 is found in thylakoid as oligomers, Hcf106-cpTatC exists in the membrane as large multimeric complexes of ~700 kDa size with the latter serving as the primary binding site for the precursor protein. However, chemical cross-linking experiments on precursor-bound thylakoids demonstrated a direct interaction between precursor and both cpTatC and Hcf106. Tha4 assembles with the precursor-receptor complex as a required prelude to the translocation step forming an active multimeric translocon where Tha4 oligomers form the protein-conducting channel [67, 68]. It is yet not clear how this channel is formed. One model suggests that Tha4 channels exist as pre-formed oligomers of varying sizes to fit different precursors whereas a second model suggests that Tha4 assembles according to the size of the precursor. Single-particle electron microscopy and random conical tilt reconstruction of TatA complexes (bacterial homologue of Tha4) have revealed ring-shaped structures of variable diameter suggesting that the number of TatA protomers changes to adjust the size of the channel to the size of the substrate being transported [69,70]. Recent in vivo single-molecule imaging has shown that TatA forms complexes exhibiting a broad range of stoichiometries with an average of 25 TatA subunits per complex. Fourier analysis of the stoichiometry distribution suggests the complexes are assembled from tetramer units. TatA complexes did not form in cells lacking TatB-TatC, suggesting that TatB-TatC complex controls the oligomerisation of TatA [71] (see Figure 1.4 for a description of the translocation process).

1.10 Protein expression in plants

The transfer and expression of foreign genes in plant cells has become an essential tool in plant biology research. Genes are introduced in plants as chimeric genes with an epitope tag enabling subcellular detection and functional investigation of the expressed proteins. Plant cell biology studies involve transient expression of proteins and often generation of transgenic plants, i.e. plants incorporating the gene of interest within their genome, from the resulting transformed cells. Transgenic cell culture selection and generation of plants can be very-time consuming and may take from 2 to 4 months. Transient expression is a particularly useful alternative for testing new constructs and generating data in short periods of time [72].

Various techniques have been developed to introduce foreign genes into plants.

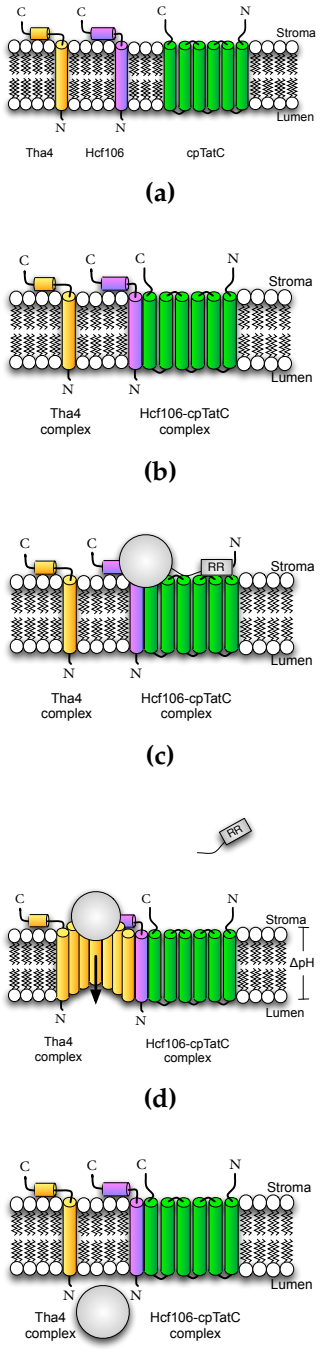

Figure 1.4: A schematic diagram showing the steps of the ΔpH-dependent pathway in chloroplasts based on current models. a) The ΔpH-dependent pathway protein components. b) In the resting state, Tha4 and Hcf106-cpTatC exist as separate membrane bound complexes. c) Precursor protein binds to the Hcf106-cpTatC complex. d) In the presence of a proton gradient, Tha4 molecules form a channel and attach to the Hcf106-cpTatC complex. Protein moves across the channel. e) The protein enters the thylakoid lumen, the proton gradient is restored and Tha4 disassembles from the Hcf106-cpTatC complex returning to the resting state.

The most widely used and successful transformation methods are the *Agrobacterium tumefaciens*-mediated DNA transfer method, which makes use of the naturally evolved crown gall-inducing mechanisms of DNA transfer present in this soil pathogen and the particle bombardment transfer method, which involves the acceleration and delivery of microprojectiles coated with DNA into the target cells. Other methods involve the direct transfer of DNA to plant protoplasts using polyethylene glycol (PEG), calcium phosphate or electroporation [73].

1.10.1 Transient expression in tobacco protoplasts using the PEG-mediated method

Tobacco mesophyl protoplasts are widely used for transient expression. Leaves from *in vitro* grown plants digest easily and produce a high yield of sterile protoplast suspension. Protoplasts are transfected with a small volume of highly concentrated and purified DNA plasmid which contains the gene encoding for the protein of interest. The level of expression can be controlled by altering the amount of DNA added to the sample. Transient expression was the main method used for this project.

1.11 Green fluorescent protein and variants

The discovery of fluorescent proteins that emit light upon irradiation was a breakthrough for the study of intracellular processes by microscopy. Green fluorescent protein (GFP) was purified from jellyfish *Aequoria victoria* in 1974 [74]. In an intermolecular energy transfer reaction of the bioluminescent system of *Aequoria victoria* the photoprotein Aequorin undergoes an intramolecular reaction upon binding to calcium and emits blue light which excites the GFP acceptor protein [74, 75]. GFP is 238 residues-long protein that folds into an 11-stranded beta barrel with a coaxial helix with the chromophore forming from the central helix [76] (protein structure shown in Figure 1.5). GFP does not fluoresce immediately after translation. Instead, it undergoes a post-translational modification to create its chromophore from protruding side chains of the S65, Y66, G67 residues. This post-translational modification entails three major synthetic steps: 1) Backbone cyclisation via covalent bond formation between glycine nitrogen G67 and carbonyl carbon atoms S65, 2) Dehydration of the oxygen of the same carbonyl and 3) Y66 oxidation [77]. Wild-type (WT) GFP has two absorption maxima at about 395 nm and 475 nm. Excitation at the primary absorption peak at 395 nm results an emmision maximum at 508 nm.

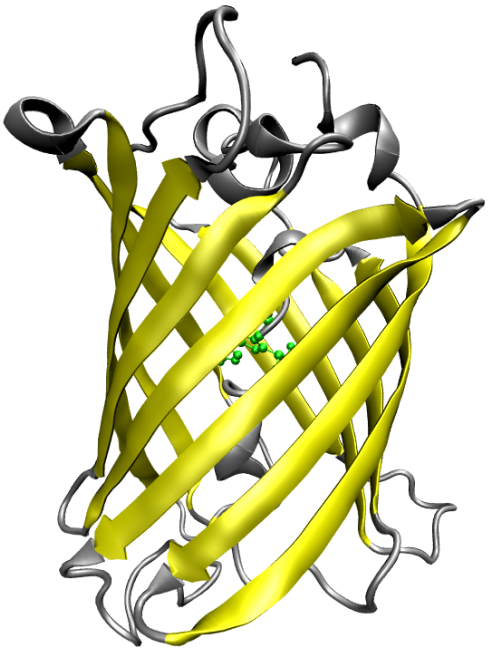

Figure 1.5: The three dimensional structure of wild type GFP was produced using the Protein Data Bank (PDB) entry 1GFL and the Visual Molecular Display (VMD) software. The protein consists of an 11-stranded beta barrel with a coaxial helix with the cromophore forming at the centre from protruding side chains of S65, Y66, G67 residues. Beta-sheets are highlighted in yellow and the 3-residue chromophore is shown in green.

Mutagenesis of the original GFP gene resulted in fluorescent variants of altered excitation and emmision spectra, supressed thermosensitivity and increased fluorescent efficiencies. For example, S65T mutation results in a single enhanced excitation peak at 488 nm [76]. The mGFP5 variant has I167T, V163A and S175G mutations which result in excitation peaks of almost equal amplitude making it ideal as a multi-purpose spectral variant which can be used for applications requiring either long-wavelength UV- or blue-light excitation [78]. Additionally, changes to codon usage eliminate any potential plant intron recognition sequences making it a suitable fluorescent tag for plant in vivo studies [78, 79]. Enhanced GFP (EGFP) presents a 35-fold increase in fluorescence and optimised human codons [80, 81]. It was shown that EGFP can enable in vivo studies of transport and sorting mechanisms involved in chloroplast biogenesis since it is not of plant origin and acts as a neutral passenger inside plant cells [82]. Additionally GFP colour variants have been produced such as Yellow Fluorescent Protein (YFP), Cyan Fluorescent Protein (CFP) and Red Fluorescent Protein (RFP).

Fluorescent proteins are vital for research as protein and organelle markers in living and fixed cells. Fusing a GFP or a GFP-variant gene at the N or C terminus of a protein of interest and introducing the chimeric gene into cells or organisms that express the recombinant protein has proven a valuable tool for studying the localisation, targeting and dynamics of a protein [83]. The production of colour GFP variants has enabled simultaneous detection of several proteins of interest. GFP and its mutants can also be used to monitor gene expression by producing a transgenic organism with the fluorescent protein encoding sequence placed under the transcriptional control of the promoter belonging to a gene of interest. This will provide direct measure of the gene expression [63]. Although fluorescently-tagged proteins usually retain their functional role, it is believed that the fluorescent tag may interfere with the protein physiological function. However, Nenninger and colleagues have recently demonstrated that even 6 GFP molecules in a row do not impede a proteins motion [84].

1.12 Laser scanning confocal microscopy

In conventional microscopy of whole cells much of the depth or volume of the sample is uniformly and simultaneously illuminated. Fluorescent light comes from excited molecules above and below the plane of focus resulting in superposition of fluorescent images from molecules at many depths in the cell, making it difficult to determine the various cellular structures [83]. Confocal microscopy, based on the principle advanced by Marvin Minsky in 1955 and patented in 1957, offers many advantages over conventional optical microscopy such as eliminat-

ing out-of-focus information and enabling collection of serial optical sections from thick specimens [85]. In laser scanning confocal microscopy, a laser beam focuses on a point in the sample and then moves laterally from point to point in the sample controlled by a scanning device. The sequences of points of light emitted from the specimen converge through a pinhole aperture at a position which is confocal with the illuminating pinhole and are detected by a photomultiplier tube (PMT). The output from PMT is used to display sharp, cross sectional images of the sample on a computer screen.

1.13 Fluorescence recovery after photobleaching and fluorescence loss in photobleaching

The mobility of a protein is closely related to its biological function and photobleaching methods are commonly used to probe protein mobility inside host membranes. In a fluorescence recovery after photobleaching (FRAP) experiment, as depicted in Figure 1.6, a high intensity laser irreversibly damages the fluorophore of a fluorescently tagged protein inside a region of interest (ROI) and an attenuated laser is used to monitor the re-distribution of non-fluorescent and fluorescent molecules inside this ROI. With appropriate models, FRAP recovery curves can give information about a protein's diffusion coefficient, the presence of more than one diffusing population and the existence of an immobile fraction.

In fluorescence loss in photobleaching (FLIP), as depicted in Figure 1.7, the high intensity laser stays on throughout the duration of the experiment irreversibly damaging the fluorophore of any fluorescently tagged protein diffusing into the region of interest (ROI) with images of the whole fluorescent population being taken at regular intervals to monitor the loss of total fluorescence and providing information on compartment connectivity.

1.14 Derivation of the diffusion equation

Diffusing protein molecules follow a random walk in three dimensions where all directions are equally likely and independent of the direction taken at the previous step. For simplicity, the one dimensional case is described here.

Suppose the number of particles distributed along the x-axis is known at time t, i.e. there are $N(x)$ particles at position x and $N(x+\delta)$ particles at position $x+\delta$. Each particle can move a length δ to the right or to the left with equal probability in time interval τ. We can consider an imaginary line perpendicular to the x-axis between positions x and $x+\delta$.

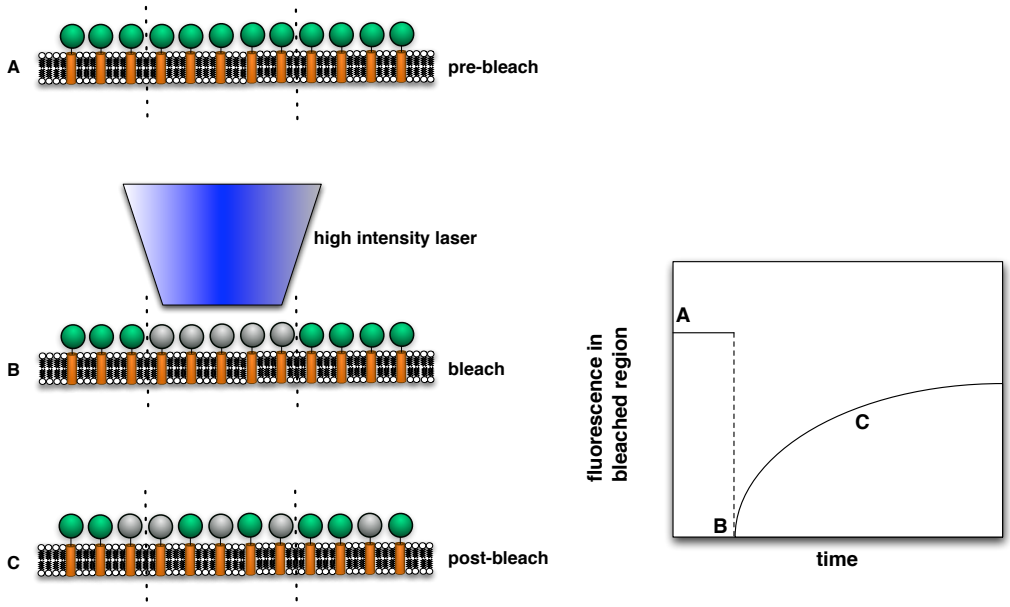

Figure 1.6: Fluorescence recovery after photobleaching (FRAP) diagram. A) The fluorescence intensity is recorded prior to the experiment. B) High intensity laser is used to photobleach a region. C) Low intensity laser is used to monitor recovery of fluorescence.

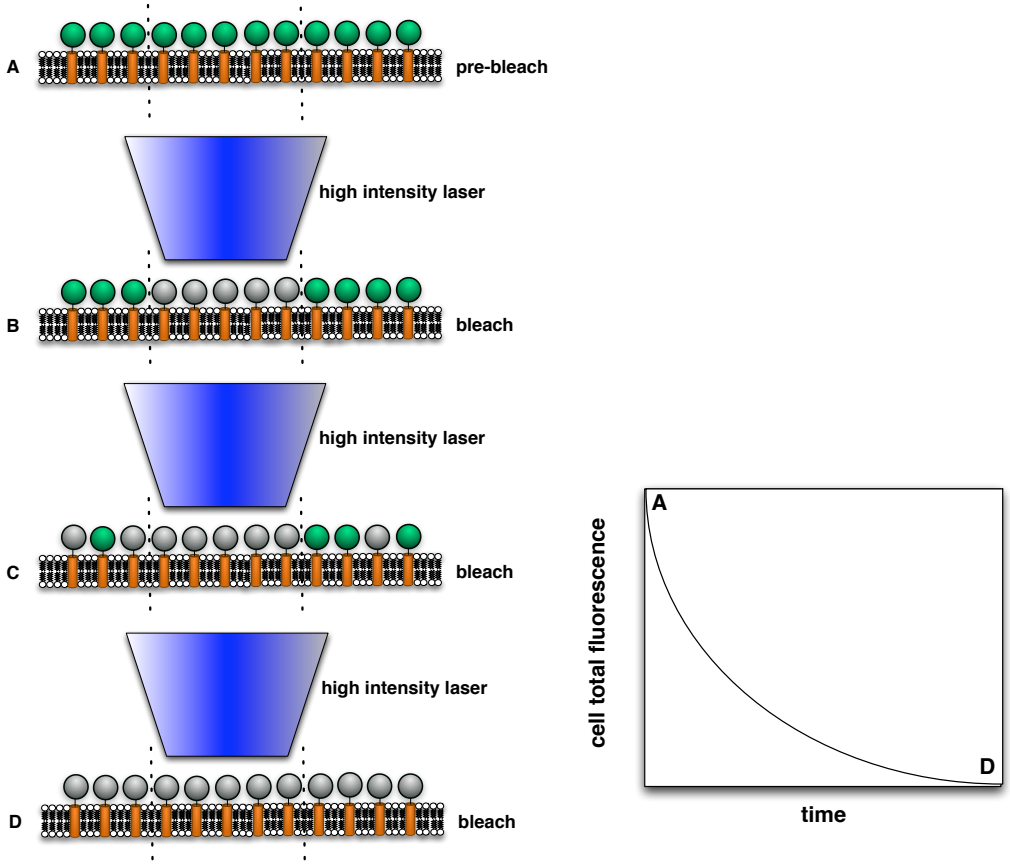

Figure 1.7: Fluorescence loss in photobleaching (FLIP) diagram. A) The initial fluorescence is measured. B-C) High intensity laser bleaches diffusing molecules. D) Loss in fluorescence gives information on molecule mobility.

At time $t+\tau$, half of the $N(x)$ particles will end up at $x+\delta$ position whereas half of the $N(x+\delta)$ particles will end up at the x position. The net number of particles crossing the imaginary line to the right is

$$-\frac{1}{2}N(x+\delta)+\frac{1}{2}N(x)=-\frac{1}{2}\left[N(x+\delta)-N(x)\right] \tag{1.1}$$

This net number of particles moving to the right through this imaginary line can be converted into flux by dividing by the area A the particles move through, and time τ, i.e. number of particles per unit area and per unit time.

$$j=-\frac{1}{2}\left[N(x+\delta)-N(x)\right]/A\tau \tag{1.2}$$

If we multiply both numerator and denominator of the above expression with δ^2 and rearrange we get

$$j=-\frac{\delta^2}{2\tau}\frac{1}{\delta}\left[N(x+\delta)/A\delta-N(x)/A\delta\right] \tag{1.3}$$

where $\delta^2/2\tau$ is the diffusion coefficient D, $N(x+\delta)/A\delta$ is the number of particles per unit volume at point $x+\delta$ i.e. the concentration $C(x+\delta)$ at the point $x+\delta$ and $N(x)/A\delta$ is the concentration $C(x)$ at point x. Inserting these definitions into equation (1.3)

$$j=-D\frac{1}{\delta}\left[C(x+\delta)-C(x)\right] \tag{1.4}$$

Taking the limit $\delta\to 0$, i.e. making δ very small, equation (1.4) becomes Fick's first equation which states that the net flux at point x and time t is proportional to the slope of the concentration function.

$$j=-D\frac{\partial C}{\partial x} \tag{1.5}$$

We now introduce the principle that particles are not created or destroyed by considering the change of concentration in a volume $A\delta$. In time τ, $j(x)A\tau$ particles enter the volume on the left side and $j(x+\delta)A\tau$ leave on the right side. The rate of increase of particles in the volume is the difference between these divided by τ. Dividing by the volume $A\delta$ gives the rate change of concentration

$$\frac{1}{\tau}\left[C(t+\tau) - C(t)\right] = -\frac{1}{\delta}\left[j(x+\delta) - j(x)\right] \tag{1.6}$$

After, taking the limit $\tau \to 0$ and $\delta \to 0$, equation (1.6) becomes the continuity equation,

$$\frac{\partial C}{\partial t} = -\frac{\partial j}{\partial x} \tag{1.7}$$

Combining Fick's equation (1.5) and the continuity equation (1.7), we derive the diffusion equation in one dimension

$$\frac{\partial C}{\partial t} = D\frac{\partial^2 C}{\partial x^2} \tag{1.8}$$

This corresponds to a random walk with mean square displacement proportional to time in the limit of step size tending to zero.

Extending the above equation to two dimensions results in

$$\frac{\partial C}{\partial t} = D\left[\frac{\partial^2 C}{\partial x^2} + \frac{\partial^2 C}{\partial y^2}\right] \tag{1.9}$$

and in general can be written

$$\frac{\partial C}{\partial t} = D\nabla^2 C \tag{1.10}$$

where ∇^2 is called the Laplacian.

The diffusion equation is usually applied to a finite area with specified conditions on the boundaries. For protein diffusion we will assume a no flux boundary condition.

1.15 Theoretical analysis of photobleaching experiments

A FRAP experiment outputs a sequence of fluorescence intensity values from inside the bleached region with respect to time. When these data are compared to established theoretical models, quantitative information such as the mobility of the fluorescently tagged population, the binding states and binding strength of each state can be extracted. Simple models incorporating diffusion of only one species are disscussed here; extended models are discussed in Appendix C.

1.15.1 Early theoretical FRAP models

The earliest attempts of Axelrod and colleagues [86] and Soumpasis [87] to model photobleaching experiments are purely analytical and predict recovery curves for the idealised cases of pure two-dimensional diffusion monitored by a laser beam of either a Gaussian intensity profile or a uniform circular disc profile. These models assume that the fluorescently labeled membrane component is uniformly distributed in an infinite membrane plane.

It is assumed that the photobleaching of fluorophores to non-fluorescent species follows an irreversible first-order reaction with rate constant $\alpha I(r)$. The concentration of unbleached fluorophore $C(r,t)$ at position r and time t can be calculated from

$$\frac{dC(r,t)}{dt} = -\alpha I(r) C(r,t) \tag{1.11}$$

where $I(r)$ is the bleaching intenisty.

After a bleaching of duration time T the fluorophore concentration profile at the start of the recovery phase $t = 0$ is given by

$$C(r,0) = C_0 \exp\left(-\alpha T I(r)\right) \tag{1.12}$$

where C_0 is the initial condition for fluorophore concentration.

The amount of bleaching induced in time T is expressed by a parameter

$$K = \alpha T I(0) \tag{1.13}$$

The equation for lateral diffusion of a single species of fluorophore follows the diffusion equation described in section 1.14. With diffusion coefficient D, the diffusion equation is

$$\frac{\partial C(r,t)}{\partial t} = D\nabla^2 C(r,t) \tag{1.14}$$

where the boundary condition is $C(\infty, t) = C_0$.

The fluorescence at time t $F_k(t)$ is equal to the sum of the number of the fluorophores being illuminated and can be expressed, in polar coordinates, as

$$F_k(t) = \frac{q}{A} \int I(r) C_k(r,t)\, d^2 r \tag{1.15}$$

where the parameter q represents the product of all quantum efficiencies of laser light absorption, emmission and detection, A is the attenuation factor of the beam during the fluorescence recovery, $I(r)$ is the intensity profile of the bleaching laser in the membrane plane and $C_k(r,t)$ is the concentration of unbleached molecules at radial distance r and time t obtained from solving the differential equation (1.14).

The origin in polar coordinates is taken to be the centre of the bleached area.

Fluorescence recovery curves can be transformed into a fractional form, thus making the recovery independent of the absolute intensity, by

$$f_K(t) = \frac{[F_k(t) - F_k(0)]}{[F_k(\infty) - F_k(0)]} \tag{1.16}$$

Gaussian intensity profile

For a Gaussian intensity profile, $I(r)$ is given by

$$I(r) = \frac{2P_0}{\pi w^2} \exp\left(-\frac{2r^2}{w^2}\right) \tag{1.17}$$

where w is the half-width at e^{-2} of the Gaussian distribution and P_0 is the total laser power.

Using the scheme described earlier in section 1.15, the closed form solution for a Gaussian intensity profile in fractional form is

$$f_K(t) = 1 - \frac{(t_D)^2}{1+2t} K^{2+t_D/(1+2t)} \frac{\Gamma(\nu)}{\Gamma(t_D)} \frac{P(2K|2\nu)}{P(2K|2t_D)} \tag{1.18}$$

where $\nu = t_D/(1+2t)$, the characteristic diffusion time $t_D = w^2/4D$, $\Gamma(\nu)$ is the gamma function and $P(2K|2\nu)$ is the χ^2 probability distribution.

Circular intensity profile

For a circular disc profile, $I(r)$ is given by

$$I(r) = \begin{cases} \dfrac{P_0}{\pi w^2} & \text{for} \quad r \le w \\ 0 & \text{for} \quad r > w \end{cases}$$

With the assumption of full recovery, the closed form solution for circular intensity profile is

$$f(t) = \exp\left(-\frac{2t_D}{t}\right)\left[I_0\left(\frac{2t_D}{t}\right) + I_1\left(\frac{2t_D}{t}\right)\right] \tag{1.19}$$

which is independent of the bleaching parameter K. I_0 and I_1 are modified Bessel functions.

If there are two diffusing populations, a fast and a slow one, the recovery curve can be expressed as

$$f(t) = f_F(t) + \theta_F[f_S(t) - f_F(t)] \tag{1.20}$$

both components have identical photobleaching characteristics, diffuse isotropically and independently and recovery is complete.

One of the limitations of the Axelrod and Soumpasis models is the assumption of planar membranes. In reality, biomembranes adopt 'wavy' conformations like $h(x, y) = A\cos(kx)\cos(ky)$, where A is the amplitude and k the spatial frequency, therefore the actual diffusion of resident molecules can be up to twice as large as the predicted from the model [88].

1.15.2 Strip FRAP on spherical membranes

Biological membranes can adopt geometries different to the planar assumptions of the earlier models. Ellenberg et al. proposed the following formula to model the diffusion of lamin B receptor in inner nuclear membranes which is roughly spherical. When a rectangular strip of a cross-section of a spherical membrane is bleached, the fluorescence recovery is given by [89]

$$f(t) = f(\infty)\sqrt{1 - \frac{w^2}{w^2 + 4\pi Dt}} \tag{1.21}$$

which agrees within 5% with the solution of the diffusion equation in one dimension for recovery into an interval of zero intensity, where $f(t)$ is the intensity as a function of time, zero of time t was taken as the midpoint of the bleach, f(∞) is the final intensity reached after complete recovery, w is the strip width and D is the effective one-dimensional diffusion constant. This equation assumes one dimensional recovery which is reasonable because the membrane is bleached across its length and full depth.

1.16 Computer simulations

Computer simulations are a powerful tool for the investigation of how biological molecules behave in experimentally inaccessible domains. Computer simulations confer flexibility for testing hypotheses and comparing with the experimental data. They mimic the set of processes taking place in a system and attempt to infer for the *in vivo* situation.

Firstly, a mathematical model describing the essential features of the system is proposed, often involving ordinary or partial differential equations. In cases where the model is too complicated to be solved analytically i.e. it is difficult or impossible to write a closed form expression, numerical methods may facilitate solving the mathematical model. Numerical methods can reduce continuous

problems with infinitely many degrees of freedom defined by differential equations to discrete problems or set of equations with only finitely many unknowns.

1.16.1 Finite-difference method

In physical systems in which a property, such as concentration, varies continuously in space and in time, the rates of change from point to point are described by partial differential equations. A classical numerical method for approximating the solution to partial differential equations is the finite differences method. The area over which diffusion occurs is discretised using a rectangular grid and the concentration is defined at the grid points. The spatial derivatives of the differential equation are replaced by difference quotients for each grid point. These quotients are algebraic expressions involving the grid points above and below, and to the left and right of the grid point in question. The time derivatives are also replaced by difference quotients which relate the conentration at the current time to the concentration at previous times. At each iteration the difference quotients for the spatial derivatives represent a system of n equations with n unknowns which can be solved. The result can be used to integrate the time derivatives to obtain the concentration at the next time point.

1.16.2 Finite-element methods

The finite element method, although similar in principle, is often preferred to the finite difference method in solving linear-steady state problems over irregular multi-dimensional domains of complex boundaries. The differential equation of the physical problem is expressed in terms of an integral to be minimised – also called a variational problem. The domain over which the problem occurs is discretised by nodes which are connected with lines to define the elements, typically triangles in two dimensions or tetrahedrons in three dimensions. The quantity of interest is interpolated between the nodes of each element in terms of bilinear relations involving the nodal values. The intergral to be minimised is evaluated using the bilinear relations over each element. The node values that make the derivative of the integral zero provide the solution to the differential equation.

1.16.3 Monte Carlo method

The nature of many physical systems is stochastic, i.e. dependent on chance. Applying the Monte Carlo method to model stochastic systems involves selecting from a set of randomly generated numbers to determine how a system evolves in

time.This approach mimics the inherent randomness of the behaviour of a physical system. The key features of the Monte Carlo method can be demonstrated via a two-dimensional random walk of a particle on a square grid of unit length side. At time $t = 0$ the particle is at the origin and at each time step can move only +1 or -1 in the x or y directions with an equal probability for each of the four directions. A random number r is generated with a uniform probability density from 0 to 1 and the direction of motion is chosen according to the following scheme:

$$\begin{aligned}
&\text{if } 0 \leq r \leq 0.25 \text{ particle moves in } -x \\
&\text{if } 0.25 < r \leq 0.5 \text{ particle moves in } +x \\
&\text{if } 0.5 < r \leq 0.75 \text{ particle moves in } +y \\
&\text{if } 0.75 < r \leq 1 \text{ particle moves in } -y
\end{aligned}$$

Each direction is therefore equally likely, and consequently, over many runs the mean displacement is zero, i.e. mean position of particle remains at the centre. However, because the square displacement R^2 is always positive, the mean square displacement of a particle moving unit length steps is nonzero, and can be shown to be equal to the total number of steps n,

$$< R^2 >= n \tag{1.22}$$

1.16.4 Particle Strength Exchange method

The Particle Strength Exchange (PSE) method is a deterministic particle method which can be used to simulate diffusion, convection-diffusion and other fluid dynamics probelms. The PSE scheme was developed by Degond and Mas-Gallic for the case of isotropic [90] and anisotropic diffusion [91]. According to the PSE scheme, the Laplace operator of the diffusion equation is replaced by an integral operator which is discretised over space using particle locations as quadrature points. This discretisation is substituted into the original differential equation resulting in a set of coupled ordinary differential equations. Using the particle strengths at $t = 0$ as the initial conditions, the differential equations are solved using the Euler method providing concentration spatio-temporal information. In order to solve the diffusion equation

$$D\nabla^2 c(x) = \frac{\partial c}{\partial t} \tag{1.23}$$

using the Particle Strength Exchange scheme, the Laplacian operator of the diffusion equation is replaced by an integral operator.

$$\nabla^2 c(x_1) \simeq \epsilon^{-2} \int [c(x_2) - c(x_1)]\eta(r)\, dx_2 \tag{1.24}$$

where $r = \sqrt{|x_1 - x_2|^2}$ is the distance between x_1 and x_2 and the 2D Gaussian kernel for distance r is given by

$$\eta = \frac{4}{\pi} e^{-r^2} \tag{1.25}$$

In this integral (1.24), the difference in concentration c at point x_1 with respect to each point x_2 of the integral domain is weighted according to the 2D Gaussian kernel η applied to the spatial separation. As a result the neighbouring points exert greater influence than further away points.

The integral operator is replaced by a summation and the integration domain is discretised in space by being divided into n squares. The total concentration c_p of each square is assigned to a simulation particle p at their centres[1]. A point x_1 located within a particular square is represented by the particle p at the centre x_p of that square. The integral becomes a sum over all particles other than p

$$\int [c(x_2) - c(x_1)]\eta(r)\, dx_2 \simeq \sum_{q \neq p} (c_q - c_p) A_q \eta(r) \tag{1.26}$$

where the A_q is the area of the square surrounding particle q and $r = \sqrt{|x_p - x_q|^2}$ is the distance between particles p and q.

This discretisation is then incorporated in the initial diffusion equation (1.27)

$$\frac{\partial c_p}{\partial t} \simeq D\epsilon^{-2} \sum_{q \neq p} (c_q - c_p) A_q \eta(x_q - x_p) \tag{1.27}$$

Using the Euler method, and by assigning suitable concentrations to each particle as the initial conditions, we numerically integrate a set of n coupled ordinary differential equations

$$c_p(t + \Delta t) = c_p(t) + \frac{\partial c_p}{\partial t} \Delta t \tag{1.28}$$

using the approximation obtained in (1.27) for the derivative. The solutions $c_p(t)$ give the concentration profile for a diffusion in space and time.

To simulate a FRAP experiment using the PSE scheme, we first define the bleached region B and the set of bleached particles $P_B = \{p : x_p \in B, 1 \leq p \leq n\}$. We

[1]Note that the simulation particles do *not* correspond to actual particles, such as proteins. They are introduced only as a computational device.

initially assign the concentration to each bleached particle such that

$$\sum_{p \in P_B} c_p = c_0 \tag{1.29}$$

where c_0 is the post-bleach intensity obtained from the experimental.

The PSE simulation then proceeds as previously described and the recovery profile is obtained from

$$F(t) = \sum_{p \in P_B} c_p(t) \tag{1.30}$$

and then transformed to fractional recovery $f(t)$ as usual.

1.17 Aims of the project

This project aims to shed light on the lateral diffusion of proteins in membrane compartments of chloroplasts. Using an interdisciplinary approach we attempt to provide answers to the following questions:

1. How is the intricate structure of the chloroplast thylakoid membrane affecting the diffusion of its resident proteins?

2. Can we use computational approaches to overcome experimental limitations, simulate the experimental observations and extract quantitative predictions of the actual molecular diffusion constants?

3. How do proteins diffuse in other membrane compartments of chloroplasts?

2

Materials and methods

2.1 pDHA expression system

The pDHA expression system allows 35S promoter-directed gene expression. It is a derivative of the Cauliflower mosaic virus 35S gene expression cassette pDH51 and contains the 5′ untranslated region of alfalfa mosaic virus coat protein mRNA which has been observed to enhance the translation efficiency of mRNA [92, 93]. The CaMV 35S is a constitutive promoter which means that it cannot be regulated or switched off by the host's gene regulation system.

2.2 Plasmid construction

A DNA fragment containing the *hcf106* gene was amplified with the forward primer F1 5′-TCATCATCTAGAATGGCCATGGCGTTACAGATTA-3′ and reverse primer R1 5′-TTCTCCTTTACTATCTTGCCTTGGAGGAGATGCAG-3′. *mGFP5* was amplified with the forward primer F2 5′-CAAGGCAAGATAGTAAAGGAG AAGAACTTTTCACTG-3′ and reverse primer R2 5′-TGATGACTGCAGTTATTT GTATAGTTCATCCATGCC-3′. The amplified fragments were used to generate the fusion between *hcf106* and *mGFP5* with the forward primer F1 and reverse primer R2. The resulting product was digested with XbaI and PstI and cloned into pDHA expression vector under the regulation of 35S promoter. DNA of 1 mg/mL concentration was purified from overnight bacterial cultures using a Maxi Prep commercial kit (Qiagen).

2.3 Acquired constructs

The constructs used for transient expression are listed in the following table:

Construct	Provider
TP-mGFP5	Alessandra Di Cola, University of Warwick
pre-mGFP5	Alessandra Di Cola, University of Warwick
pre-ΔTPP-mGFP5	Alessandra Di Cola, University of Warwick
atOEP7-mGFP5	Lorenzo Frigerio, University of Warwick

2.4 Tobacco seed sterilisation and plant growth in room conditions

All of the following operations were performed in a sterile hood. *Nicotiana tabacum* cv. Petit Havana SR1 seeds (about 30 seeds) were sterilised in 1.5ml eppendorf tubes. Seeds were incubated, with mixing, in the presence of 1 ml 70% (v/v)

EtOH for 1 minute before being left to sediment. The supernatant, along with floating seeds, was removed and discarded. 1 ml 10% (v/v) bleach with a drop of tween was added to the seeds pellet and incubated with continual agitation for 10 minutes. Seeds were left to rest and the supernatant and floating seeds were discarded. The seeds pellet was washed with 1 ml sterile water 4 times, leaving to rest and removing supernatant and floating seeds between washes. Seeds were then plated, in the last water wash, onto a short sterilised glass Weck jar containing sterilised MS-agar (Murashige and Skoog (MS), 2% sucrose 0.8% bacto agar, adjusted to pH 5.8 with 1 M KOH). The sterilised seeds were incubated under artificial illumination (12h light / 12h dark cycle, optimal for transient expression efficiency) at a constant temperature of 25 ℃ and once germinated, individual seedlings were transferred into sterilised glass Weck jars containing sterilised MS-agar. These tobacco plants were used as the source of protoplasts for the transient expression of DNA constructs.

2.5 Maintenance of *Nicotiana tabacum* plants in greenhouse conditions

Nicotiana tabacum cv. Petit Havana SRI plants (~8 weeks old) were transferred from a glass jar to a large pot containing a 1:1 mix of multipurpose compost (B&Q, UK) and fine vermiculite (1-3mm, Sinclair, UK) in a greenhouse. Plants were maintained at a constant temperature of 20℃ and illuminated with sodium lamps with a regime of 16h light / 8h dark. These tobacco plants were used as a seed supply.

2.6 Transient expression in tobacco protoplasts

2.6.1 Preparation of protoplasts from tobacco leaves

All solutions used were stored at −20℃ when not in use and filter sterilised. All operations were carried out in a sterile hood. Cut tips were used when dealing with protoplast suspensions. 10x enzyme mix (Macerozyme Onozuka R-10 (2% (w/v)), Cellulase Onozuka R-10 (4% (w/v)) in K3 medium (3.78 g/l Gamborg's B5 basal medium with minimal organics (Sigma), supplemented with 750 mg/l $CaCl_2.2H_2O$, 250 mg/l NH_4NO_3, 136.2 g/l sucrose, 250 mg/l xylose, 1 mg/l 6-benzylaminopurine (6-BAP), 1 mg/l alpha-naphtalenacetic acid (NAA), pH 5.5) was diluted to a final concentration of 1x with K3 immediately before use, and poured into 10 cm petri dishes in 7 ml aliquots. 2 to 5 week old green leaves were

cut from a sterile tobacco plants. Using a sterilised scalpel, the abaxial surface of the leaf was carefully scarified every 1 mm taking care not to cut through the whole leaf. Wet or curled parts of leaves due to contact with the jar walls were discarded. Operating quickly to avoid excessive dehydration, the leaves were floated on the enzyme mix in the Petri dish, such as the abaxial surface was in contact with the enzyme mix without wetting the adaxial surface. Plates were filled as much as possible with whole leaves and fragments to fill in any gaps and incubated overnight in the dark at 25 °C. The following morning, the digestion mix was gently removed using a sterile Pasteur pipette and discarded, leaving protoplasts still attached to the leaves. 3 ml of K3 was added drop wise over the leaves, and the plates were gently agitated to release the protoplasts. Using a fresh sterile Pasteur the released protoplast solution was recovered and filtered through a sterilised 100 µm brass sieve, previously flamed and wetted with K3, into a a Petri dish. Another 3 ml K3 was added to the leaves, and any protoplasts released by this second wash were filtered as before. The filtered protoplasts were transferred to a 50 ml sterile Falcon tubes and centrifuged at 100g (600 rpm, Beckman GPR bench centrifuge, GM3.7 rotor) for 20 minutes at room temperature, in order to separate broken from viable protoplasts. While viable protoplasts float, the pellet of broken protoplasts and most of the K3 above it was removed, using a Pasteur pipette connected to a 25 ml pipette, leaving 5 ml K3 containing the floating layer of viable protoplasts. The K3 was then diluted 4-fold with W5 medium (9 g/l NaCl, 0.37 g/l KCl, 18.37 g/l $CaCl_2.H_2O$ 0.9 g/l glucose) added drop-wise down the wall of the tube. The solution was gently mixed until the protoplasts were evenly distributed and pelleted by centrifugation at 100g (600 rpm, Beckman GPR bench centrifuge, GM3.7 rotor) for 10 minutes at room temperature and the supernatant was discarded. The resulting pellet was gently resuspended in the same volume of W5. Protoplasts were pelleted again and the supernatant was discarded. Finally, protoplasts were carefully resuspended in up to 10 ml W5 and incubated in the dark for 30 minutes at 25 °C, after removing a 50 µl sample for protoplast counting.

2.6.2 Determining the number of protoplasts per unit volume of suspension

A 50 µl sample of the protoplast solution in W5 was diluted in 450 µl K3. An aliquot of 10 µl was loaded onto the counting chamber of an improved Neubauer hemacytometer using a cut tip and covered with a slide. Observing under a microscope using 40x magnification (4x objective), only those protoplasts appearing round were counted as viable.

2.6.3 Protoplast transfection using polyethylene glycol (PEG) method

After 30 minutes of dark incubation, protoplasts were pelleted by centrifugation at 100g (600 rpm, Beckman GPR bench centrifuge, GM3.7 rotor) for 5 minutes at room temperature and the supernatant was discarded. Protoplasts were resuspended to a final concentration of 10^6 viable protoplasts per ml with MaCa buffer (0.1% MES, 20 mM $CaCl_2$, 0.5 M mannitol, pH 5.7). The protoplast suspension was subjected to a 45 ℃ heat shock for 5 min and allowed to cool at room temperature for at least 10 minutes. 1 ml of protoplast suspension was added in a 15 ml sterile Falcon tube already containing the DNA for transfection (40 μg in no more than 100 μl per million cells). The protoplasts were gently mixed with the DNA solution and the tube was then placed tilted on a rack, and 1ml 40% (w/v) PEG 4000 (40 g polyethylene-glycol 4000 dissolved in 60 ml of 0.1 M $Ca(NO_3)_2.4H_2O$ and 0.4 M mannitol in water, pH adjusted to between 8 and 10 with 1 M KOH, and volume brought to 100 ml) was added dropwise to the upper part of the tube and allowed to slide down the wall so that the impact with the cell suspension was gentle. The solution was mixed gently by inverting the tube several times and incubated at room temperature for 30 minutes, mixing from time to time in order to dissolve cell clumps. Protoplasts were washed by slowing adding W5 in 3 ml aliquots taking over 15 minutes to fill the tubes and throroughly mixing between each addition. Protoplasts were pelleted by centrifugation at 100g (600 rpm, Beckman GPR bench centrifuge, GM3.7 rotor) for 10 minutes at room temperature, the supernatant was discarded, and the pellet was resuspended in 1 ml K3. Protoplasts were allowed to recover overnight in the dark at 25 ℃.

2.6.4 Chloroplast isolation

After the overnight recovery step, the protoplasts were washed in 4 ml W5 and pelleted with centrifugation at 100g for 10 minutes at 4 ℃. The pellet was resuspended in 4 ml HS buffer (1X) (50 mM Hepes-KOH and 330 mM sorbitol, pH 8.0). Using a syringe, protoplasts were slowly forced through a pore size mesh three times in order to break and release their chloroplasts. The cell suspension was carefully applied on the side of a tube containing pre-cooled 4 ml 35% Percol pad (800 μl HS(5X), 1.4 ml Percoll and 1.8 ml H_2O). After centrifuging for 8 minutes at 1400g at 4 ℃, the intact chloroplasts pelleted and the broken chloroplasts formed a layer at the interface between the Percoll pad and the HS solution. The broken cells and the supernatant were carefully removed and the chloroplast pellet was resuspended in 8 ml of HS(1X). The chloroplast suspension was centrifuged for 2 minutes at 3000g at 4 ℃.

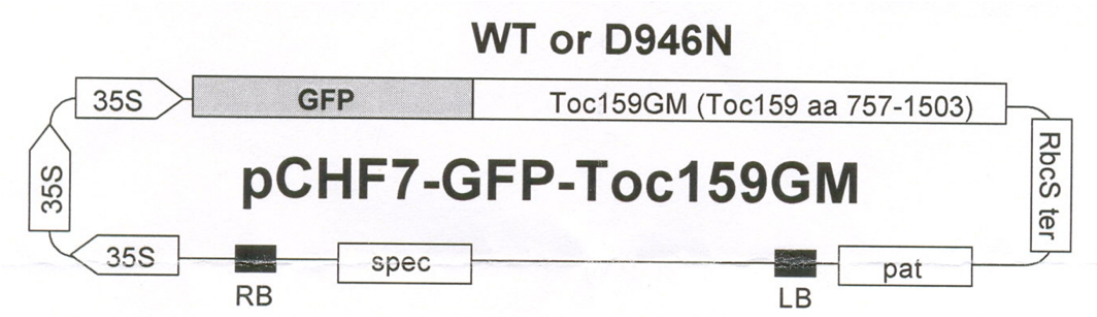

Figure 2.1: Schematic diagram of the layout of the pCHF7-GFP-Toc159GM vector. Courtesy of Prof. Felix Kessler.

2.6.5 Determining chloroplast concentration

The absorbance coefficient of chlorophyll (a/b) at 652 nm was used to estimate the concentration of chloroplasts in the suspension. An aliquot of 5 µl chloroplast solution was added in 1 ml 80% (v/v) acetone in a 1.5 ml Eppendorf tube and mixed by inverting the tube (three replicates). The sample was centrifuged at 13000 rpm for 5 minutes to pellet insoluble material. The supernatant was transferred into a 1 ml quartz cuvette (10 mm light path) and the absorbance at 652 nm was measured against an 80% acetone blank using a spectrophotometer. The chlorophyll concentration of the chloroplast sample was calculated using the formula A_{652} x 5.6 µg chlorophyll(a/b)/µl and it was adjusted to 1 mg/ml according to the method outlined in [94].

2.7 Toc159 transgenic plants

The seeds for the Toc159 transgenic *A. thaliana* (ecotype Wassilewska) plants were provided by Professor Felix Kessler (Universite de Neuchatel). Due to the homozygous ppi2 (toc159) mutation, plants transfected with Constructs 2 and 3 (see table below) do not express the endogenous Toc159 full length. The single point mutation D946N in Construct 3 disrupts the interaction of Toc159 with Toc34. A summary of the constructs used appears in the following table:

Construct 1	TOC159/TOC159 + pCHF7-GFP-TOC159GM
Construct 2	ppi2/ppi2 + pCHF7-GFP-TOC159GM
Construct 3	ppi2/ppi2 + pCHF7-GFP-TOC159GM D946N

2.8 *Arabidopsis thaliana* seed sterilisation and plant growth

All of the following operations were performed in a sterile hood. Seeds were transferred in 1.5 ml eppendorf tubes. The seeds were initially sterilized by a 2 minute incubation in 50% bleach/tween. Seeds were left to rest and the supernatant and floating seeds were discarded. The seeds pellet was washed with 1 ml sterile water 4 times, leaving to rest and removing supernatant and floating seeds between washes. Seeds were then plated, in the last water wash, onto square petri plates containing sterilised MS-agar (Murashige-Skoog medium). The plates were incubated for 2 days in the dark at 4 ℃ for vernalisation to occur and subsequently transferred to the 24 hour light room and were allowed to grow for 10 days [95].

2.9 Maintenance of *Arabidopsis* plants in greenhouse conditions

The 10-day old plants were transferred to pots containing a 1:1 mix of multipurpose compost (B&Q, UK) and fine vermiculite (1–3 mm, Sinclair, UK) previously soaked with intercept dissolved in water. Plants were maintained in the green house at a constant temperature of 20 ℃ and illuminated with sodium lamps with a regime of 16h light / 8h dark.

2.10 Preparation of protoplasts and chloroplasts from *Arabidopsis* leaves

Well-expanded leaves from 3-4 week-old plants (usually leaf numbers five to seven) before flowering were selected. 1 mm leaf strips were cut from the middle part of each leaf using a fresh sharp razor blade. The leaf strips (from 10-20 leaves) were quickly transferred into a petri dish containing 10 ml enzyme solution (1.5% (w/v) cellulase 'Onozuka R10', 0.4%(w/v) 'Macerozyme R10', 0.4 M mannitol, 20 mM KCl, 10 mM $CaCl_2$, 20 mM MES (pH 5.7)) by dipping both sides of the strips using a pair of flat-tip forceps. The leaf strips were vacuum infiltrated for 30 minutes in the dark using a desiccator. The digestion continued without shaking in the dark for at least 3 hours at room temperature. The enzyme solution turned green after a gentle swirling motion indicating the efficient release of protoplasts. The enzyme/protoplast solution was diluted with an equal volume

of W5 (154 mM NaCl, 125 mM $CaCl_2$, 5 mM KCl, 2 mM MES (pH 5.7)) and filtered through a sterilised 100 µm brass sieve, previously flamed and wetted with W5 to remove the undigested leaf tissues. The flow through was collected in a 50 ml falcon tube and the protoplasts were pellet after a 5 minute centrifugation at 100 g. After removing the supernatant the protoplasts were resuspended in the same volume of W5 and re-centrifuged to pellet the protoplasts to ensure complete removal of the enzymatic solution. Chloroplasts were released from protoplasts using the same protocol as for tobacco chloroplast isolation.

2.11 Protoplast fractionation

Arabidopsis protoplasts were subjected to three freeze-thaw cycles and then centrifuged at 9800g at 4 ℃ for 5 min in a microcentrifuge to remove cell debris. The cell extracts then were fractionated into soluble and membrane fractions by ultracentrifugation in 1 ml samples at 100 000g for 30 minutes. 25 µl of supernatant, and the whole pellet resuspended in 25 µl of HS buffer, were both used in SDS-PAGE.

2.12 SDS polyacrylamide gel electrophoresis

Sodium dodecyl sulphate polyacrylamide gel electrophoresis (SDS-PAGE) was performed using the methods of Laemmli using a vertical gel electrophoresis system (CBS). The resolving gel was a 15% acrylamide (5.4 ml "Acrylogel 2.6 (40%)" solution (40% acrylamide, 2.6% Bis-acrylamide), 5.4 ml dH20 and 3.6 ml resolving buffer (0.4% SDS, 1.5 M Tris-HCL pH 8.8). Polymerisation of the resolving gel was initiated with the addition of 32 µl APS (10%) and 8 µl of TEMED. The gel was overlaid with 0.5 ml of water-saturated butanol which was aspirated before the addition of the stacking gel solution. The stacking gel was 5% acrylamide (0.6 ml "Acrylogel 2.6 (40%)" solution (40% acrylamide, 2.6% Bis-acrylamide), 3.0 ml dH20 and 1.2 ml separation buffer (0.4% SDS, 0.5 M Tris-HCL pH 6.8). The stacking gels was polymerised upon addition of 30 µl APS (10%) and 3 µl of TEMED. In order to form wells, a comb was inserted before gel polymerisation was complete. Gels were placed into gel tanks and submerged in 1x protein gel running buffer (25 mM Tris-HCL pH 6.8, 192 mM glycine, 0.1% SDS). A 2x concentrated sample buffer (4% SDS, 10% beta-mercaptoethanol, 20% Glycerol, 100 mM Tris-HCL pH 6.0, 0.002% Bromophenol Blue) was added to the samples which were subsequently denatured by heating at 95 ℃ for 4 minutes, briefly centrifuged and loaded onto the gel. The electrophoresis was carried out at a fixed current of 35

mA for 4 hours.

2.13 Western blots

Proteins were transferred from the acrylamide gel to PVDF membrane (Peqlab PVDF Membrane, 0.45 μm) in a semi-dry Western blotting system (Sigma Aldrich, UK) with Western Transfer Buffer (100 ml 10X Tris-Glycine (250 mM Tris, 2 M Glycine), 700 ml dH_2O a semi-dry Western blotting system (Sigma Aldrich, UK) with Western Transfer Buffer (100 ml 10X Tris-Glycine (250 mM Tris, 2 M Glycine), 700 ml dH_2O, 200 ml Methanol). Two sheets of Whatman 3MM Chromatography paper were soaked in Western Transfer Buffer solution and placed on the blotter and a sheet of PVDF membrane previously soaked in methanol was placed on top of them. A glass rod was rolled over the membranes to remove any air bubbles trapped between the layers as this may cause uneven transfer. The acrylamide gel was placed on the PVDF membrane and covered with another 2 sheets of Western Transfer Buffer soaked Whatman paper. Air bubbles were once again removed by rolling a glass rod. Transfer was carried out by applying a constant current of 200 mA for 2 hours. The protein markers were visible on the PVDF membrane indicating efficient protein transfer. The membrane was placed into blocking solution PBS-T (137 mM NaCl, 2.7 mM KCl, 10 mM Na_2HPO_4, 2 mM KH_2PO_4 with 0.1% Tween 20) containing 5% (w/v) dried skimmed milk powder for an 1 hour. The membrane was washed in PBS-T and then incubated with anti-GFP for an hour while shaking (2 μl anti-GFP rabbit serum (Invitrogen) in 20 ml PBS-T). The solution was removed and several washes were done in PBS-T for 1 hour. The membrane was incubated with the secondary antibody (Anti-Rabbit IgG (H+L), HRP Conjugate, Promega) for 1 hour, again followed by several washes over the course of 2.5 hours to eliminate increased background signal. Immunoreactive bands were detected using the ECL (enhanced chemiluminescence) kit (Amersham Biosciences). X-ray films (super RX film, Fujifilm) were developed on an AGFA Curix 60 automatic developer according to the manufacturers instructions.

2.14 FRAP and FLIP experiments

Both FRAP and FLIP experiments were performed on a Leica TCS SP5 laser scanning confocal microscope at room temperature. The samples were mounted on polylysine slides. The 488 nm line of the argon laser was used for both imaging and photobleaching in combination with a 63x oil immersion objective (NA 1.4) with a scan resolution of 512x512 pixels, with a scan rate of 400 Hz. GFP

fluorescence signal was collected in the 500-530 nm range while the chlorophyll autofluorescence was detected in the 670-700 nm range. Fluorescence intensities were corrected for imaging photobleaching. The dimensions of bleaching area and the frame rates vary for different experiments.

2.15 Image pre-processing

A custom-made MATLAB function was written to correct for cell motion for the cases when polylysine-coated slides were not used. The intensity pixels are thresholded and converted to black and white image. Noise pixels were removed by deleting any pixel not connected to more than ten others. Black pixels (including the ROI) inside the cell are replaced by white. Distinct objects in the image were labelled and the object containing the ROI centre was identified as the cell of interest. The centre of mass of the identified cell is calculated. For each frame the position of the centre of mass of the cell is compared to its position at pre-bleach and the position of ROI is adjusted to compensate for cellular translational motion.

2.15.1 Correction for imaging photobleaching during FRAP

Photobleaching during the recovery phase was corrected by monitoring the loss in fluorescence intensity in a separate ROI chosen to be as far as possible from the bleached ROI. The fluorescence intensity observed for the bleached ROI at time t was then corrected by multiplying the bleached ROI intensity by the ratio of the intensity of the correction ROI before bleaching and at time t. The corrected recovery profile is therefore

$$f(t) = \hat{f}(t)\frac{c(0)}{c(t)} \tag{2.1}$$

where $\hat{f}(t)$ is the uncorrected recovery profile, $c(0)$ is the intensity of the correction ROI prior to bleaching and $c(t)$ is the intensity of the correction ROI at time t.

2.15.2 Correction for imaging photobleaching during FLIP

It is not possible to use a correction ROI within the cell to correct for photobleaching during a FLIP experiment (unless a separate in-field cell is used) because the whole cell fluorescence intensity is the measured quantity of interest and consequently photobleaching cannot be distinguished from fluorescence loss due to diffusion. Therefore the rate of photobleaching is assayed by imaging a cell without bleaching using the same acquisition rate and laser intensity as in the imaging

frames of the FLIP experiment. The observed loss in fluorescence is then used in equation (2.1) as for FRAP.

2.16 Model fitting

The FRAP experimental data for Hcf106 and autofluorescence were fitted to the Soumpasis equation (1.19). The assumptions of the model this equation is derived from does not apply to thylakoid diffusion; the fitting is used to for comparison only. The FRAP data wass also fitted to an exponential equation; again for comparison only. The FRAP experimental data on proteins in chloroplast outer membrane were fitted according to the Ellenberg model (section 1.15.2). Diffusion constants were calculated by fitting each function to the experimental data by the MATLAB nonlinear least-squares algorithm in the Curve Fitting Toolbox.

2.16.1 Extracting thylakoid network information from confocal images

Images of chloroplast autofluorescence revealing the grana as bright red patches (see Figure 2.2) were captured and processed using a custom made MATLAB software. Using Otsu's image processing method (a built-in MATLAB function), the grayscale image was thresholded and converted into foreground and background classes by maximizing the difference of variances between those classes. The black pixels represent the chloroplast. A convex hull, a polygon boundary, was computed for this set of black pixels using a standard MATLAB function (shown in red in Figure 2.3) .

A simple model of the thylakoid network was created where circles of 0.4 μm diameter represent granal features in two dimensions and stromal lamellae are represented by rectangles. Approximately a third of granas, represented by circles, are placed randomly inside the convex hull such that the separation between them is greater than a threshold (Figure 2.4a). This small batch of grana are distributed first to allow capture of the brightest spots in the image, while avoiding congestion when moving the full number of grana. Monte Carlo simulation is used to maximise the intensity inside the circles according to the Metropolis-Hastings algorithm. In detail, the grana are moved according to a random walk. A step is accepted without condition if the intensity inside the circle increases. Otherwise, if the intensity decreases the move is accepted with probability

$$P = \alpha \exp(-\Delta I/T) \tag{2.2}$$

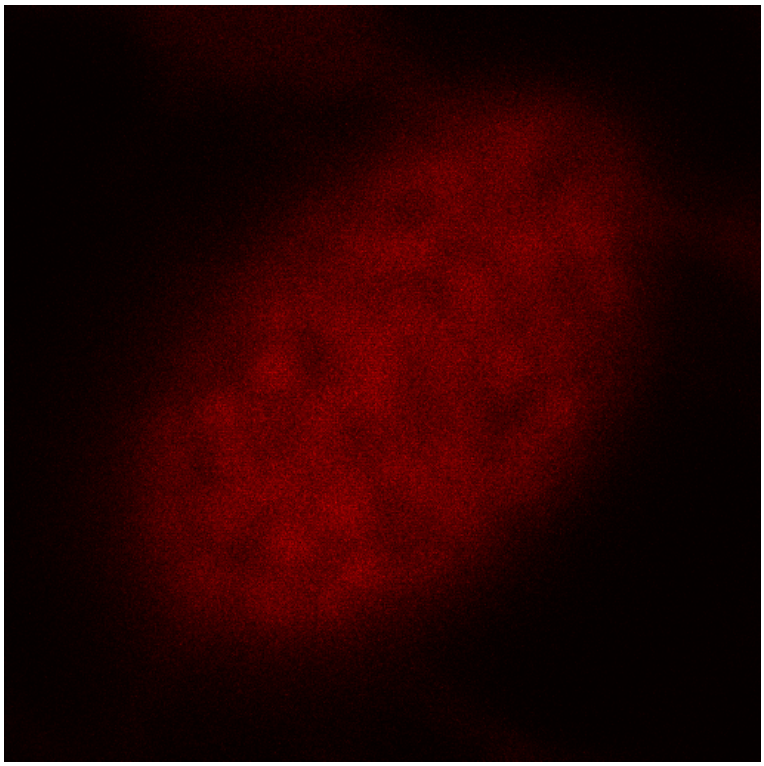

Figure 2.2: A 512x512 pixel image of chloroplast autofluorescence. Stacks of grana are visible as bright red patches. Images such as this one are used to fit the model thylakoid network by aligning model grana over the parts of the image with brightest autofluorescence.

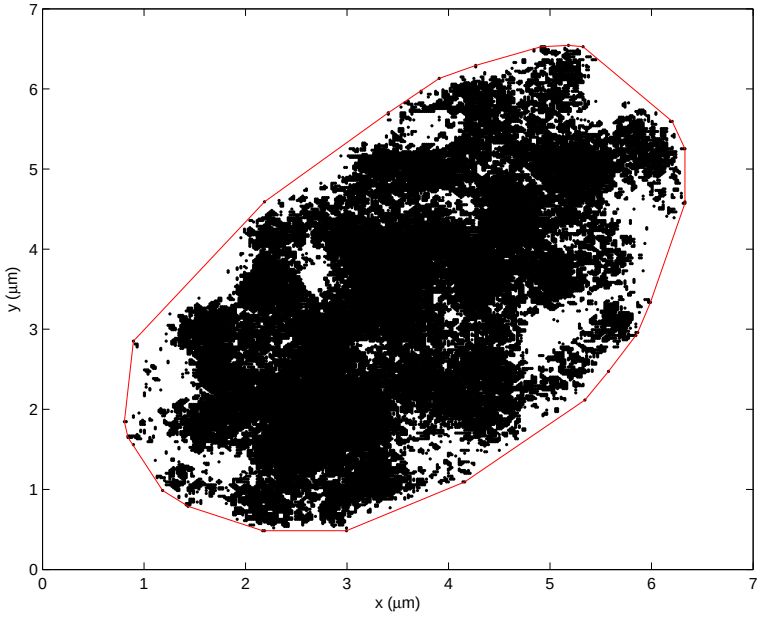

Figure 2.3: The thylakoid autofluorescence image is converted to black and white pixels using an intensity threshold obtained with Otsu's method; in the image shown the black pixels are above the threshold. The convex hull of all the black (i.e., chloroplast) pixels is computed and shown in red. The convex hull is used as a bounding region to randomly place grana in their starting positions.

where ΔI is the change in intensity, T is the mean intensity of the whole image and α is an acceptance factor. At each iteration every grana is given the chance to move. After 500 iterations grana are fixed at their positions (Figure 2.4b).

The rest of the grana are then placed within the convex hull but are not allowed to be closer to previously placed grana than a separation threshold (Figure 2.5a). In this case the threshold is less strict than previously to accommodate the larger number of grana. Using the same Monte Carlo scheme as previously the intensities within the newly placed grana are maximised after a further 9500 iterations (Figure 2.5b). The trajectory of the average of the mean intensity inside the grana during the course of the Monte Carlo simulation is shown in Figure 2.6, and is indicative of the convergence of the simulation after 10 000 iterations. The first batch of grana attain positions that maximise the mean intensity they enclose. The significant drop in mean intensity value just after the 500th iteration is due to the introduction of the second batch of grana at random and suboptimal positions. It is apparent that a 10 000 iteration Monte Carlo simulation is sufficient to place the grana over the chloroplast areas of maximal intensity.

Although it seems possible to estimate the positions of the grana from the variations of intensities it is clearly not possible to extract any information about their connectivity via lamellae. Therefore it is necessary to employ a heuristic approach. All granas are connected to their nearest neighbour. 75% of the grana are also connected with their second nearest neighbour. Also, 10% of the grana are connected to three most nearest grana (Figure 2.7). These proportions were found to produce reasonable networks.

The position and size of bleached area matches the experimental bleach ROI for each experiment and is shown in white.

2.16.2 Ensuring the network is connected

If a network is not connected, i.e., it has two disjoint parts, it is discarded and another network is generated. To check whether a network is connected, the following matrix is calculated

$$S = \sum_{i=1}^{n} A^i \tag{2.3}$$

where n is the number of grana and A is the adjacency matrix of the network. If matrix S has entirely nonzero elements then the network is connected. Otherwise it is has disjoint parts.

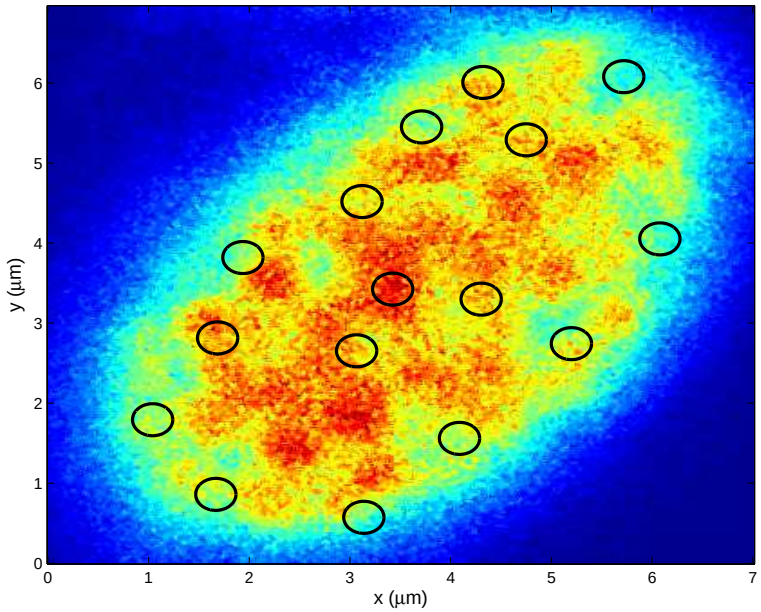

(a)

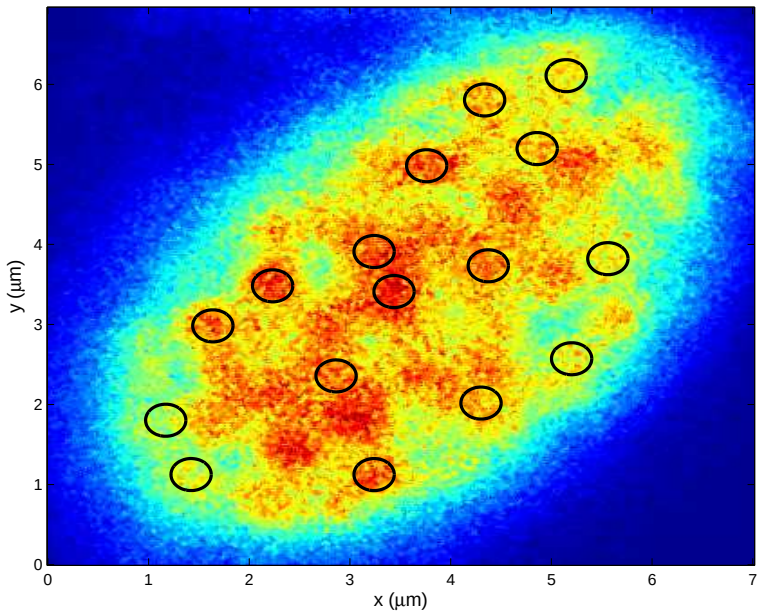

(b)

Figure 2.4: (a) The first batch of grana are assigned random positions within the convex hull, such that their mutual separation is greater than a predefined value. This results in an even spread of grana, but the grana do not fit to the image intensity at this point. (b) The final positions of the first batch of grana after 500 iterations. These grana are now fixed in these positions from this point onwards. Some of the highest intensity grana positions have been captured.

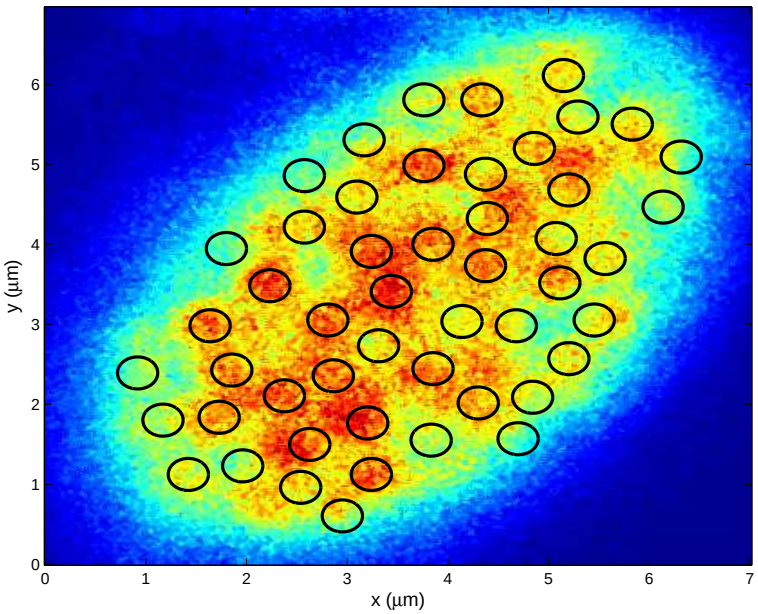

(a)

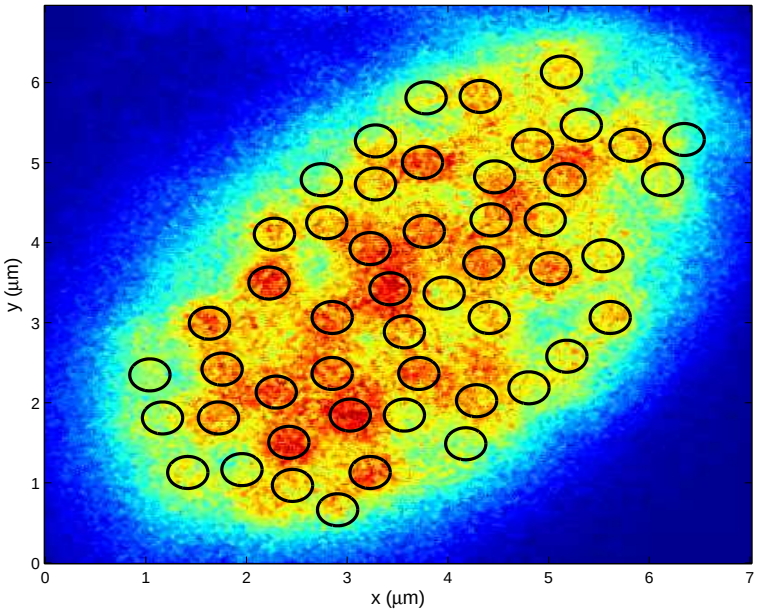

(b)

Figure 2.5: (a) The remaining grana are placed within the convex hull, avoiding previously placed grana and maintaining a less stringent mutual separation. (b) The final positions of all the grana after the 10 000th iteration. Clearly, the grana have occupied the regions corresponding to the brightest thylakoid autofluorescence.

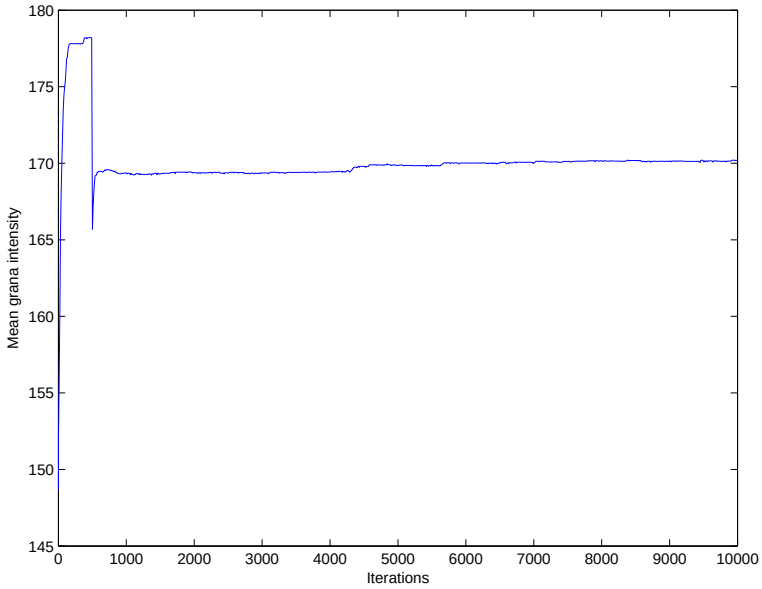

Figure 2.6: The trajectory of mean grana fluorescence during the course of the Monte Carlo simulation. The first batch is simulated for 500 iterations, after which the rest of the grana are placed, resulting in a significant drop in mean fluorescence as the placing is random and suboptimal. The trajectory provides an indication of the convergence of Monte Carlo simulation; it is clear that after 10 000 iterations the average of the mean intensity has reached a maximum.

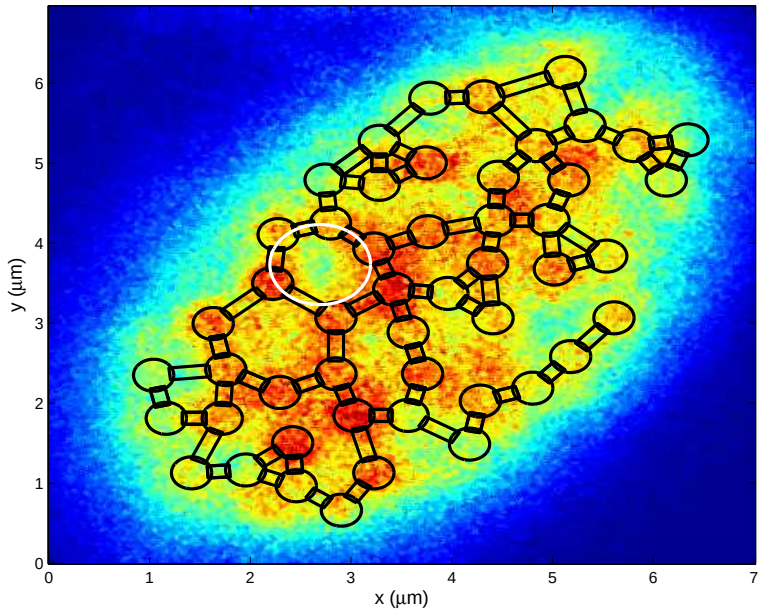

Figure 2.7: From the final grana positions a network is produced by connecting every grana to its nearest neighbour, followed by also connecting around 75% to its second nearest neighbour, and finally connecting around 10% to its third nearest neighbour. The area bleached during the experimental FRAP is shown as a white circle.

2.16.3 PSE implementation

After generating a network, the PSE simulation is setup. An n by n grid of points with interspacing h is created where h is the width of the domain divided by n. Only the particles that are inside the thylakoid network are kept. A subnetwork inside the original network is created by shrinking the original network down by a factor ϵ. Particles that are inside the large network but outside the subnetwork are identified as boundary particles. For each boundary particle, a mirror particle is created, positioned by finding the nearest edge of the network and reflected across that point. Verlet lists are then created by dividing the area into square cells and making a list of the particles that each square encloses. For each particle in each Verlet list, Euclidean distances to all the particles in its nearest neighbouring cells are calculated. The nearest neighbouring cells are defined as those immediately above, below, left and right of the current cell. The next step is to identify the particles within the bleached region and to set their strengths accordingly (see Figure 1.16.4). The resulting PSE simulation structures are stored so multiple simulations can be run on the same network.

In the simulation phase, for each timestep the sum of (1.26) is evaluated for every real particle by summing the contribution of its nearest neighbours (including nearby mirror particles) through the kernel function. This sum is then used to iterate (1.28). After all real particles have been updated the mirror particles are updated with the strength of their corresponding boundary particle. At chosen intervals an image is formed by calculating the contribution of each particle to the intensity at each pixel, weighted by the kernel function. After all the steps are completed the FRAP intensity recorded for the particles within the bleached region is normalised. The total strength of all particles before and after the simulation is monitored to ensure conservation of strength imposed by the Neumann (no-flux) boundary conditions.

2.16.4 Method validation

In all the simulations presented in this thesis $n = 250$. Simulations proceeded for as long as the corresponding experimental data. Initial strength was arbitrarily set to 1; since the resulting FRAP is normalised, this has no effect. The timestep was $\delta t \leq 0.1h^2/4D$.

In order to validate the implementation of the PSE scheme, FRAP experiments were simulated on a uniform plane using a bleaching circular region of $0.5\,\mu$m radius and a range of diffusion coefficients for 0.1, 0.01 and $0.001\,\mu\text{m}^2/\text{s}$. The Soumpasis model with the appropriate diffusion coefficient is in close agreement with the PSE simulations proving that the PSE approach does indeed simulate

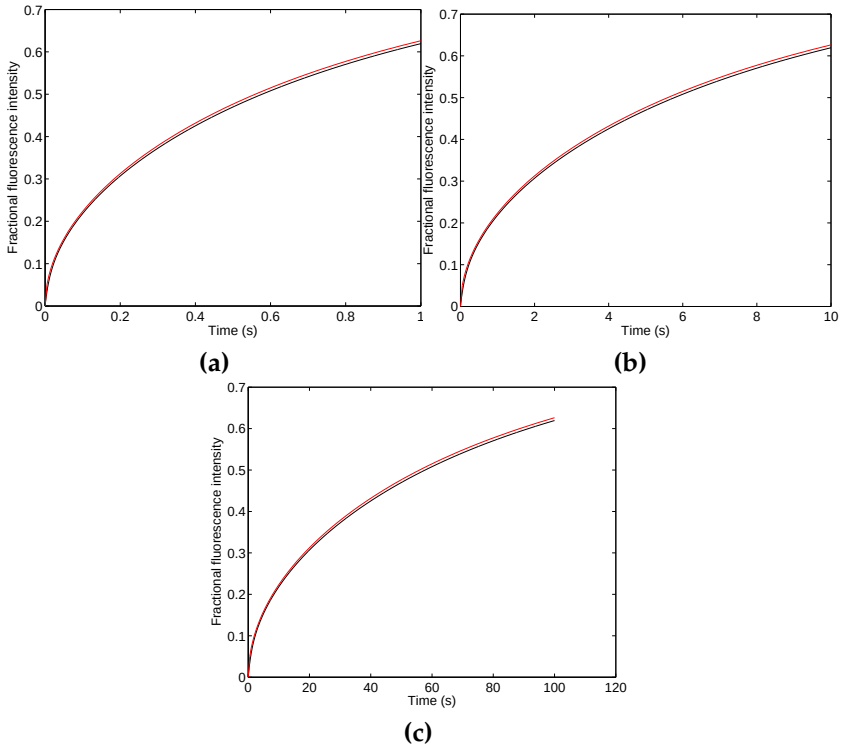

Figure 2.8: The PSE scheme was validated by applying it to simulate diffusion on a uniform plane for three different diffusion coefficients. The PSE simulated result is shown in black whereas the red line shows the Soumpasis fitted model for the corresponding diffusion and a bleaching circular region of 0.5 μm radius a) Diffusion of 0.1 $\mu m^2/s$, b) diffusion of 0.01 $\mu m^2/s$ and c) diffusion of 0.001 $\mu m^2/s$. The close agreement between the theoretical curve and the simulation at each value for D provides evidence that the PSE scheme and implementation correctly simulates FRAP diffusion.

the FRAP experimental setup. The PSE results were plotted together with the theoretical fit as described in Soumpasis et al. [87] and shown in Figure 2.8.

3

Studying the mobility of thylakoid proteins using FRAP and FLIP

3.1 Introduction

The characterisation of a protein's mobility yields information about its functional role as well as providing insight into the protein's host environment inside the cell. There is very limited information on how non-photosynthetic proteins diffuse inside chloroplast membrane compartments. We have studied the mobility of a thylakoid membrane protein, Hcf106, a core component of the plant Tat protein translocase in plants which localises in the non-appressed stromal thylakoids [68,96], by means of FRAP and FLIP on the GFP fluorescence from a Hcf106-GFP fusion introduced by transient expression. We have also studied the mobility of the chlorophyll-containing complexes (PSII, LHCII and PSI) by using FRAP on the autofluorescence.

3.2 Mobility of photosynthetic proteins in chloroplasts

The diffusion of proteins in chloroplast thylakoid membranes is believed to be important for processes including light harvesting and photodamaged-PSII repair cycle [97]. There are only a few studies that have analysed the mobility of thylakoid proteins and those studies have focused on the mobility of the light-harvesting complex of PSII, LHCII. Consoli and colleagues investigated the mobility of LHCII in thylakoid membranes from *Spinacia oleracea*. Phosphorylated LHCII molecules were labelled with a 0.8 μm diameter microsphere using anti-phosphothreonine and nonphosphorylated LHCII were similarly labeled with a polyclonal antibody specific to the stroma-exposed loop of LHCII. According to the authors it is probable that only LHCII particles in the most superficial grana margins and in the top stroma lamellae were labelled due to steric hindrance. Both non-phosphorylated (LHCII) and phosphorylated (P-LHCII) conformations were found to exhibit average diffusion of 8.4×10^{-3} $\mu m^2/s$ and 2.7×10^{-2} $\mu m^2/s$ respectively in fairly restricted corrals with only few complexes exploring larger domains of the membrane [98].

Kirchhoff and colleagues established a novel fluorescence recovery after photobleaching method for studying the mobility of LHCII. Conducting FRAP experiments on isolated grana membranes from *Spinacia oleracea* fused to PC lipid bilayers labeled with BODIPY FL-C12 revealed that around 73±3% of LHCII is immobile within an observation period of 9 minutes and the remaining fraction was assessed as highly mobile, able to escape from grana within a few seconds undergoing diffusion of 4.6×10^{-3} $\mu m^2/s$ [99].

Goral and colleagues found the majority of chlorophyll proteins to be immobile in the grana of wild type spinach (*Spinacia oleracea L.*) and *Arabidopsis*

chloroplasts over the period of 10 minutes. However approximately 15% of chlorophyll molecules were found to be able to exchange between grana and stromal membranes in the presence of certain kinase molecules which are responsible for phosphorylation of PSII core proteins and light-harvesting complexes [97].

3.3 Hcf106 and autofluorescence FRAP studies

In order to investigate the mobility characteristics of the chloroplast thylakoid protein Hcf106, tobacco protoplasts were transfected with a construct encoding for GFP-tagged *Arabidopsis thaliana* Hcf106. Figure 3.1 shows a tobacco protoplast expressing Hcf106-GFP. The image was captured 18 hours post transfection. The red panel shows the autofluorescence from thylakoid pigments, which serves as a chloroplast marker, and the green panel shows the presence of GFP tagged proteins within the chloroplasts. The image confirms that Hcf106-GFP was efficiently targeted to the chloroplasts. Chloroplasts were subsequently isolated from transfected protoplasts. Figure 3.2 shows a mixed population of transfected and non-transfected chloroplasts, and it is clear that the transfected population exhibit a far higher level of green fluorescence than the non-transfected chloroplasts do. The green background fluorescence could be associated with multi-photon excitation artifacts [100] or with emission of light from excited chlorophyll in range similar to excited GFP emission spectrum. A higher magnification, line-averaged image of single chloroplast is shown in Figure 3.3. The autofluorescence exhibits a punctuated pattern compatible with the granal thylakoid network configuration while the GFP fluorescence forms a web-like pattern resembling the stroma lamellae structural features. The merged image confirms that the GFP and autofluorescence signals do not overlap.

The lateral mobility of the membrane protein Hcf106 and the autofluorescence was studied by means of fluorescence recovery after photobleaching (FRAP). In this technique, a region of fluorescence is irreversibly bleached using the confocal laser and the recovery of fluorescence in the region, signifying diffusion of neighbouring molecules, is monitored. Photobleaching during recovery is corrected as described in section 2.15.1. Figure 3.4 includes images from key stages of a FRAP experiment of a chloroplast expressing Hcf106-GFP. The first column of the panel shows the green and red images captured immediately before bleaching along with the merged image. The second column consists of images taken just after bleaching and the third column includes images acquired at the end of experiment. Neither the green GFP fluorescence nor the red autofluorescence seem to recover within the bleached region during the experimental time course.

The FRAP experiments from 12 chloroplasts with Hcf106-GFP were analysed

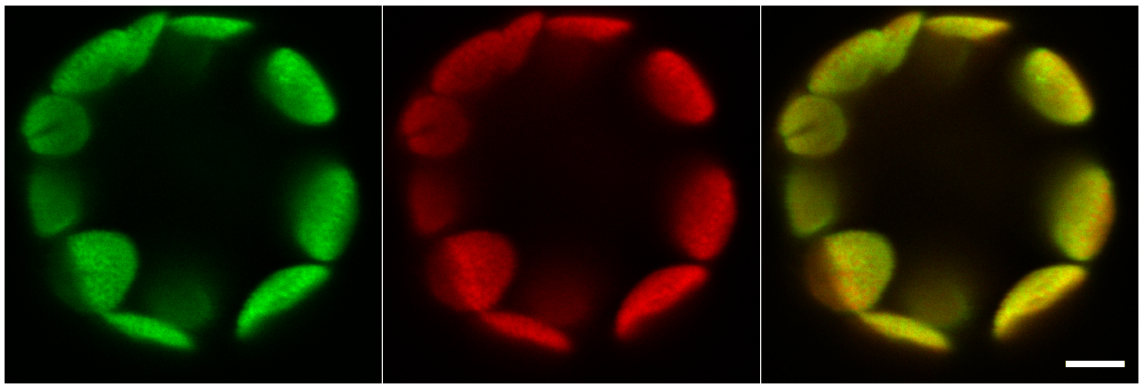

Figure 3.1: Hcf106-GFP localises in stromal lamellae within the thylakoid membranes of transfected tobacco protoplasts. Tobacco leaf protoplasts were transfected with a plasmid encoding for Hcf06-GFP fusion. Protoplasts were analysed by confocal microscopy 18 hours post transfection. The 488 nm line of the argon laser was used to excite the fluorescent population and emission was monitored in the 500-530 nm range for GFP detection and 650-700 nm range for detection of thylakoid autofluorescence. Scale bar 5 μm.

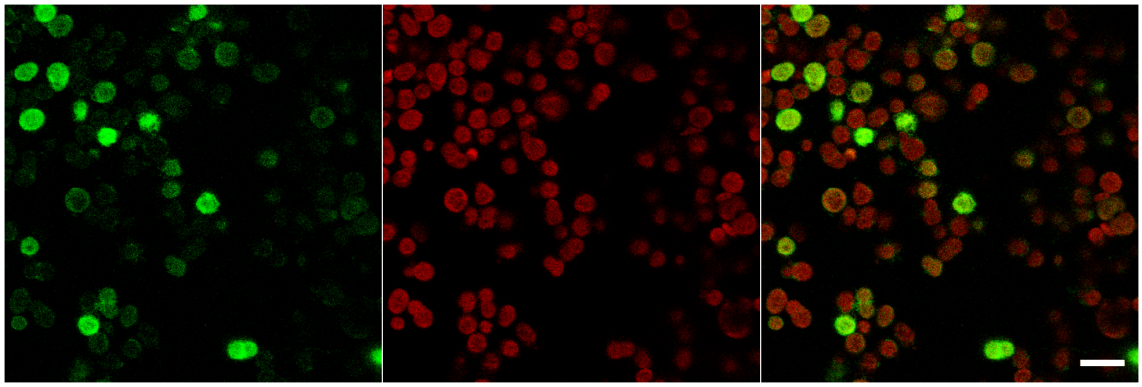

Figure 3.2: A mixed population of chloroplasts isolated from transfected and non-transfected protoplasts from a transient transfection of tobacco protoplasts with Hcf106-GFP expressing construct. The chloroplasts with Hcf106-GFP exhibit significantly higher green fluorescence than the chloroplasts from non-transfected protoplasts. The background green in WT chloroplasts is due to emission from excited chlorophyll or multiple photon excitation artifacts. Scale bar 20 μm.

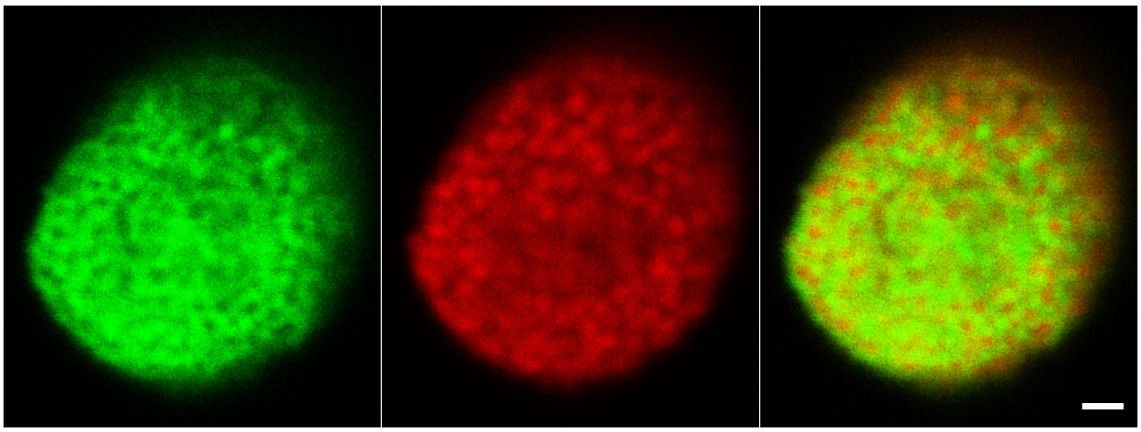

Figure 3.3: A higher resolution image of a single chloroplast using 16 line averaging. The autofluorescence exhibits a punctuated pattern reflecting the grana network and shape. GFP fluorescence shows a rod-like pattern and appears to originate primarily from regions where the autofluorescence is absent confirming that Hcf106-GFP localises in the stroma lamellae. Scale bar 1 μm.

and their average fractional recovery profiles for the green and red channels were plotted against time. On average, the fluorescence due to GFP recovered by 11.3±2% of its pre-bleach intensity. A similar behaviour is exhibited by the chlorophyll fluorescence which recovers only by 11.1±1% when compared to its original intensity within the 19 seconds of observation. FRAP experiments with longer observational time were also carried out. For the longer FRAP setup, the GFP fluorescence recovered by 19.4±2% of its pre-bleach intensity value on average whereas the chlorophyll fluorescence recovered by 17.6±4% of its original intensity within 262 seconds of observation.

Student's t-test was used to assess whether the mean recovery of Hcf106-GFP and autofluorescence recover to statistically significantly different values. For the 12 short FRAPs the t-test fails to reject the null hypothesis that the mean recoveries are the same ($p > 0.5$). For the 7 longer FRAPs the null hypothesis that the mean recoveries are the same is also not rejected ($p > 0.5$). Therefore, the data does not support the conclusion that Hcf106-GFP recovers more or less than autofluorescence.

3.4 FLIP experiments on Hcf106 and controls

In light of the results from the FRAP experiments, Fluorescence Loss in Photobleaching (FLIP) was employed to confirm and complement the experimental findings from the FRAP studies. FLIP can yield information on how accessible the region being bleached is to other areas of the organelle. Failure to deplete the whole organelle's fluorescently tagged population indicates that the region of in-

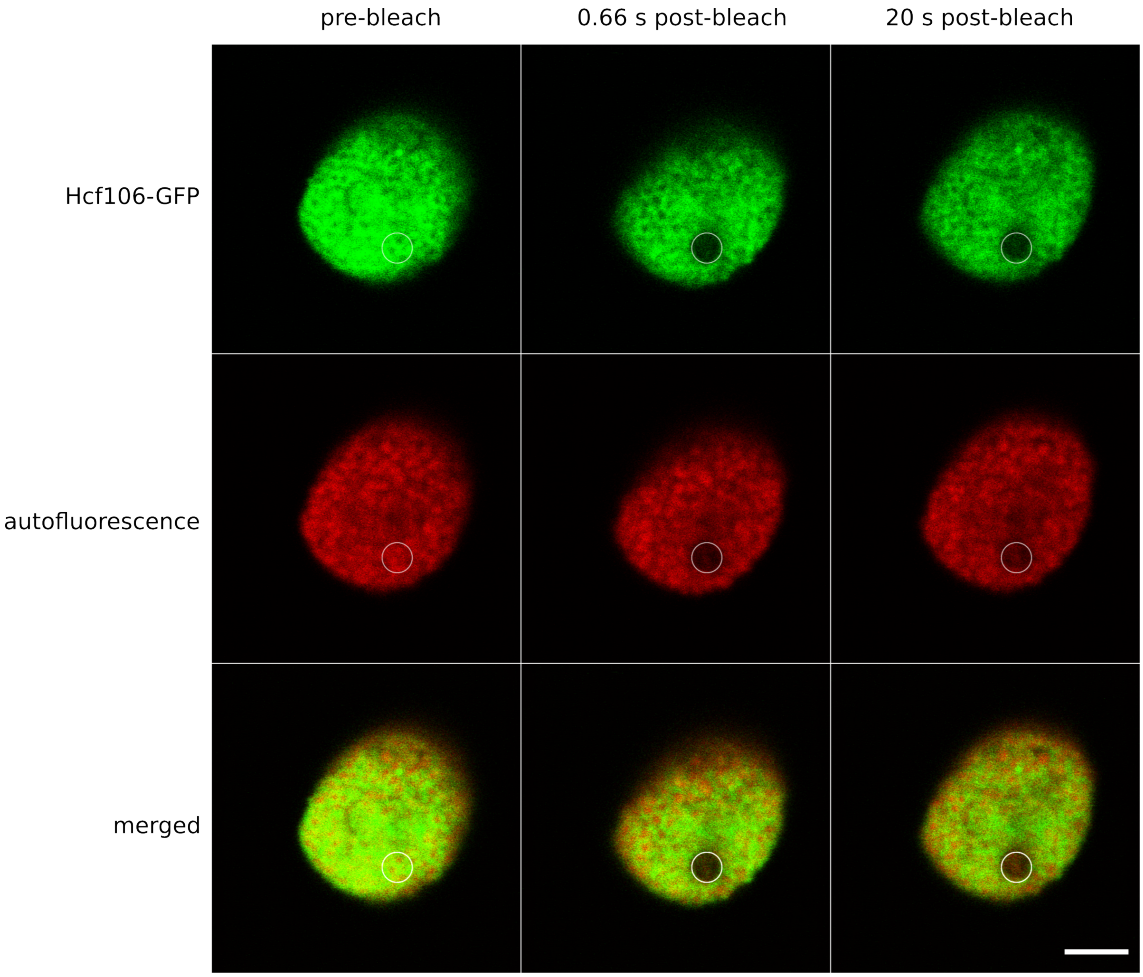

Figure 3.4: An example of images acquired during a FRAP experiment on an isolated chloroplast from a protoplast expressing Hcf106-GFP. The images in the first column show the pre-bleach stage, the second column the first post-bleach frame and the third column the last post-bleach frame of the experiment. The bleached region is marked by the white circle and is 1 μm diameter. Within the 20 seconds of the experiment the Hcf106-GFP fluorescence and red autofluorescence fail to recover within the bleached region. Scale bar 2 μm.

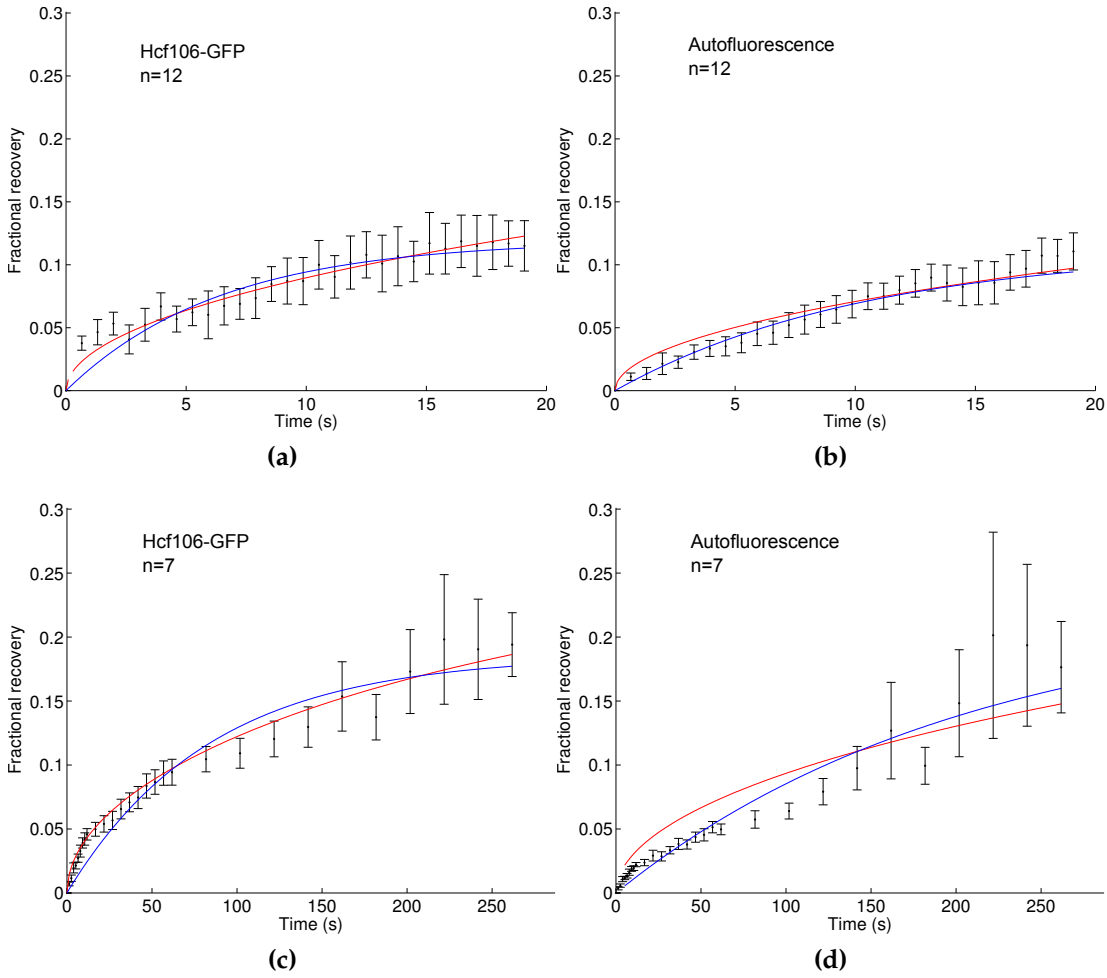

Figure 3.5: The average recovery profiles from chloroplast experiments for the green and red channels are plotted as fractional recovery against time, and fitted against the Soumpasis model (red line) and an exponential (blue line). a) During 12 short FRAP experiments, the green fluorescence due to GFP-tagged Hcf106 molecules recovers only to 11.3±2% of its pre-bleach intensity on average within 19 seconds of observation. b) During the same 12 short FRAP experiments, the autofluorescence behaviour is monitored using a second channel. The chlorophyll fluorescence recovers only by 11.1±1% within the bleached. c) FRAP experiments were also performed at longer time scales. Specifically, the recovery after photobleaching within 7 chloroplasts was monitored for more than 4 minutes. The GFP fluorescence was found to recover by 19.4±2% of its pre-bleach intensity value on average. d) The chlorophyll fluorescence recovered by 17.6±4% of its original intensity within the 262 seconds of observation. Error bars show standard errors.

terest is isolated and therefore fluorescently tagged molecules cannot redistribute. Photobleaching due to imaging is corrected as described in section 2.15.2.

The results from 8 FLIP experiments on chloroplasts with Hcf106-GFP along with three control experiments are summarised in Figure 3.7. The first control, pre-mGFP5, has the presequence of the 23-kDa oxygen-evolving complex subunit which is synthesized in cytosol as a 33-kDa precursor protein with a N-terminal tandem of signalling sequences, the first for targeting to the chloroplast and the second for recognition by the TAT translocon and targeting to the thylakoid lumen. The presequence is linked to mGFP5 via a 13 amino acids linker from cytochrome b6. The second control, pre-ΔTPP-mGFP5, is a construct with the terminal residue of the presequence (Ala 73) deleted. Since the lumen peptidase TPP cleaves after the A-D-A motif, removing the A blocks processing of the protein and results in the accumulation of an intermediate-size protein that is tightly associated with the thylakoid membrane and largely resistant to proteolysis [101]. The final construct, TP-mGFP5, has the transit peptide for chloroplast targeting but lacks the thylakoid targeting signal therefore, once it enters the chloroplasts it is processed into pure mGFP5 diffusing in the stroma. All four constructs were made in pDHA vector. For the FLIP experiments, using the bidirectional microscope mode, a circular region of interest of 0.4 μm diameter was repeatedly bleached for 50 frames at 0.754 s frame separation while an image of the whole organelle was captured after every bleaching frame to measure the total fluorescence intensity. After correcting for observational photobleaching the total fluorescence intensities were on average as follows: After 37 seconds, the total fluorescence on average for Hcf106-GFP decreased to 91±2% ($n = 5$), for pre-ΔTPP-mGFP5 decreased by 85±2% ($n = 5$), for pre-mGFP5 82±3% ($n = 5$) and for TP-GFP by 56±1% ($n = 5$), where the variations given are standard errors. Analysis of variance (ANOVA) shows that the mean fluorescence decreases from each sample group are not equal ($p < 0.0001$, see table 3.1). Furthermore, multiple pairwise comparison indicates that the mean fluorescence decrease of the TP-GFP sample is significantly more than those of the other three samples ($p < 0.001$), as can clearly be seen in the box plot in Figure 3.6.

Since Hcf106 experiments were performed using a 1 μm diameter circular bleaching ROI, FLIP experiments were also repeated using a bleaching region of the same size for consistency and comparable results. The results are summarised in Figure 3.8.

In summary, the FLIP experiments suggest a pronounced constraint on the movement of Hcf106 protein throughout the chloroplast, consistent with the failure of photobleached thylakoid areas to recover during the FRAP experiments.

Source of variation	d.f.	Sum of squares	Mean square	F	p-value
Samples	3	0.3526	0.1175	18.94	1.6258×10^{-5}
Residual	16	0.0993	0.0062		
Total	19	0.4518			

Table 3.1: One-way analysis of variance (ANOVA) of FLIP samples of TP-GFP, Hcf106-GFP, pre-ΔTPP-mGFP5 and pre-mGFP5. Probability of obtaining the listed F-statistic is extremely small assuming the mean fluorescence loss of each sample is equal. Therefore, we conclude significant differences (see text for details).

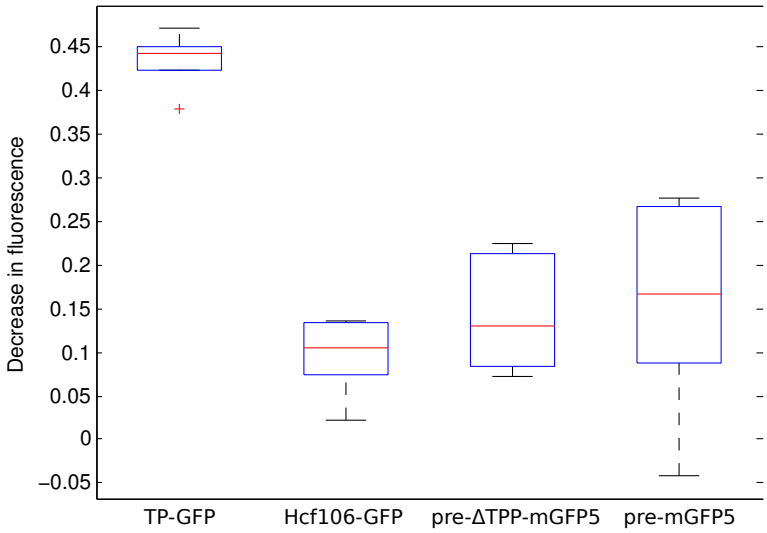

Figure 3.6: Box plot of fluorescence loss in FLIP experiments. The fluorescence loss for Hcf106-GFP, pre-ΔTPP-mGFP5 and pre-mGFP5 is significantly lower than for TP-GFP ($p < 0.001$, see text). The red line is the median and the box is the 95% confidence interval about the mean. The whiskers show the range of the data, excluding the outliers shown as red pluses.

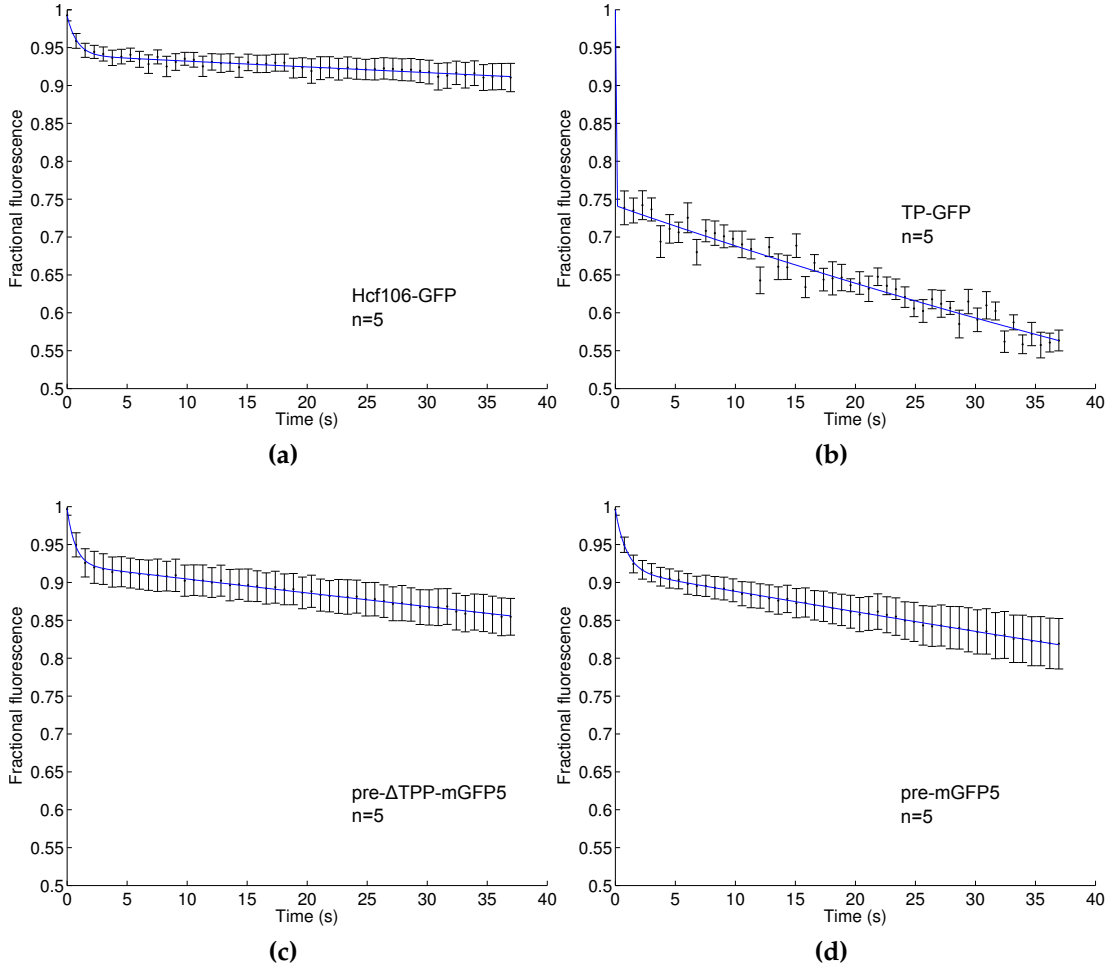

Figure 3.7: FLIP fractional fluorescence profiles of Hcf106 and controls, fitted to a double exponential decay curve (blue line). After 37 seconds the total fluorescence on average decreased to a) 91%±2 for Hcf106-GFP (n = 5), b) 56%±1 for TP-GFP (n = 5), c) 85%±2 for pre-ΔTPP-mGFP5 (n = 5) and d) 82%±3 for pre-mGFP5 (n = 5). The bleaching region was circular with diameter 0.4 μm. Error bars show standard errors.

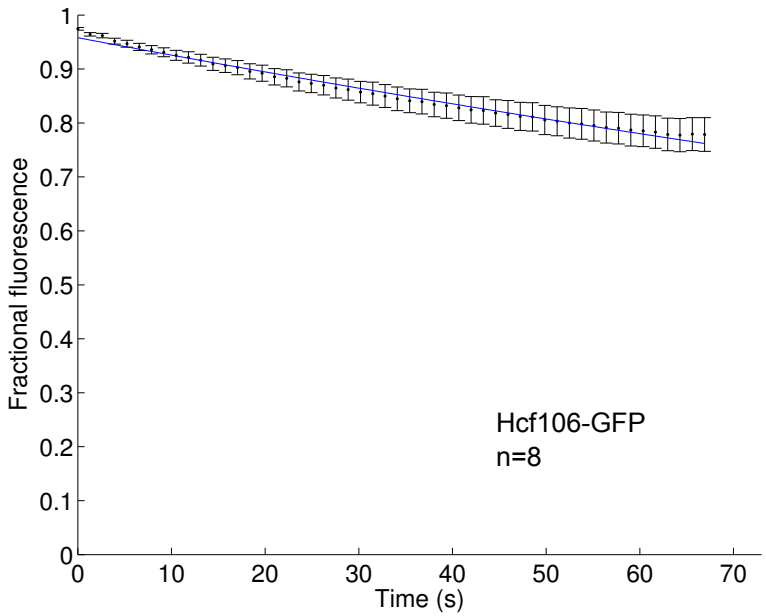

Figure 3.8: The average loss of fluorescence intensity as shown from 8 FLIP experiments on chloroplasts with Hcf106-GFP, fitted to a double exponential decay curve (blue line). A 1 μm diameter circular bleaching region was used. Within the 70 seconds of the experiment the fluorescence intensity is depleted by only 20%. Error bars show standard errors.

3.5 Summary

In this chapter, the lateral diffusion of the thylakoid membrane protein Hcf06 as well as the mobility of chlorophyll-containing complexes contributing to the endogenous autofluorescence, have been investigated by means of two complementary photobleaching methods. FRAP studies revealed that plant-TAT translocon component Hcf106 exhibits surprisingly slow lateral diffusion similar to that of the endogenous autofluorescence. FLIP experiments confirmed the observations from the FRAP experiments as the total fluorescence of the organelle did not reduce significantly with the passage of time. Additionally, the results from the FLIP experiments may hint towards the possibility of a highly compartmentalised thylakoid membrane.

4

Investigating the behavior of thylakoid membrane proteins using PSE simulations

4.1 Introduction

The lateral mobility of components of biological membranes is important for many cellular processes. The results from photobleaching experiments on the thylakoid membrane protein Hcf106 and autofluorescence were presented in the previous chapter. Although FRAP and FLIP can give qualitative information on how proteins diffuse inside the thylakoid network [102], these membranes do present difficulties for obtaining quantitative information by FRAP. In general, a theoretical model of the FRAP experiment is required to extract quantitative results such as the diffusion coefficient of the fluorescently-tagged protein and asymptotic recovery levels. Key to the model is a solution of the diffusion equation (see section 1.14) over the domain accessible to the protein. Analytically solvable models, such as the Soumpasis model or Ellenberg model (described in section 1.15), require a predictable membrane geometry, e.g. planar or spherical, and membrane uniformity over the area of the measurement [103]. Therefore, when applying FRAP techniques to extract quantitative information about diffusive characteristics of proteins, it is absolutely crucial to take into consideration the actual domain of diffusion. For a complex membrane, such as the endoplasmic reticulum (ER) or the thylakoid, the assumptions of the analytical models are clearly not satisfied, and their predictions cannot be trusted.

To make quantitative FRAP measurements on complex membranes, the diffusion equation must generally be solved numerically on the particular domain, which is often highly specific to the individual cell and individual measurement. Where the domain can be observed and reconstructed, such as the ER membrane, a numerical solution is possible [104]. However, producing a three-dimensional model of the thylakoid membrane in order to simulate diffusion of the protein on a known geometry is not possible. The heterogeneity and complex nature of the thylakoid membrane, the diffraction limit of the illuminating laser and the limited axial resolution of the confocal microscope impose limitations which prevent three-dimensional membrane reconstruction. Consequently, quantitative analysis of FRAP experiments on the thylakoid membranes of higher plants presents a considerable challenge. In an attempt to quantitatively analyse the FRAP experiments measuring the diffusive behavior of proteins in thylakoid membranes presented in Chapter 3, the Particle Strength Exchange method of solving the diffusion equation on complex domains is employed. This method is capable of handling surfaces of high curvature and complex shape, which are often encountered in biology, and allows estimation of geometry-corrected molecular diffusion constants.

4.2 Previous computational studies of protein diffusion in thylakoid membranes

Grana of thylakoid membranes are very crowded membrane environments with around 80% of their area occupied by protein molecules. The majority of PSII and its light harvesting complex II (LHCII) exist in appressed membrane domains of the thylakoid network and are found densely packed in semi-crystalline arrangement. However, phosphorylated LHCII are able to dissociate form PSII and diffuse from grana to stroma-exposed thylakoids. This is believed to be of functional importance for balancing the excitation energy and protection against photodestruction of PSII [105].

Various studies have attempted to explain the lateral migration of LHCII from grana to stoma-exposed thylakoids by using numerical simulations. Drepper and colleagues induced phosphorylation of light-harvesting chlorophyll a/b protein complex LHCII of photosystem II at 0 °C under illumination. Increasing the temperature to 20 °C, phosphorylated LHCII diffused from appressed grana to nonappressed membrane regions. The redistribution of phosphorylated molecules was followed by a rapid detergent fractionation of the two membrane areas. The long-range diffusion of phosphorylated LHCII was investigated by means of Monte Carlo simulations by incorporating all protein components of thylakoid as mobile particles to compensate for steric hindrance due to the archipelago effect [106]. The dimensions of the integral complexes, their density in appressed and non-appressed regions and their relative mobility was taken into account to build a realistic model of the thylakoid membrane. According to the Monte Carlo scheme followed, at each iteration complexes were moved by 1 nm steps corresponding approximately to the distance between lipid molecules in the membrane. Each molecule moves in one of six randomly selected directions spaced at 60 degrees intervals. Hard-sphere collisions were introduced, i.e. when a molecule ended up at a position occupied by some other molecule, its motion changed in the direction of the angle of a hard-sphere reflection until it had covered distance of 1 nm. Fitting the Monte Carlo simulations to experimental data suggested that the diffusion constant of phosphorylated-LHCII is around 2×10^{-4}–4×10^{-4} $\mu m^2/s$ suggesting that they are highly restricted in the appressed thylakoid membrane [105].

More recently, Kirchhoff and colleagues, used a computational method for estimating the diffusion coefficient of LHCII from FRAP experiments on isolated grana patches. One-dimensional fluorescence profiles were extracted from each image in the direction perpendicular to the line bleach by summing fluorescence across the membrane patch. To compare fluorescence distributions before and after the bleach, the profiles were normalized to the same total fluorescence. The

postbleach profiles were subsequently subtracted from the prebleach profile, and the mobile fraction was estimated by comparing the postbleach profiles. An iterative computer routine was used to predict the fluorescence evolution due to random diffusion for a set of arbitrary diffusion coefficients. To obtain an estimate for the actual diffusion coefficient the predicted recovery curves were fitted to the experimental data and coefficient giving the best fit was accepted. The results from this study suggest that 73±3% of LHCII is immobile with the remaining fraction undergoing diffusion of 4.6×10^{-3} $\mu m^2/s$ [107].

4.3 Previous applications of PSE

In order to estimate the influence of complex organelle geometry on FRAP measurements, Sbalzarini et al. used the Particle Strength Exchange method to study the mobility of the soluble, fluorescent protein ssGFP-KDEL in the Endoplasmic Reticulum (ER) lumen of VERO cells. GFP is synthesised with an N-terminal cleavable signal sequence responsible for efficient ER targeting and a C-terminal sequence Lys-Asp-Glu-Leu (KDEL) which is responsible for retention of the protein within the ER lumen [108]. Using GFP-KDEL as a marker, before each FRAP experiment, 50 0.1 μm serial confocal sections were collected at 0.8 μm/pixel resolution. These z-stacks were used to reconstruct a 3D gray level iso-surface in space using Imaris3 image analysis software. FRAP experiments were conducted on the same domain and the reconstructed volume of the ER lumen was used as the computational domain for the PSE simulations. The experimental curves were then compared to the simulated data and the molecular diffusion constant for GFP-KDEL was estimated to be 34 ± 0.95 $\mu m^2/s$ on average. Ignoring the effect of organelle shape, the molecular diffusion coefficient is underestimated by a factor of 1.8 to 4.2. The estimated diffusion coefficient of GFP-KDEL is at least 2.5 times slower when compared to the diffusion of pure GFP in water at room temperature suggesting that ER lumen is a viscous compartment [104].

The PSE method was also employed to provide quantitative information on the diffusion of proteins in the ER membrane using the transmembrane protein tsO45-VSV-G (temperature sensitive vesicular stomatitis virus glycoprotein), C-terminally tagged with green fluorescent protein. Using FRAP models derived for planar membranes, such as Soumpasis et al. model [87] would not be appropriate as these yield inaccurate molecular diffusion constants if applied to curved, complex membranes. After being compared to FRAP experimental recovery curves, the PSE simulations yield a molecular diffusion coefficient of 0.16 ± 0.07 $\mu m^2/s$, more than two times lower than the previously published diffusion coefficient of 0.45 ± 0.03 $\mu m^2/s$ which did not take into account the membrane geometrical

shape. As expected, the simulations confirmed that the diffusion behavior of molecules in the ER membrane is significantly slower (recovery half time differs by 4) compared to the diffusion of soluble molecules in the lumen of the same ER domain even if the molecular diffusion constants are identical [109].

4.4 PSE FRAP on thylakoid membranes

Due to the limitations of confocal microscopy, it is not possible to three-dimensionally reconstruct the thylakoid membrane. Therefore, to perform numerical simulations it is necessary to provide a model structure for the thylakoid to serve as the diffusion domain. It is known that PSII and LHCII are highly concentrated within grana. Moreover, the autofluorescence in chloroplast images (e.g., Figure 2.2) is localised in circular regions. As PSII and LHCII are autofluorescent, this leads to the conclusion that the bright circular regions are grana. Therefore, it seems reasonable that a procedure to select these regions and extract their positions will provide an approximate top-down view of the thylakoid network. Unfortunately, it is not as clear for the stromal lamellae connecting sections and some abstraction needs to be made. To avoid subjective bias, a model thylakoid network was computationally generated for nine FRAP experiments performed on chloroplasts containing Hcf106-GFP, consisting of circles representing grana and rectangles representing stromal lamellae, using the Monte Carlo procedure described in section 2.16.1.

The Monte Carlo approach to fitting thylakoid network models appears to be accurate in capturing the peak intensities of autofluorescence confocal images. The networks include 40 to 60 granas spanning the whole chloroplast area and are shown in Figure 4.1, for the nine FRAP experiments A through I. Although the bleaching region is shown as a sharp circle in reality bleaching spreads out in an approximately Gaussian fashion, and this is simulated in the PSE scheme. The bleaching region was chosen to be relatively small compared to the organelle's size. Choosing a large bleaching region could bias the recovery profiles due to depletion of a significant proportion of the fluorescent population. However for smaller bleaching regions the area underneath is more variable which could potentially impair the observed recovery i.e. bleaching over whole granas or edges of lamellaes can result in different recovery profiles.

4.4.1 PSE for Hcf106 data

For each experimental dataset, an optimisation algorithm is employed to find the best fitting diffusion coefficient D. For each iteration of the algorithm, a simulation

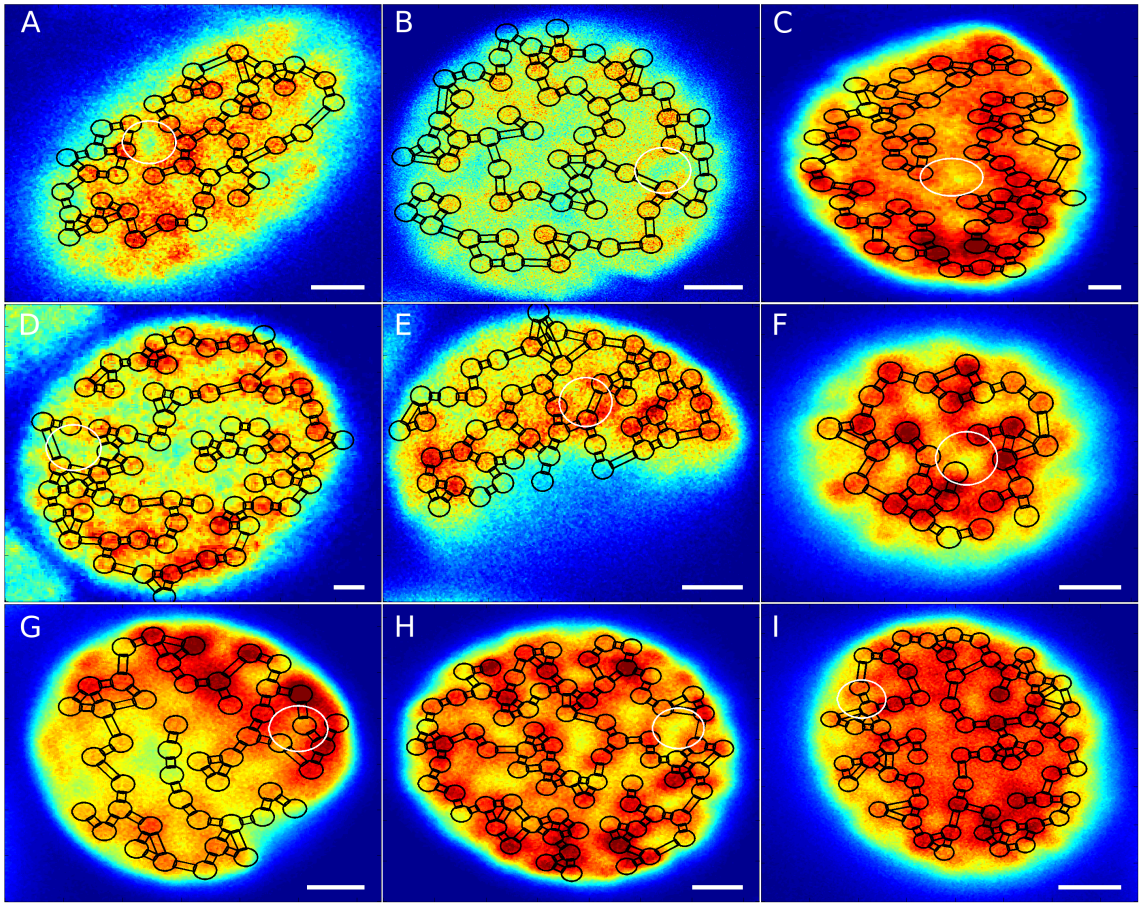

Figure 4.1: The model thylakoid networks fitted by the Monte Carlo simulation for the nine different chloroplasts (A to I) subjected to FRAP, overlaid on the images used to fit them (false colour scale, red is high intensity; blue is low). It is evident that the Monte Carlo fitting procedure successfully maximised the fluorescence intensity enclosed by the network. However in some images, e.g. B and E, some grana have clearly been marginalised by the minimum separation rule imposed during fitting. The regions bleached in the experiments are shown as white circles with diameter 1 μm. Scale bars 1 μm.

is run and the sum of square residuals is computed. The objective of the algorithm is to minimise this sum.

For the first set of simulations a uniform diffusion was assumed i.e. diffusion can occur throughout the network at a constant rate. The majority of experimental data seem to undergo diffusion at two time scales, recovering very fast at the beginning and much slower for the rest of the experiment. However, experiments C, D, and H, seem to fit the uniform diffusion very well giving the least sum of squares residuals (Figure 4.2), and predicting for the diffusion constant $0.015\,\mu m^2/s$, $0.042\,\mu m^2/s$ and $0.0059\,\mu m^2/s$, respectively. That could be due to the fact, in those cases, that the bleaching does not cover a substantial membrane area. Only a small fraction of fluorescence is bleached, for which recovery fits a single diffusion coefficient.

The second set of simulations involves diffusion that is restricted to stroma-exposed lamellae, and is motivated by the biological evidence that membrane protein Hcf106 localises in stroma-exposed membranes. Experiments C and F appear to fit this scenario well as only a very small part of stroma-exposed lamellae is bleached. Experiment G also fits well this scenario. In this case two stroma-exposed membranes are totally bleached and the other two are bleached very marginally (Figure 4.4).

The third and fourth set of simulations were 'ratio 10' and 'ratio 100'. In these cases diffusion in grana is set to be 10 and 100 times slower, respectively, than diffusion in stroma-exposed lamellae. This scenario was based on the repeatedly reported observations that proteins diffuse slower in grana but are able to escape and diffuse faster in stromal lamellae. For most of the experiments, a ratio of diffusion coefficients appears to fit better compared to the uniform case judging from sum of square residuals. This lends support to the hypothesis that when a mixed area of grana and stroma lamellae is bleached, molecules diffuse fast in stroma-exposed lamellae but slower in the grana areas. There is no significant difference when comparing ratio 10 (Figure 4.6) to ratio 100 results (Figure 4.7). However, the fitted diffusion coefficients differ considerably; $0.082\,\mu m^2/s$ and $0.60\,\mu m^2/s$, respectively, for the stromal lamellae rate. It is quite plausible that simulations of much bigger ratios of diffusion could fit the experimental much better. Ideally a two dimensional optimisation should be employed where the diffusion coefficients for grana and stroma lamellae are fitted independently. However, multidimensional optimisation generally requires more objective function evaluations (simulations in this case), and would take considerably longer.

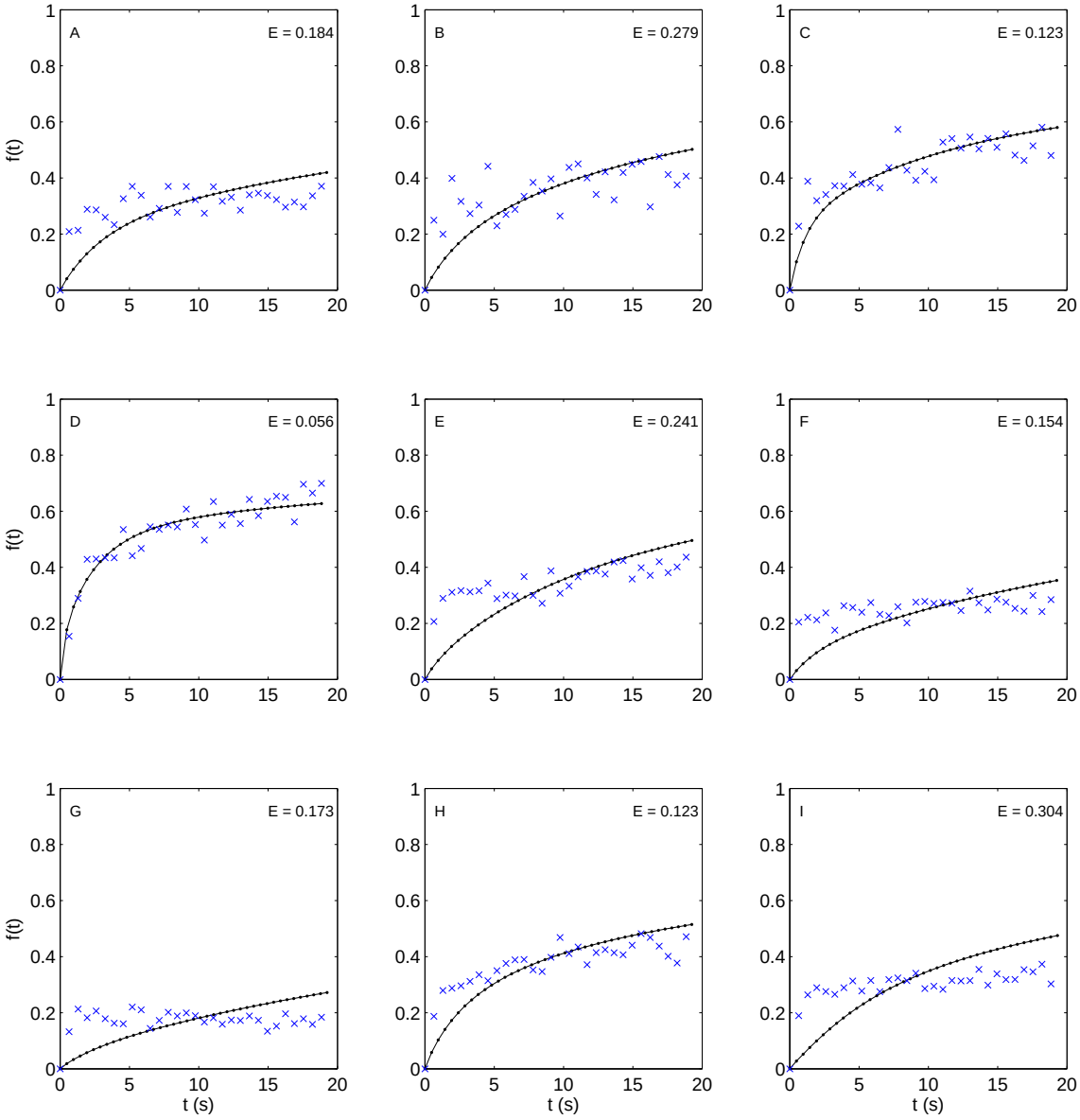

Figure 4.2: The result of PSE simulation (black lines) fitting to experiment data (blue crosses) for Hcf106-GFP, assuming a uniform diffusion coefficient throughout the model thylakoid network. Fitting is variable; C, D and H fit particularly well. Referring to the model networks in Figure 4.1, the bleached region for these simulations has relatively small overlap with the model network, while E and I, which fit poorly, have much more overlap. The fitting error E is the residual sum of squares.

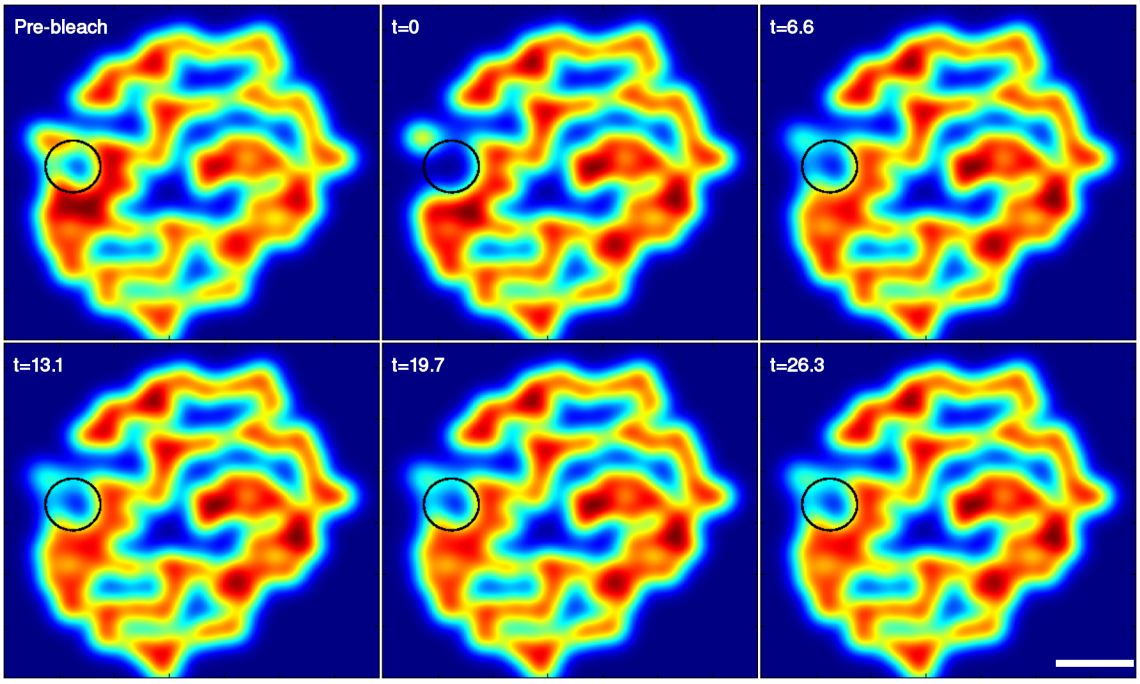

Figure 4.3: Sequence of postbleach images for simulation of FRAP experiment D for Hcf106-GFP. Bleaching is clearly visible in the ROI indicated by the black circle. After 6.6 s, partial recovery has already occurred. However, after 26 s, intensity in the ROI still has not reached the prebleach level. The fitted diffusion coefficient is 0.42 $\mu m^2/s$. Scale bar 1 μm.

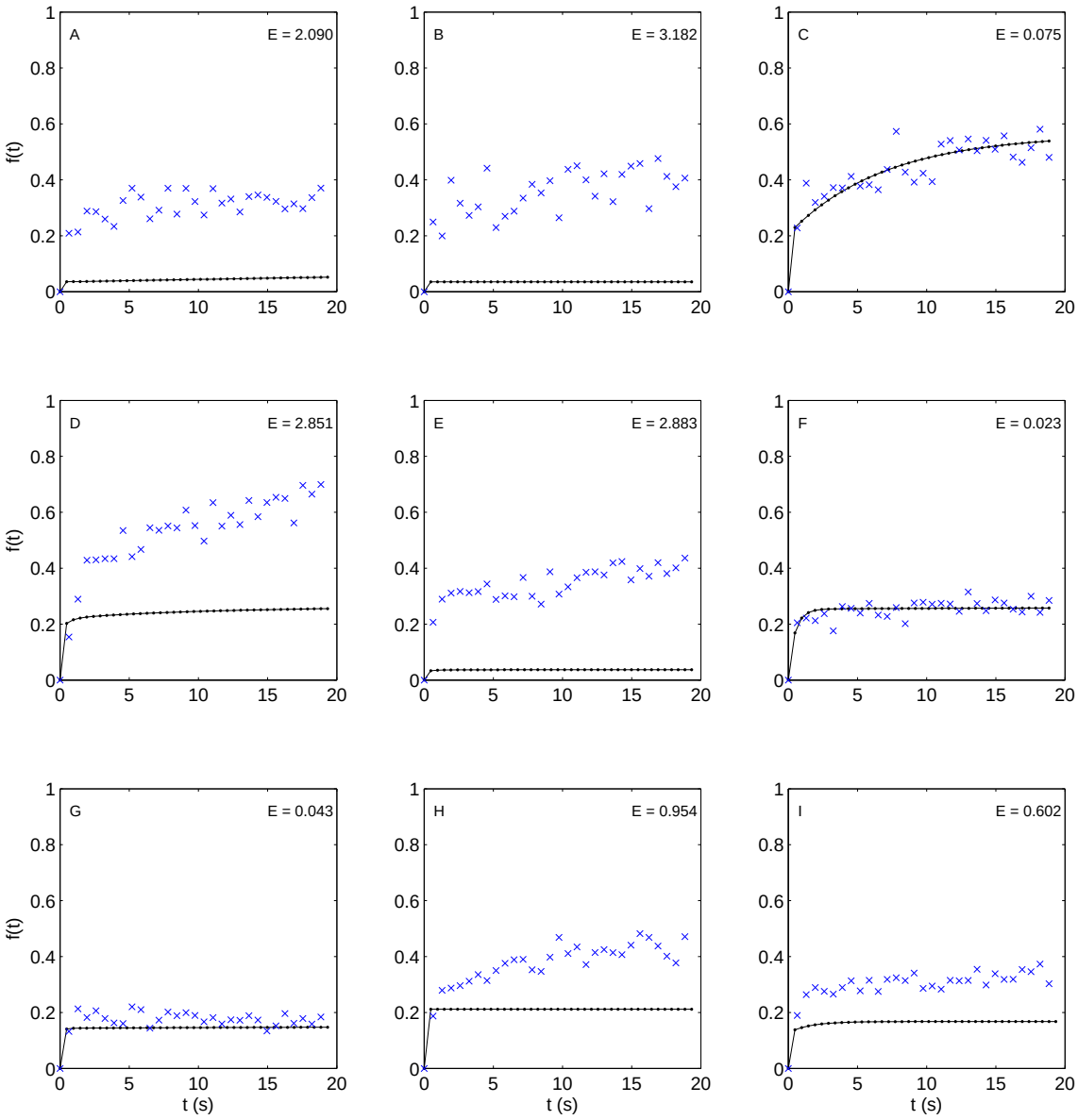

Figure 4.4: Best fit PSE simulations (black lines) to data (blue crosses) for the assumption that Hcf106 only diffuses within stroma-exposed lamellae. Clearly this assumption is not supported by the data, in terms of this model. Most of the simulations fit extremely poorly because the bleaching depletes the fluorescence population within a stromal lamellae section which cannot be replenished by diffusion through connecting grana. However, C and F fit rather well because the bleached ROI in these cases does not cover much network area, and the fractional recovery shown here actually has a small absolute value. The fitting error E is the residual sum of squares.

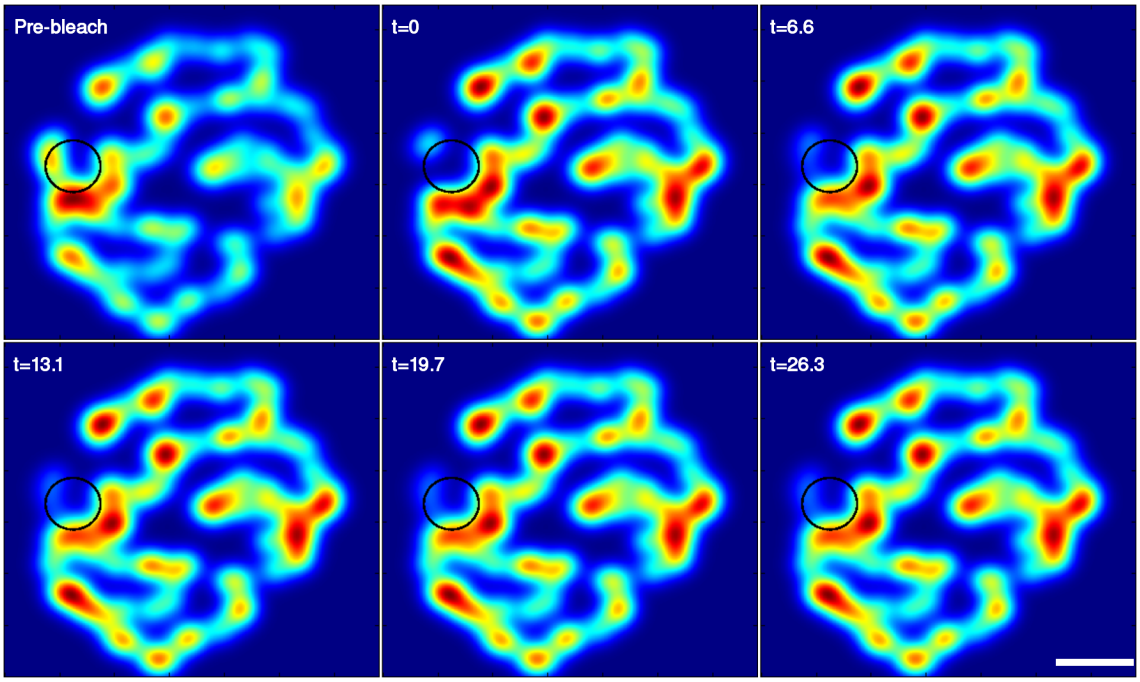

Figure 4.5: Images from simulation of FRAP experiment D under the assumption that Hcf106 is restricted to the stroma-exposed lamellae. Note that the intensity image is less dense than the others. In this case, the fluorescence inside the ROI circle is bleached but fails to recover. This is because, referring to Figure 4.1, the ROI can be seen to cover large portions of some stroma-exposed lamellae. When these are bleached they cannot recover because, as it is assumed that Hcf106 cannot cross the grana, the population of Hcf106-GFP in stroma-exposed lamellae cannot be replenished from elsewhere in the network. Consequently, the simulated recovery does not fit the data even for the high fitted diffusion coefficient (2.0 $\mu m^2/s$). Scale bar 1 μm.

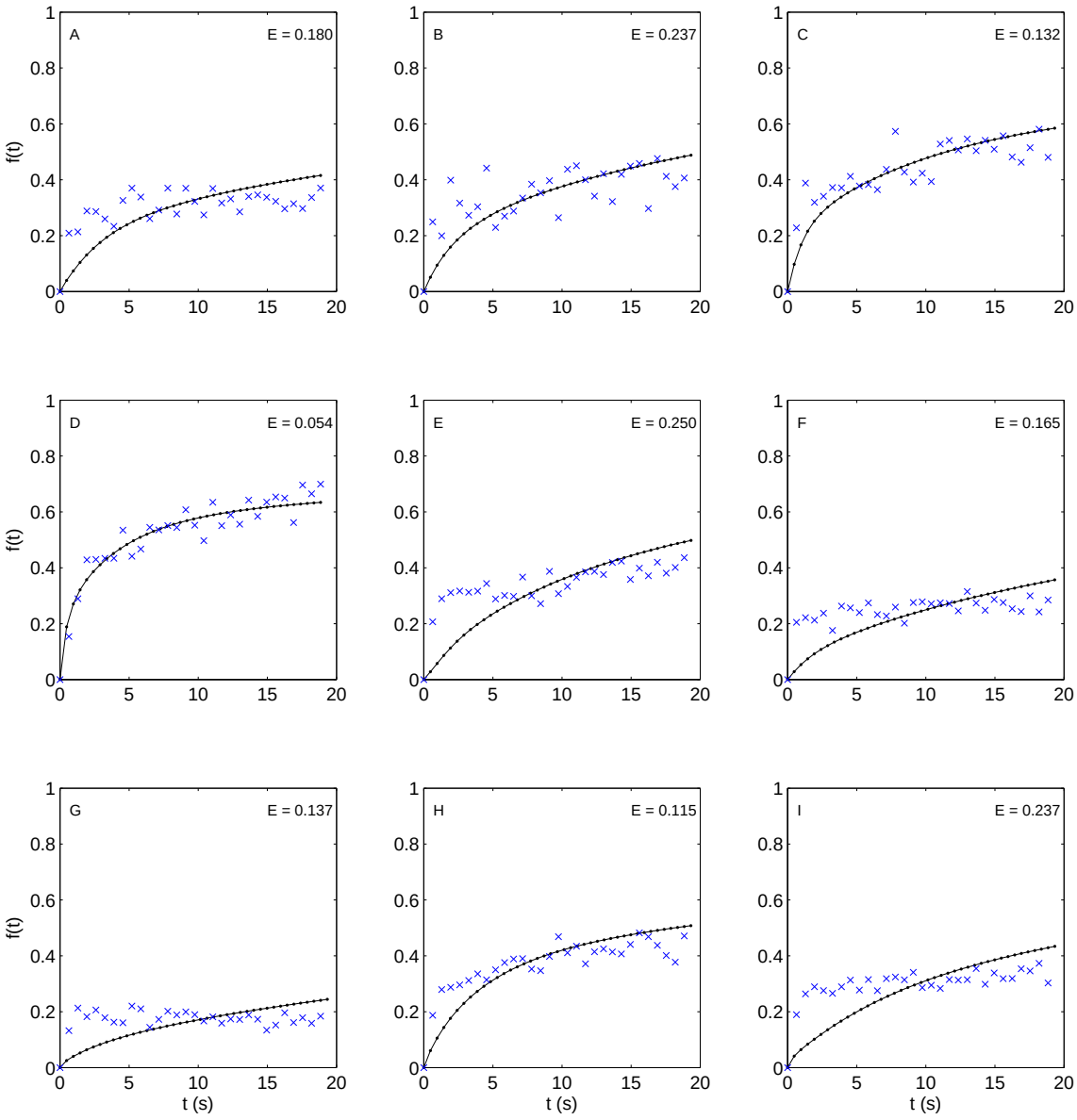

Figure 4.6: PSE simulations (black lines) fitted to experimental data (blue crosses), where the diffusion of Hcf106 in the grana is set to be 10 times lower than in the stroma-exposed lamellae. These simulations fit the data slightly better than those with the uniform diffusion assumption. The fitting error E is the residual sum of squares.

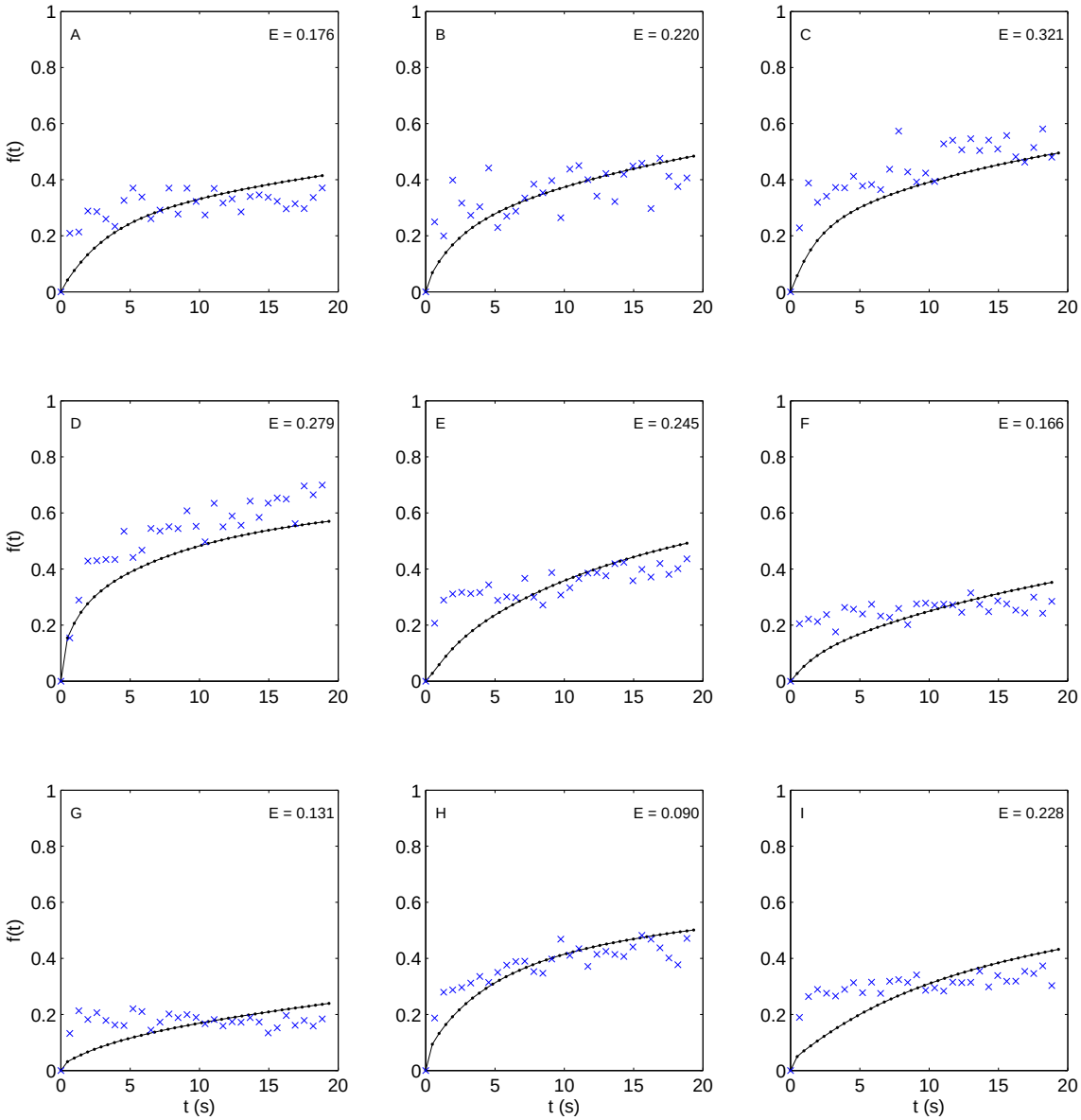

Figure 4.7: PSE simulations fitted to experimental data, as in Figure 4.6, except that the diffusion in the grana is set to be 100 times less than in the stroma exposed lamellae. These simulations fit the data slightly better than the ratio 10 simulations. The fitting error E is the residual sum of squares.

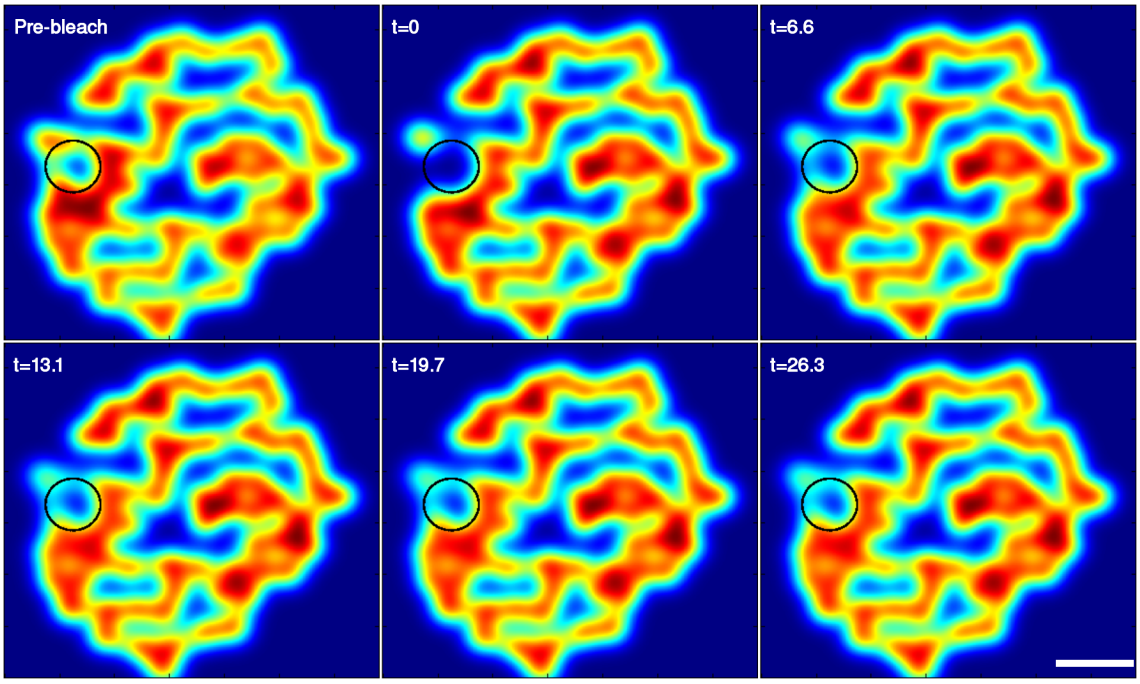

Figure 4.8: PSE images for Hcf106 from simulation of FRAP experiment D for the ratio 10 assumption where the diffusion in grana is fixed to be 10 times lower than in stroma-exposed lamellae. For the fitted stromal lamellae diffusion coefficient (0.21 $\mu m^2/s$), the fluorescent recovery is quick and matches the data well (see simulation D in Figure 4.6). Scale bar 1 μm.

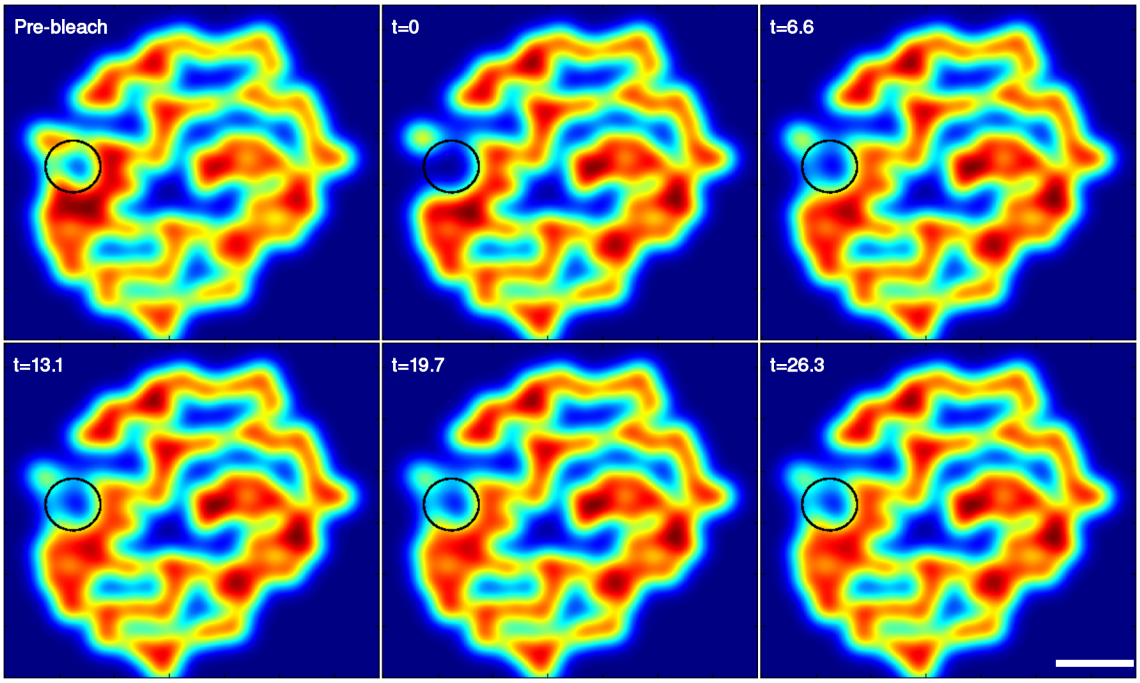

Figure 4.9: PSE images from simulation of FRAP experiment D, as in Figure 4.8, except the ratio is 100, that is, diffusion in grana is 100 times slower than stroma-exposed lamellae. Consequently, the recovery is slightly slower in this case for the fitted stromal lamellae diffusion coefficient (0.93 $\mu m^2/s$). Comparing the plots for simulation D in Figure 4.6 and 4.7, the ratio 100 does not recover quickly enough to fit the data, unlike the ratio 10 case. This is because, after the distribution of the remaining unbleached Hcf106-GFP in stromal lamellae has equilibrated, the timescale for introduction of new Hcf106-GFP from neighbouring grana is very slow. Scale bar 1 μm.

4.4.2 PSE for autofluorescence data

In an analogous way to simulation of Hcf106 data, PSE simulations can be applied to study the autofluorescence recovery. All the same assumptions as for Hcf106 are made; except an additional assumption is tested, that autofluorescent proteins cannot diffuse out of the grana.

It is immediately obvious from Figure 4.10 that, with the uniform diffusion assumption the PSE simulations fit autofluorescence much better than Hcf106, and predicts a mean diffusion coefficient of $0.025\,\mu m^2/s$. A sequence of images from the best fitting simulation is shown in (Figure 4.11).

Separately making the assumptions that autofluorescent proteins cannot diffuse in either grana, or lamellae, completely fails to the fit the data (not shown). This is not surprising as restricted diffusion on the model network is characterised by a short fast recovery state, followed by a steady state (see Figure 4.4), and the data does not support this. Moreover, other experimental evidence suggest that autofluorescent proteins can diffuse between grana [107].

Taking the middle ground assumption that diffusion is slower in grana, with ratios 10 and 100, a reasonable fit is found for most of the experiments, although not all. The mean best fit diffusion coefficients were $0.16\,\mu m^2/s$ and $0.82\,\mu m^2/s$ in stroma-lamellae for ratio 10 and ratio 100 respectively implying diffusion coefficients of $0.016\,\mu m^2/s$ and $0.0082\,\mu m^2/s$ in grana. This is in rough agreement with Kirchhoff et al. for ratio 100 [107].

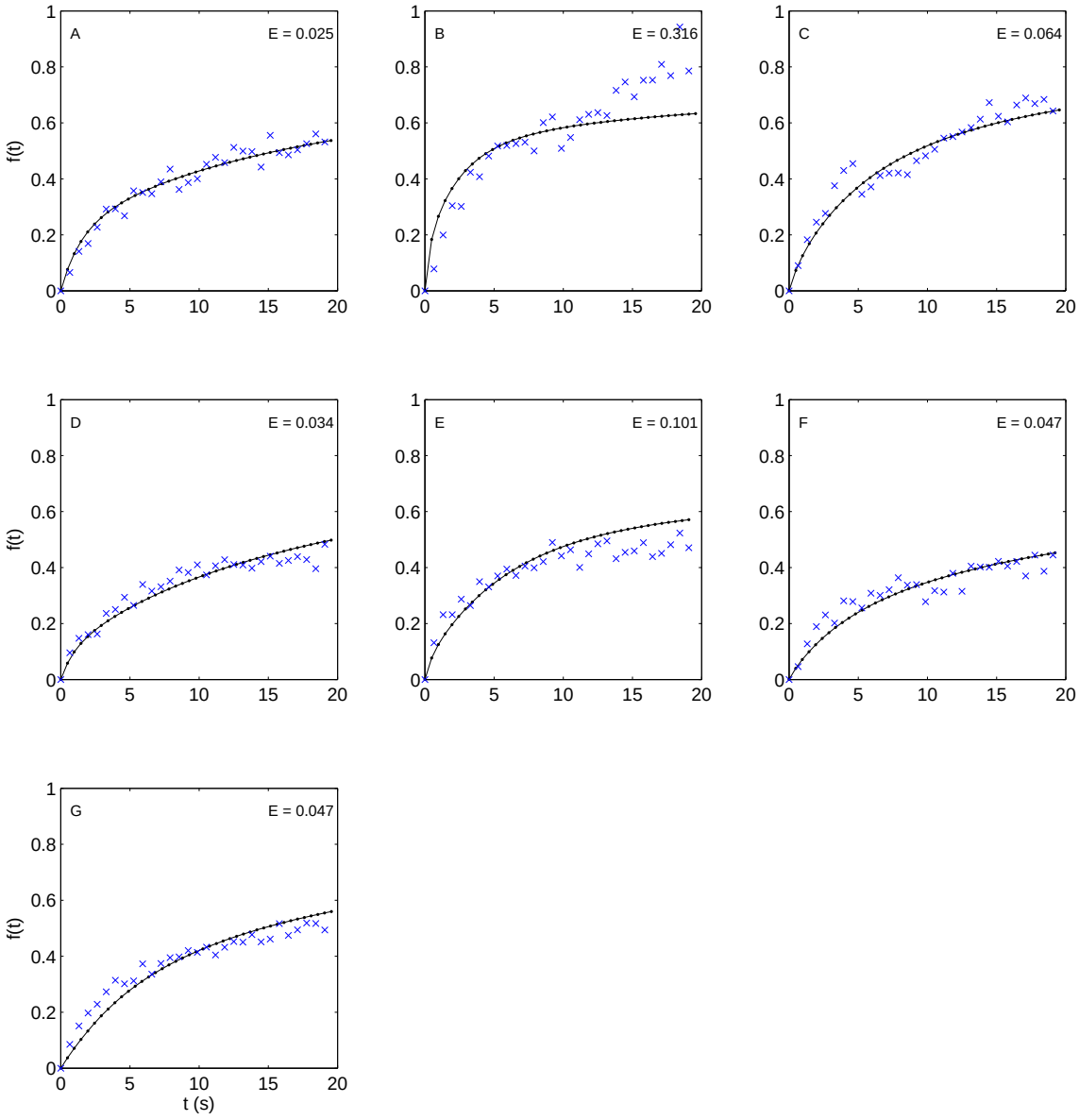

Figure 4.10: Best fit PSE simulations (black lines) to autofluorescence intensity data (blue crosses), assuming uniform diffusion throughout the thylakoid network. The simulations fit the data very well in these cases. Clearly, the assumption that autofluorescent proteins are free to diffuse in both grana and stroma-exposed lamellae is compatible with the data, and is furthermore supported by other experimental evidence [97]. The fitting error E is the residual sum of squares.

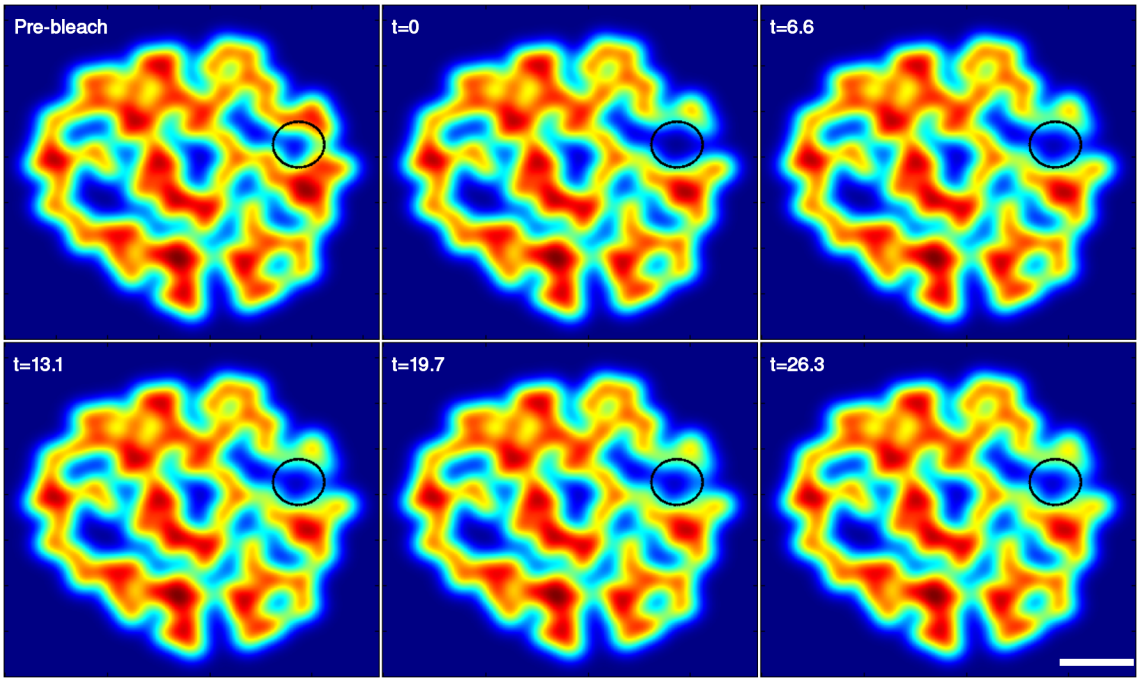

Figure 4.11: Sequence of PSE images for autofluorescence simulation of FRAP experiment F. The bleached region (black circle) shows a slow steady, but incomplete, recovery throughout the timecourse. Scale bar 1 μm.

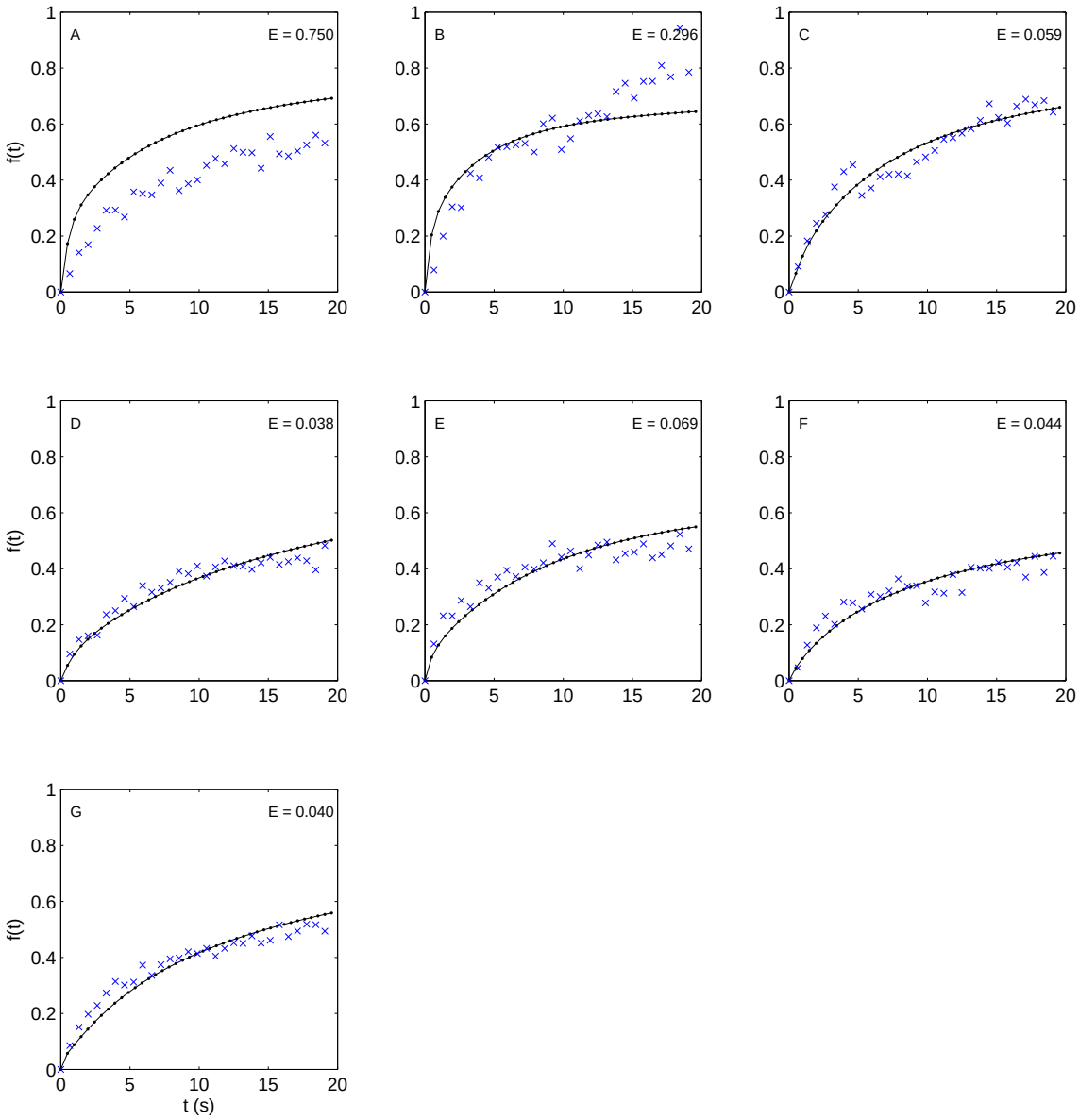

Figure 4.12: Result of fitting diffusion coefficients for PSE simulations (black circles) to autofluorescence data (blue crosses), assuming that diffusion in grana is ten times slower than in stromal lamellae. The fit is good for most experiments; particularly D, F and G. However, altogether, the fit is not as good as for uniform diffusion. The fitting error E is the residual sum of squares.

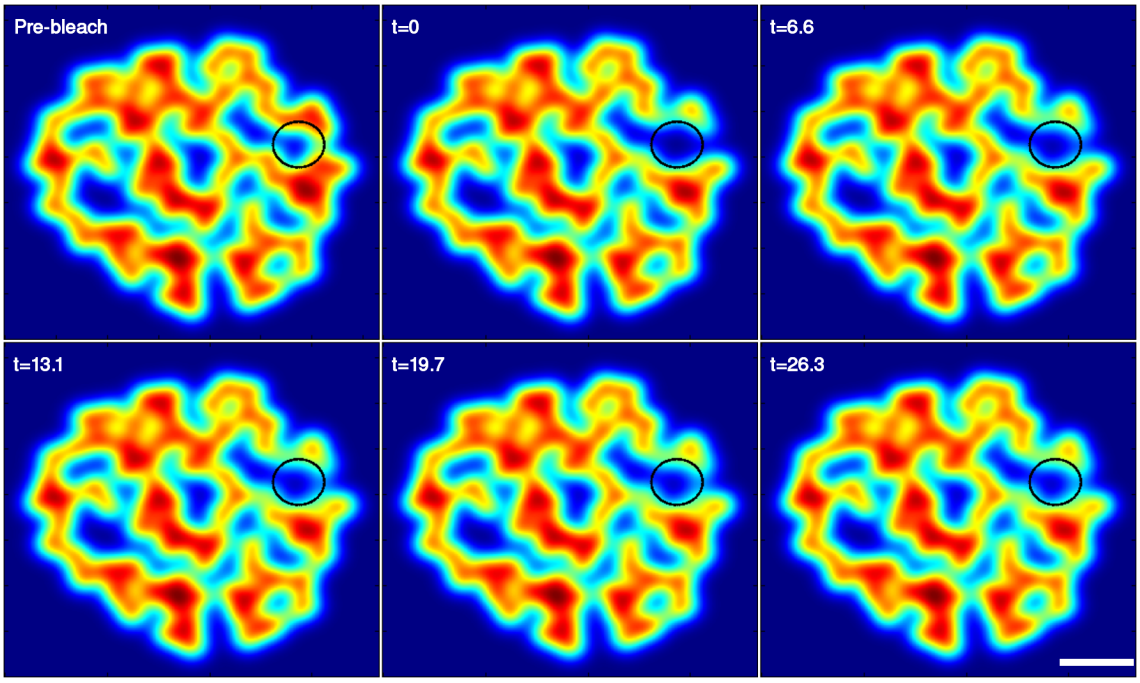

Figure 4.13: Sequence of PSE images for autofluorescence for simulation of FRAP experiment F, assuming ten-fold slower diffusion in grana. After 26 s the recovery of fluorescence in the bleached region is approximately half. Scale bar 1 μm.

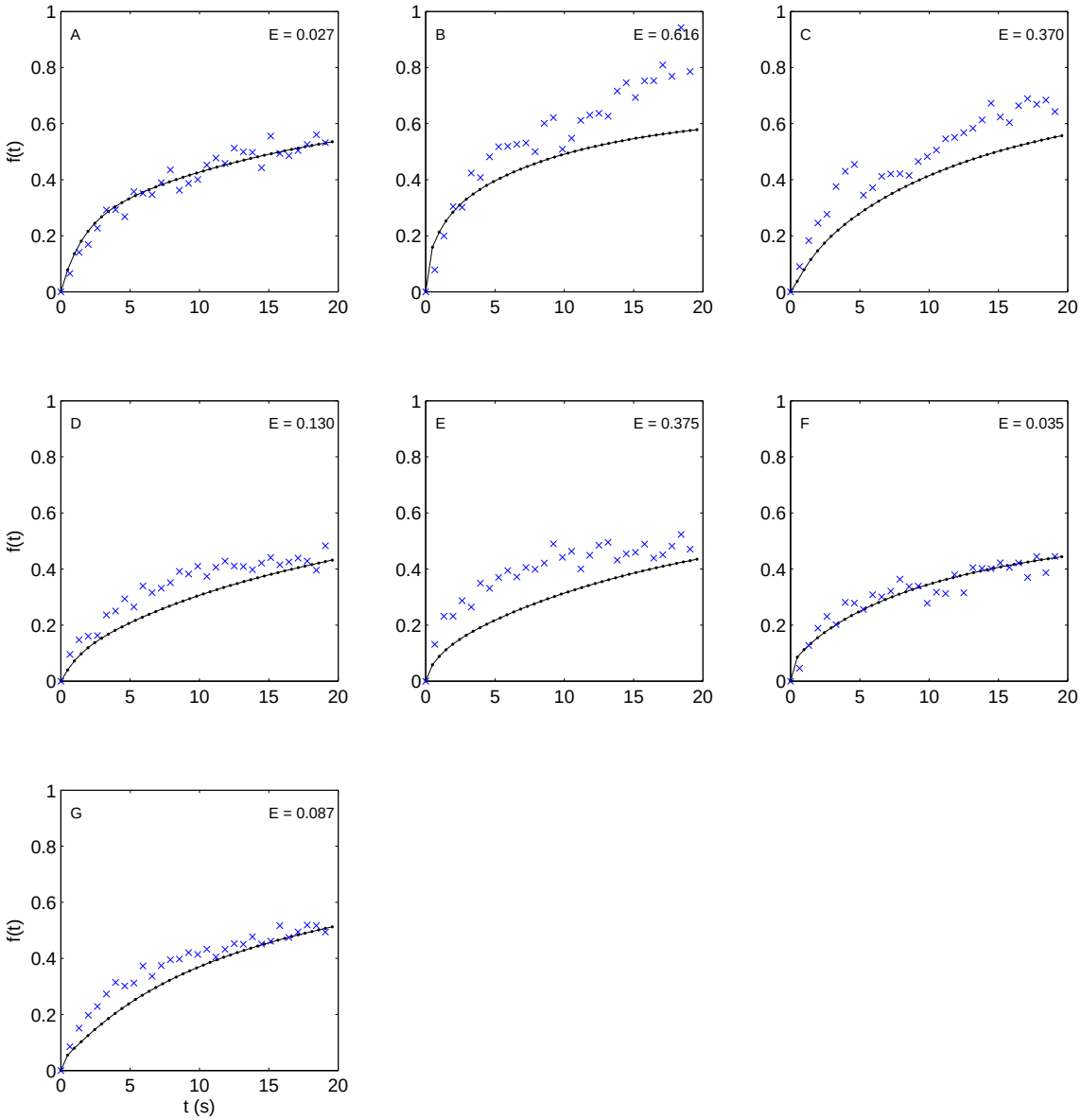

Figure 4.14: Fitting results for PSE simulations of autofluorescence, as in Figure 4.13, but with 100-fold slower diffusion in the grana. This case does not fit as well as the ratio 10 or uniform models. The fitting error E is the residual sum of squares.

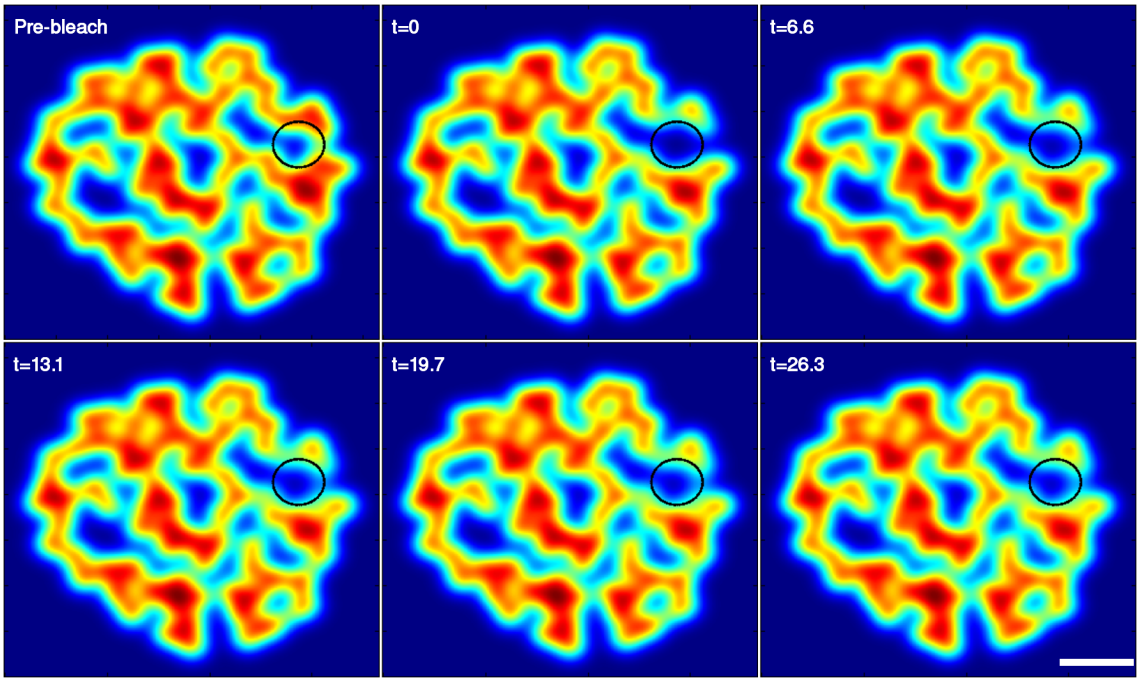

Figure 4.15: Pre-bleach and post-bleach images from autofluorescence PSE simulation of FRAP experiment F, as in Figure 4.13, but for 100 times slower diffusion in grana than stromal lamellae. Again, after 26 s the recovery fluorescence in the bleached region is approximately half. Scale bar 1 μm.

4.5 Summary

In this chapter, PSE was used to simulate diffusion on the thylakoid network, for both Hcf106 and autofluorescence. For Hcf106, based on the total sum of square residuals, assuming that Hcf106 is restricted to stromal lamellae gives the worst fit, while assuming either uniform diffusion throughout, or 10 or 100 times slower diffusion in grana fit similarly well, with ratio 10 being marginally better. The autofluorescence PSE results fit well and are in close agreement with results reported by Kirchhoff and colleagues [107]. The results suggest that autofluorescent proteins follow either uniform diffusion throughout the grana or 10 or 100 times slower in the grana.

5

Mobility of protein Toc159 in chloroplast outer membrane

5.1 Introduction

The TOC complex provides means of entry of precursor proteins into chloroplasts. Toc159 is a core membrane constituent of the TOC complex. It is believed to exist in a membrane bound state. However there has been evidence of its existence in a soluble fraction [53, 60]. The targeting and motor models, the two competing hypotheses on the mechanical function of the TOC complex, are still under debate.

5.2 FRAP of Toc159 in leaves and chloroplasts

The lateral mobility of Toc159 and a mutant was investigated using a series of FRAP experiments in leaves and isolated chloroplasts. Until now, there has been no information available on how proteins diffuse in the chloroplast outer envelope.

Kessler and colleagues have developed a series of constructs to study the functionality and assembly of the TOC complex. They employed immunofluorescence, fractionation and immunoblotting but have not observed the dynamics of the protein components *in vivo*. The mobility of three of their Toc159 constructs was measured by FRAP in this study. The three constructs are endogenous Toc159 with GFP-Toc159GM (Construct 1), ppi2 mutation with GFP-Toc159GM (Construct 2), and ppi2 mutation with GFP-Toc159GM D946N (Construct 3). G is the GTPase domain and M the transmembrane domain of Toc159.

The outer membrane of chloroplasts has a spherical geometry. Therefore the Ellenberg analytical expression, which describes fluorescence recovery in experiments where a strip bleached ROI is used on a spherical geometry (see section 1.15.2), is the most appropriate model for the Toc159 FRAP experiments. To satisfy the assumptions of this model, small rectangular ROIs were bleached and the fluorescence recovery fitted by nonlinear least squares (see section 2.16). To avoid biasing the result due to the autofluorescence contributing to the GFP channel, the recovery profile was taken only from the portion of the ROI corresponding to the membrane.

5.2.1 Construct 1: Endogenous Toc159 with GFP-Toc159GM

Construct 1 plants express the full length endogenous Toc159 protein and an N-terminal GFP tagged Toc159 missing the A domain. In confocal fluorescence images the protein can clearly be seen as a bright green halo surrounding the thylakoid autofluorescence, shown in Figure 5.3. Competition with respect to translocon incorporation may occur between the endogenous Toc159 population

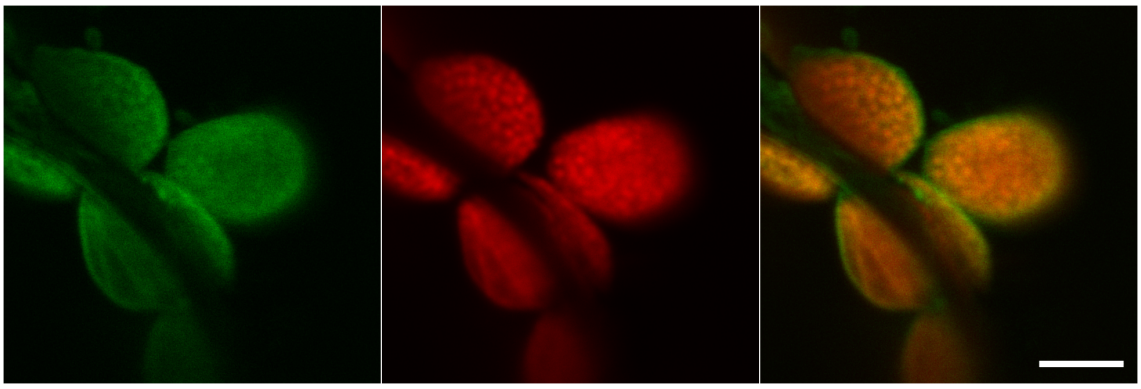

Figure 5.1: Confocal images of leaves from plants expressing the full length endogenous Toc159 protein and the truncated version Toc159 tagged to GFP at its N-terminus (Construct 1). Image of chloroplasts inside a leaf captured in green and red channel. The merged image shows a green halo around the autofluorescence. Scale bar 5 μm.

and the introduced truncated version in Construct 1 plants.

FRAP experiments were performed directly on leaf sections. A typical series of prebleach, postbleach and final images from a FRAP experiment in a leaf for Construct 1 is shown in Figure 5.4. As the panel shows, the autofluorescence is bleached and does not recover. It is difficult to determine from the images of the leaf whether the GFP was bleached or not.

Chloroplasts were isolated and subjected to the same FRAP procedure as for the leaf. Images from one of those experiments are shown in Figure 5.5. The recovery profile from the same experiment is shown in Figure 5.6. In these images the bleached region is apparent in the postbleach image. In the final image, some recovery has occurred in both the red and green channels. Analysing the intensity values shows that GFP in this construct is bleached and recovers to around 30% of its original value, on average. The experimental data were fitted using the model due to Ellenberg et al. [89]. Fitting the Ellenberg model to this data yields a diffusion constant of 0.0015 $\mu m^2/s$ and an asymptotic recovery of 78%.

5.2.2 Construct 2: ppi2 mutation with GFP-Toc159GM

Construct 2 plants express only GFP-tagged Toc159 GM. Leaf sections were observed using a confocal microscope. Green halos appear to co-localise with the outer envelope membrane as seen in Figure 5.7.

The mobility of GFP-Toc159GM protein was assessed by FRAP. On average GFP recovers to around 70% of its original value. According to the Ellenberg model fit, GFP-Toc159GM molecules undergo diffusion of 0.01 $\mu m^2/s$. The asymptotic fluorescence intensity was found to be to 98% of its orginal value.

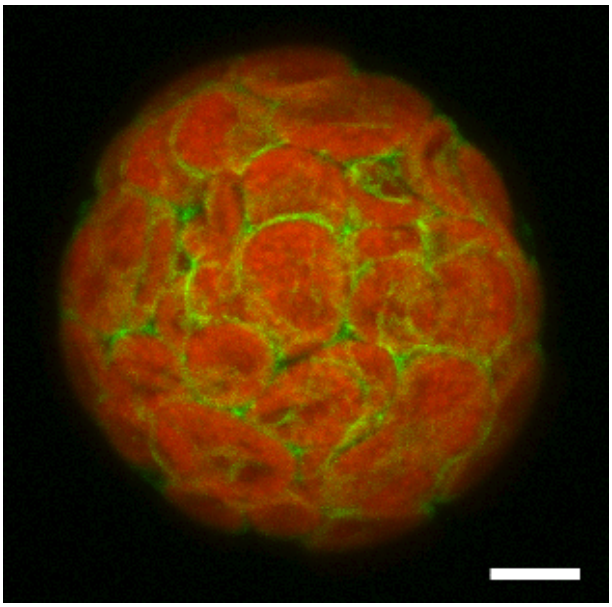

Figure 5.2: Confocal 3D image of a protoplast expressing endogenous Toc159 and Toc159GM (Construct 1). The 3D image was reconstructed from a Z-stack, a series of images taken at different focal plane heights, using the Leica LAS AF software. GFP is clearly visible in the chloroplast outer membranes. Scale bar 5 μm.

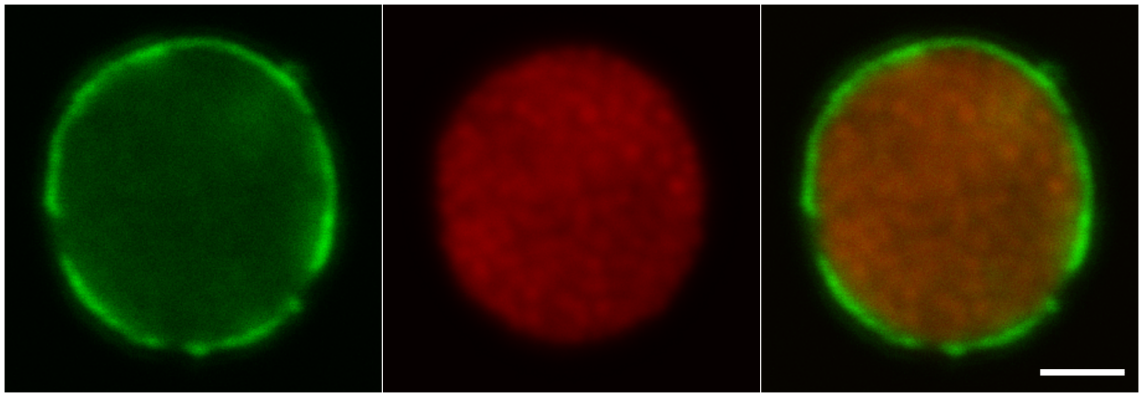

Figure 5.3: Confocal images of a chloroplast from plants expressing the full length endogenous Toc159 protein and the truncated version Toc159 tagged to GFP at its N-terminus (Construct 1). The green halo appears to be incomplete. Scale bar 2 μm.

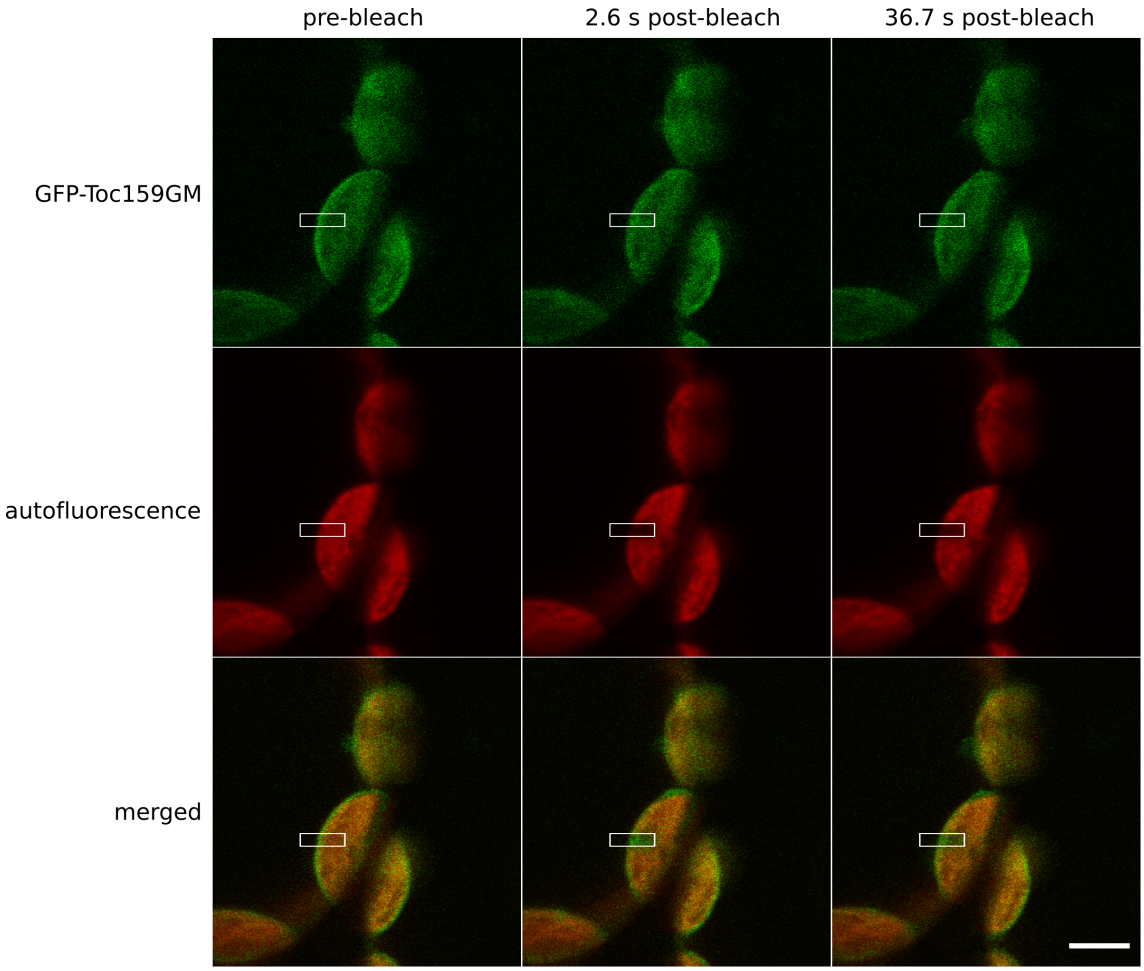

Figure 5.4: Images from a FRAP experiment on endogenous Toc159 with GFP-Toc159GM (Construct 1), showing prebleach, postbleach and final images. The bleached region (marked by white rectangle, width 1 μm) can be clearly seen in the autofluorescence postbleach images, but not so clearly in the green channel. Scale bar 5 μm.

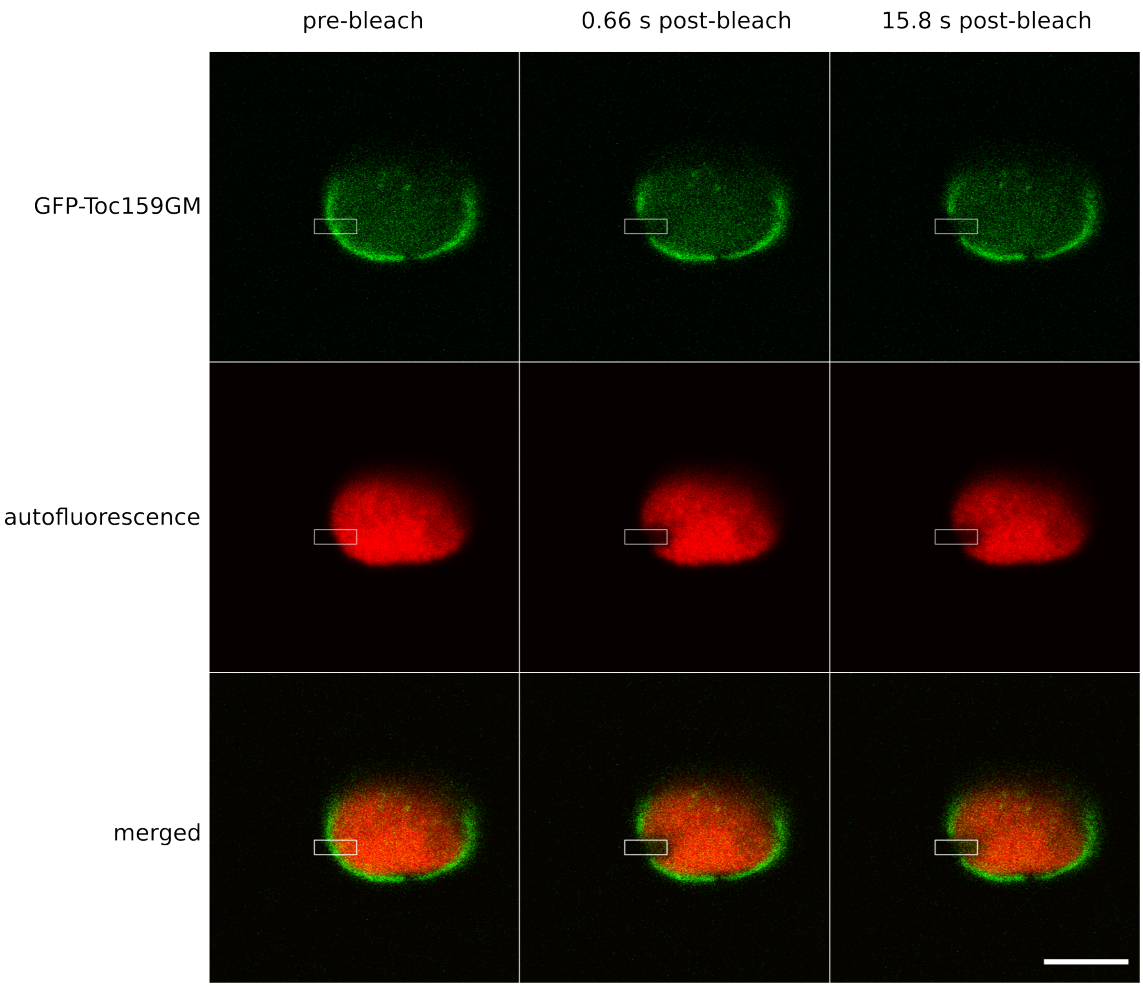

Figure 5.5: Images of a FRAP experiment on an isolated chloroplast from Construct 1 transgenic plants. The bleached region (1 µm width, marked by white rectangle) of the membrane is still clearly visible at the end of the experiment. Note the dark region at the bottom of the chloroplast is not due to bleaching. Scale bar 5 µm.

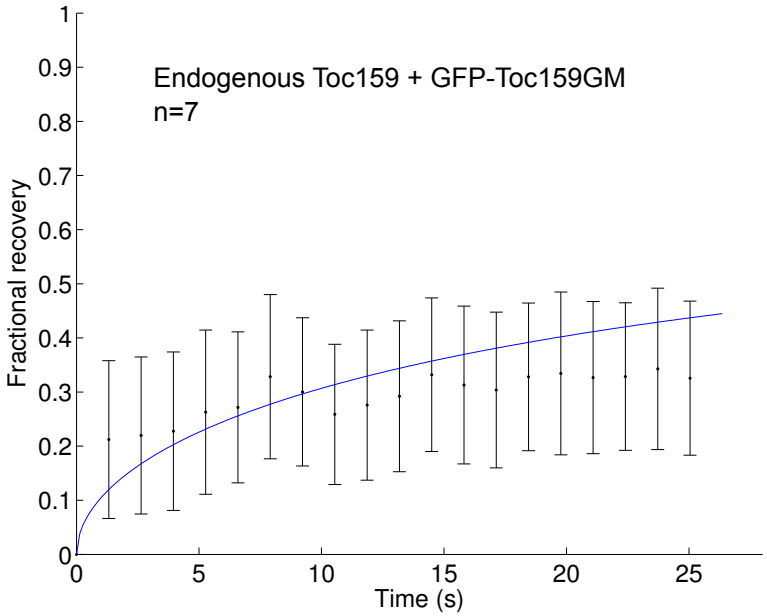

Figure 5.6: The mean average recovery profile for chloroplasts from Construct 1 transgenic plants with the fit to the Ellenberg model (blue line, $n = 7$). The bleaching region was 1 μm wide. On average the recovery is around 30% over a period of 25 s, although the fit predicts an asymptotic recovery of 78%. However, the fitted curve appears to over shoot the data for $t > 10$ s. Error bars show standard errors.

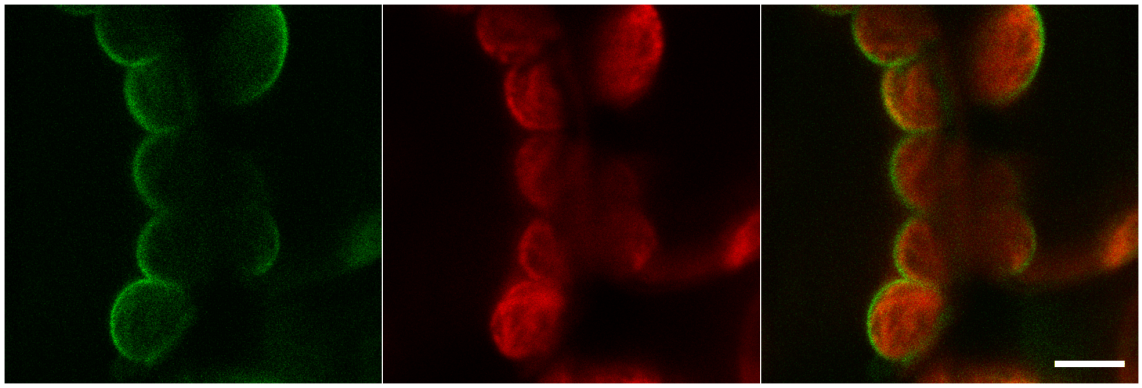

Figure 5.7: GFP, autofluorescence and merged images of a leaf from a Construct 2 plant containing the ppi2 mutation with GFP-Toc159GM. The GFP membrane halo are complete and not patchy, in the in-focus part of the chloroplasts in the image. This is in constrast to the patchy halos of Construct 1 in Figure 5.3. Scale bar 5 μm.

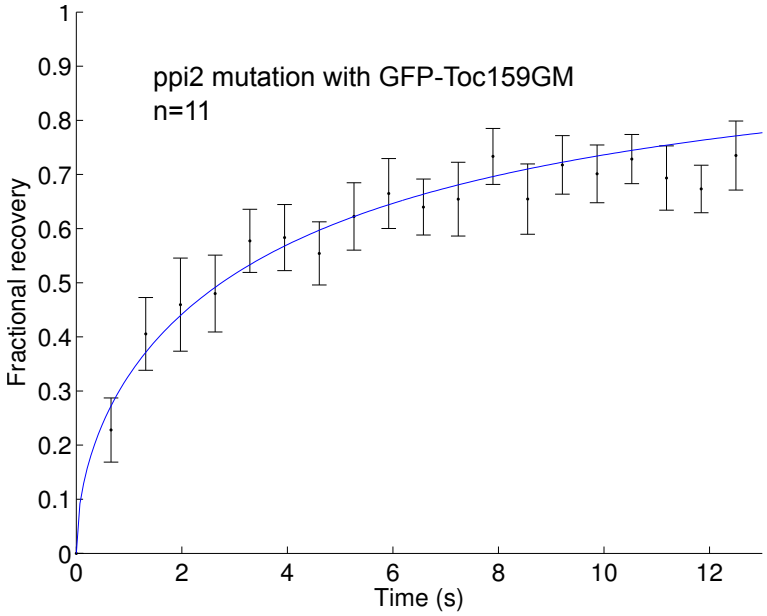

Figure 5.8: FRAP data for Construct 2 (ppi2 mutation with GFP-Toc159GM) showing high mobility. GFP-Toc159GM protein molecules recover with diffusion constant of 0.01 $\mu m^2/s$ and an asymptotic recovery of 98% (n = 11) according to fitting to the Ellenberg model (blue line). The bleached region was rectangular with 1 μm width. Error bars show standard errors.

5.2.3 Construct 3: ppi2 mutation with GFP-Toc159GM D946N

Construct 3 plants express the truncated version Toc159 GM tagged to GFP. Additionally, the mutation from aspartic acid to asparagine introduced at residue 946 is believed to disrupt the interaction of Toc159 with Toc34. Similarly to construct 1 and construct 2, halos are clearly formed in the green channel around the red autofluorescence of the thylakoid membrane, see Figure 5.9.

FRAP experiments on leaves from plants expressing GFP-Toc159GM D946N and model fitting reported a diffusion of 0.013 $\mu m^2/s$, similar to construct 2, and an asymptotic recovery of 85% as seen in Figure 5.10.

The mean recovery of fluorescence between constructs 1, 2 or 3 over the course of the experiment was compared by analysis of variance (ANOVA) (see table 5.1). There is significant difference in recovery between constructs ($p < 0.05$). Multiple pairwise comparison analysis shows construct 1 to have a significantly different recovery to constructs 2 and 3 at the 90% level (see box plot in Figure 5.11).

5.3 Protoplast fractionation

The localisation of GFP-tagged Toc159 was investigated by immunoblotting. Leaves from all three plants were digested to release protoplasts. The proto-

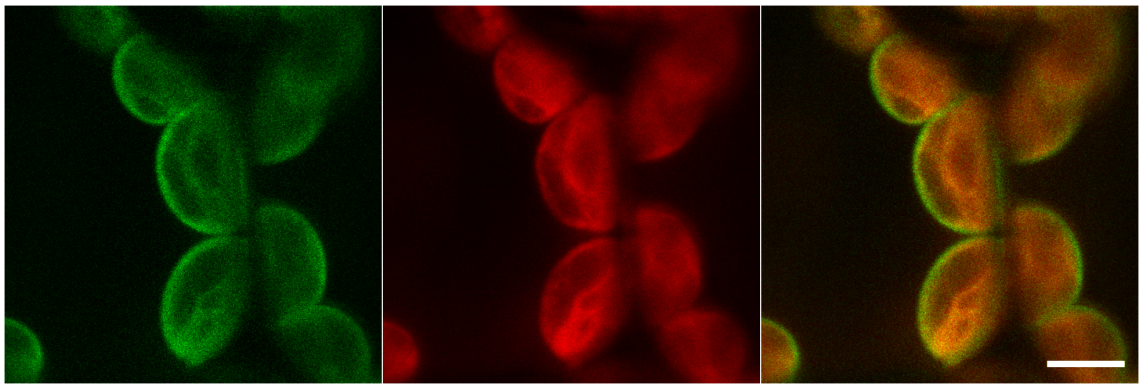

Figure 5.9: GFP, autofluorescence and merged images of a leaf from a Construct 3 plant (ppi2 mutation with GFP-Toc159GM D946N). As the complete halos clearly show, GFP-Toc159GM D946N is able to incorporate into the membrane despite the D946N mutation. Scale bar 5 μm.

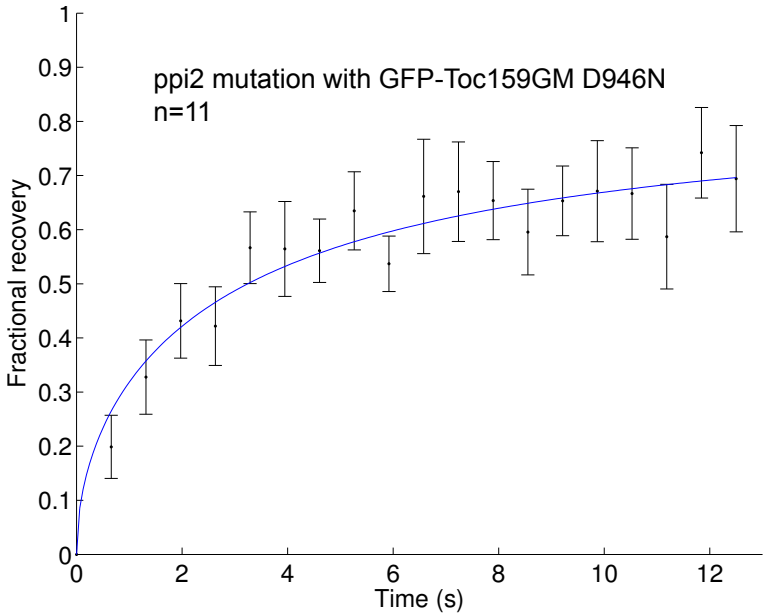

Figure 5.10: FRAP data for Construct 3 showing high mobility. The profile is very similar to the profile for Construct 2 in Figure 5.8, indicating the D946N mutation has little effect on mobility. GFP-Toc159GM D946N molecules exhibit diffusion of 0.013 $\mu m^2/s$ and an asymptotic recovery of 85% (n = 11) according to the fit to the Ellenberg model (blue line). The bleached region was rectangular with 1 μm width. Error bars show standard errors.

Source of variation	d.f.	Sum of squares	Mean square	F	p-value
Samples	2	0.7991	0.3996	3.91	0.0389
Residual	18	1.8400	0.1022		
Total	20	2.6392			

Table 5.1: One-way analysis of variance (ANOVA) of FRAP samples of endogenous Toc159 with GFP-Toc159GM, ppi2 mutation with GFP-Toc159GM, ppi2 mutation with GFP-Toc159GM D946N. The probability of obtaining the listed F-statistic is small assuming the mean fluorescence loss of each sample is equal. Therefore, we conclude significant differences in the means at the 95% confidence level (see text for details).

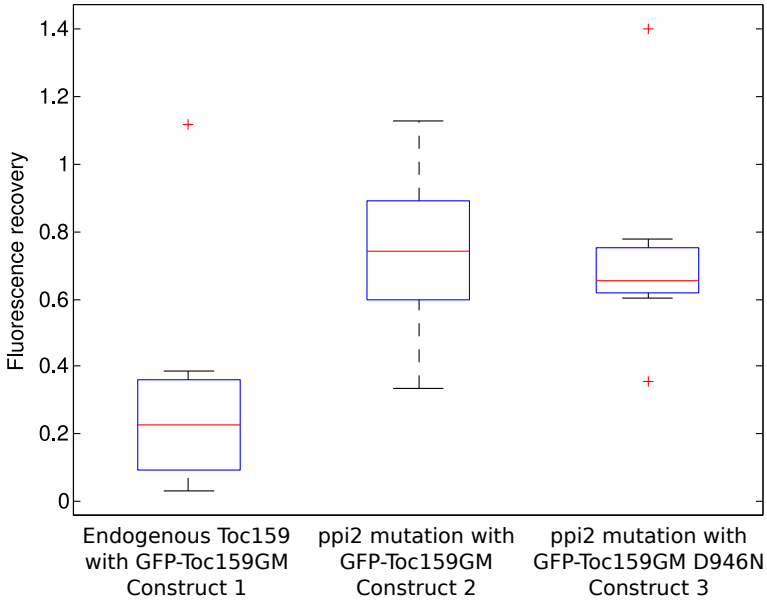

Figure 5.11: Box plot of endogenous Toc159 with GFP-Toc159GM, ppi2 mutation with GFP-Toc159GM and ppi2 mutation with GFP-Toc159GM D946N samples. Construct 1 recovers significantly less than Construct 2 and 3 (multiple pairwise comparison, $p < 0.1$). The red line is the median and the box is the 95% confidence interval about the mean. The whiskers show the range of the data, excluding the outliers shown as red pluses.

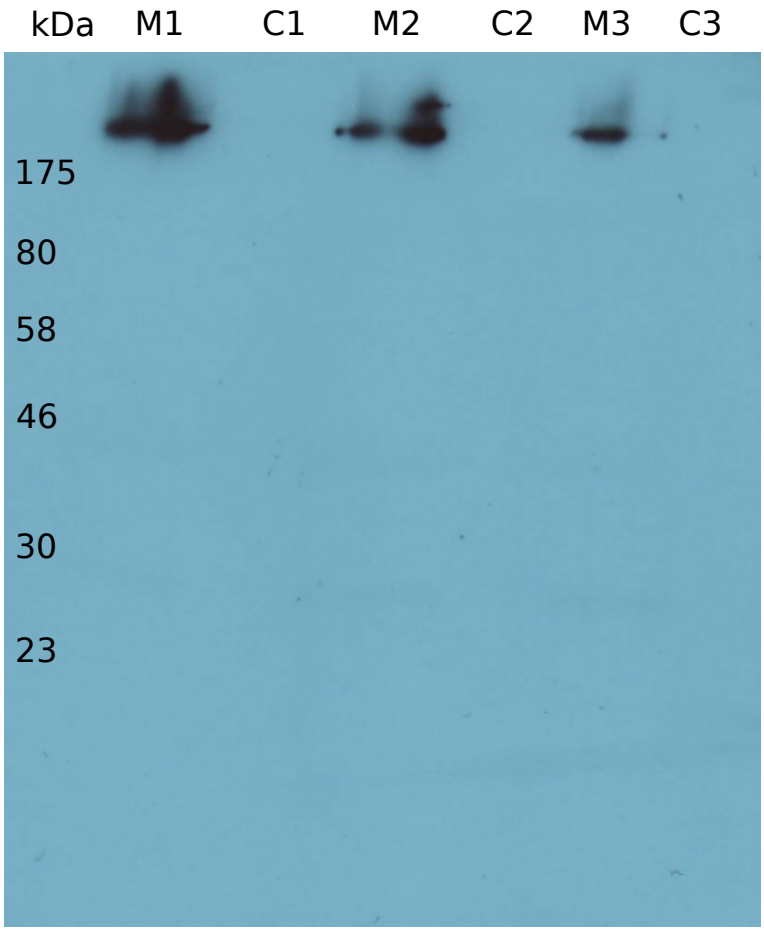

Figure 5.12: A diagnostic western blot of fractionated protoplasts from the three constructs. C1, C2 and C3 are the cytosolic fractions, and M1, M2 and M3 are the membrane fractions, from Construct 1, 2 and 3, respectively. Each membrane track shows a strong GFP band, while the cytosolic fractions contain no GFP. However, the cytosolic fraction is diluted compared to the membrane fraction and therefore cannot provide evidence for Toc159 not being cytosolic (see text for details).

plasts suspensions were subsequently fractionated into membrane and cytosolic fractions and tested against anti-GFP using a western blot, shown in Figure 5.12.

According to the immunoblotting results, GFP-tagged molecules are present only in the membrane fractions. However, the cytosolic fraction is diluted approximately 40-fold compared to the membrane fraction and it is possible that cytosolic GFP bands are simply too faint to be visible. Consequently, these results do not support the conclusion that Toc159 is predominantly localised to the membrane. Further fractionation and immunoblotting or fluorescence spectroscopy experiments would be required to determine the localisation of the GFP-tagged Toc159 conclusively.

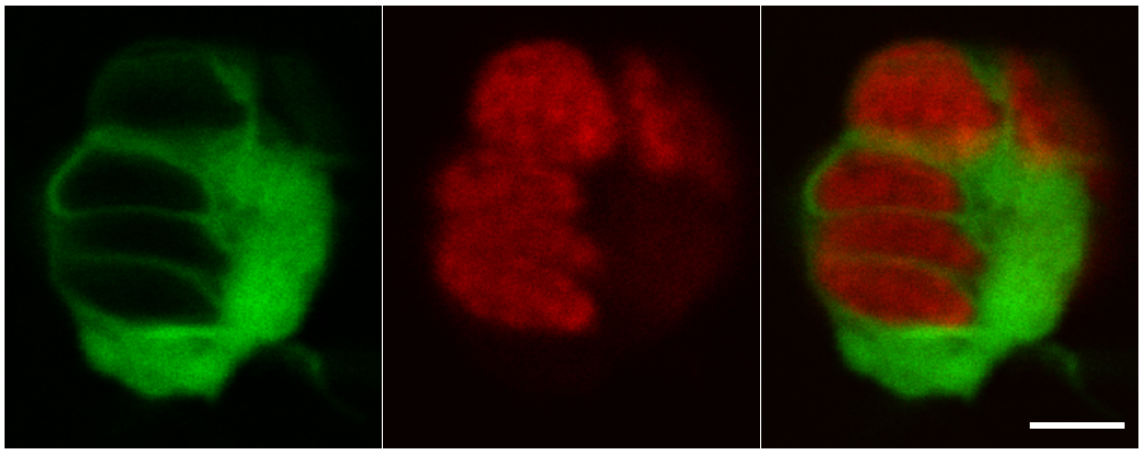

Figure 5.13: Three-dimensional reconstruction of aggregated chloroplasts transiently expressing OEP7-GFP, produced from a Z-stack of images using Leica LAS AF software. The GFP fluorescence is localised to the outer membrane. At the bottom-right GFP overexpression is visible. Scale bar 3 μm.

5.4 FRAP of AtOEP7

AtOEP7 was transiently expressed as a fusion protein with GFP in tobacco protoplasts to serve as a control for protein diffusion in the outer envelope of chloroplasts. The localisation of OEP7 in the outer envelope of chloroplasts was previously confirmed by fluorescence microscopy and fractionation analysis [110].

Chloroplasts targeted with OEP7-GFP appeared to clump and this was a consistent experimental observation. However, the protein was successfully inserted in the outer envelope resulting in bright green halos outside the autofluorescence area (Figure 5.13).

FRAP experiments, bleaching a square of 2 μm across the outer envelope, suggest that OEP7 is able to diffuse inside the outer envelope with diffusion coefficient of 0.09 $\mu m^2/s$ as estimated by fitting the Ellenberg model to the experimental data (Figure 5.15).

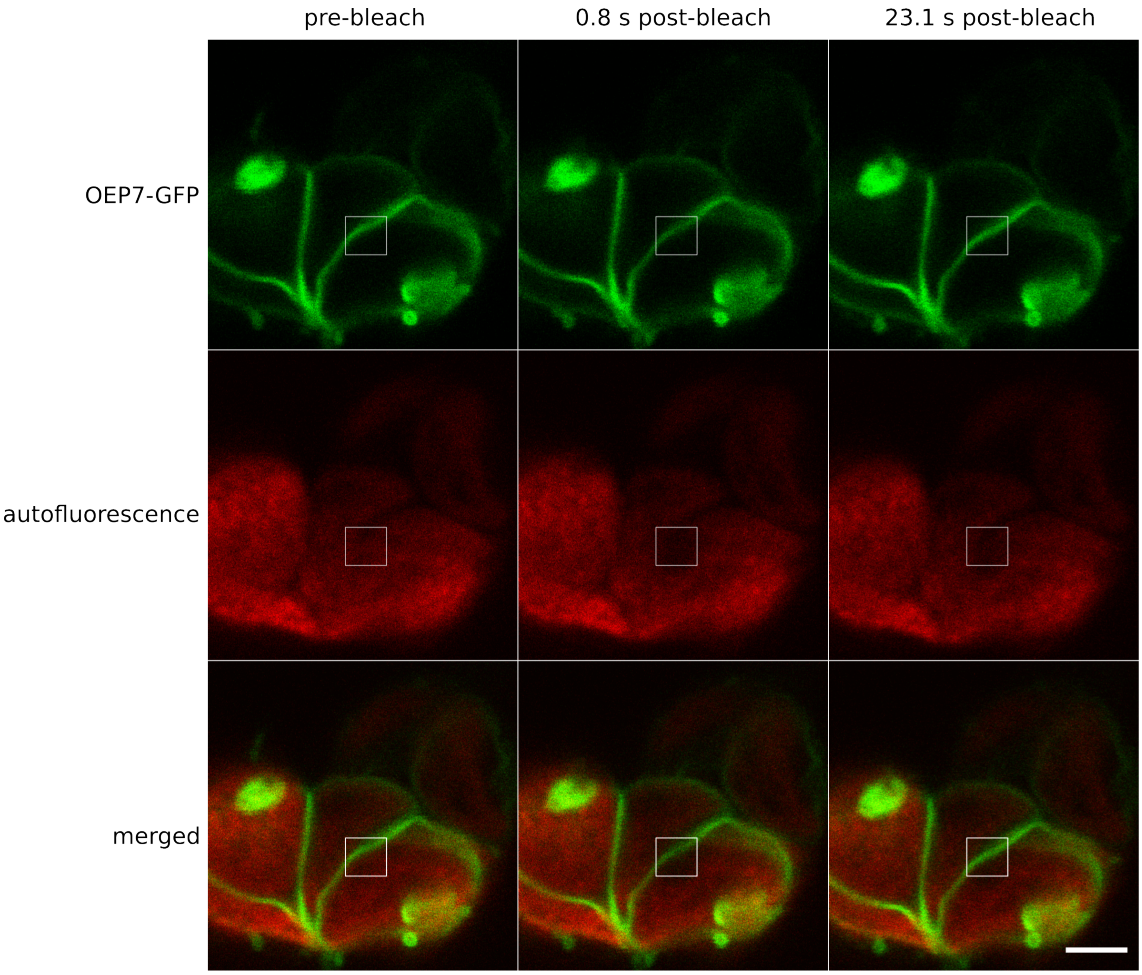

Figure 5.14: Prebleach, postbleach and final images for green and red channels of FRAP experiment on OEP7. The bleached region is marked by the 2 μm side white square. The GFP fluorescence appears slightly dimmer in the 0.8 s post-bleach frame but appears completely recovered after 23 s. Note that, because the chloroplasts are aggregated, the outer envelope of two adjacent chloroplasts are bleached simultaneously. Scale bar 3 μm.

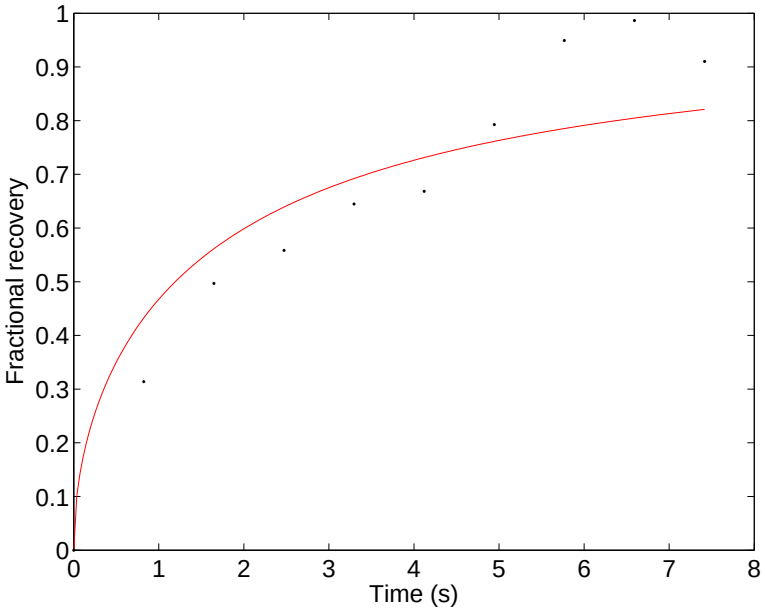

Figure 5.15: The recovery profile from a single FRAP experiment on chloroplasts containing OEP7-GFP. After 8 s the recovery is almost complete, indicating that OEP7 is highly mobile in the outer envelope. The experimental data were fitted using the Ellenberg model which resulted in a diffusion coefficient of 0.09 $\mu m^2/s$ ($n = 1$).

5.5 Summary

Based on FRAP studies on leaves, GFP-Toc159GM D946N and GFP-Toc159GM exhibit similar diffusion rates according to the Ellenberg fitted model. OEP7 was used as a control for mobility in chloroplast outer envelope and was found to be 9 times more mobile than GFP-Toc159GM D946N and GFP-Toc159GM, while GFP-Toc159GM appeared to diffuse slower in the presence of endogenous Toc159 on isolated chloroplasts.

6
Discussion

The thylakoid membrane is one of the most remarkable and intriguing biological membranes found in nature. While its detailed structure and the way it is formed is still a matter of debate in the field, the key feature is that the thylakoid presents areas of stacked membranes and areas of long, stroma-exposed membrane. Although the thylakoid proteins are found to be spatially segregated, redistribution of certain protein molecules has been observed. This spatial re-arrangement is of a great functional importance (e.g. PSII repair cycle, state transitions).

The mobility of the *Arabidopsis thaliana* thylakoid membrane protein Hcf106 was studied by means of two complementary photobleaching protocols as described in previous chapters. Hcf106 is a core subunit of the TAT-translocon in higher plant chloroplasts and according to immunoblotting reports, it is found within stroma-exposed membranes during fractionation experiments of isolated thylakoid membranes. The FRAP data demonstrated an extremely slow apparent diffusion in a degree comparable to the diffusion exhibited by photosynthetic thylakoid complexes believed to be found in highly-dense and crowded arrangements in the appressed regions of the thylakoid. The results from the FLIP experiments were consistent with the FRAP observations. Bleaching at one part of the thylakoid membrane did not deplete the total fluorescence of the organelle significantly. Unbleached fluorescently-tagged protein molecules were not able to diffuse throughout the network suggesting that the domain being bleached was inaccessible and isolated from the rest of the membrane.

The photobleaching experimental data raised a number of question and motivated a series of hypotheses. Is the majority of membrane protein Hcf106 immobile or is the observed impaired diffusion the effect of the structural organisation of its host membrane? Is there a functional importance of its mobility being either way i.e. does a potential slow diffusion confer advantages linked to its biological function as a translocon? Is Hcf106 incorporation to an active, multi-component translocon complex slowing down its motion?

There are many factors affecting protein lateral diffusion in biological membranes as discussed in Chapter 1. Could the observed Hcf106 slow diffusion be attributed to any of these factors? According to the entropic phenomenon known as the depletion or excluded volume effect, a hierarchy of molecules of different sizes forces large molecules into contact and to diffuse as one entity [4]. This does not necessarily imply a slow diffusion for the actual large complexes themselves but for the molecules diffusing around them. According to Saffman-Delbruck theory, the diffusion of a transmembrane protein is proportional to the natural logarithm of the reciprocal of the protein radius. Therefore, even large Hcf106-cpTatC complexes of 700 kDa should be rather mobile assuming a globular configuration

or even in the case where the complex adopts a disc-like conformation.

Protein diffusion may be impeded by interaction with peripheral structures. Reski and colleagues have observed persistent, highly organised filamentous scaffolds of FtsZ that are most likely involved in the maintenance of plastid integrity and in plastid division. They used the term 'plastoskeleton' for this newly described subcellular structure. However further experimental evidence across different plant species will be required before firm conclusions can be drawn [111,112].

Membrane microdomains or lipid rafts which are sphingolipid-cholesterol rich microdomains in liquid ordered phase, selectively incorporate or exclude proteins and can also hinder protein mobility [8]. Such a scenario would not be appropriate for thylakoid membranes which are mainly composed of monogalactosyldiacylglycerol (MGDG) and digalactosyldiacylglycerol (DGDG) [21,22]. It is more likely that the thylakoid membrane has a highly fluid nature [113].

Furthermore, membrane curvature may also restrict the lateral diffusion of a membrane protein. While this could be a possibility at junctions between stroma lamellae and grana margins, phosphorylated LHCII can still reversibly migrate between the two compartments despite its complicated three dimensional organisation. This could potentially suggest that the protein migration occurs when the thylakoid membrane adopts a more flexible, extended confirmation. It is known that low ionic-strength induces unstacking of chloroplasts [32]. More importantly, in high-intensity light, chloroplasts have less grana stacks and are more elongated compared to chloroplasts in low light. Grana stacking could be measured as the ratio of length of appressed membranes to the length of non-appressed membranes. As an example, spinach or pea thylakoids with 50-60% appressed membranes would give a ratio of 1.0-1.5, and this ratio may increase up to 5 times in shade leaves [33]. Transition of LHCII modulates the distribution of excitation energy between the two photosystems [114]. The major light-harvesting chlorophyll complex LHCII is reversibly phosphorylated at a threonine residue located in its N-terminus. Phosphorylation is catalyzed by a thylakoid-bound kinase that is regulated by the redox potential of the plastoquinone (PQ) pool of the chloroplast membrane. The kinase is activated when the PQ pool is reduced, such as the case of high light intensities. Therefore, we could suggest that the escape of phosphorylated LHCII molecules is facilitated by the flexible extended confirmation adopted by the thylakoid under high-light intensity conditions.

In Chapter 1, three different models of thylakoid structure were presented: quasi-helical, folded and bifurcation. The result that autofluorescent proteins are able to diffuse, albeit slowly, throughout the thlakoid, suggests that models where there are no substantial barriers to diffusion between grana and stromal

lamellae thylakoid membrane and where compartments are formed from physically connected membrane are more likely. Beyond this, the data do not support conclusions in favour of one model over the others.

While the FRAP results have revealed interesting features about the diffusion of proteins in thylakoid memranes, a series of control experiments would add strength to the findings. Ensuring that the outer membranes of chloroplasts are intact is important as it supports the physiological relevance of the observed results. The intactness of the chloroplasts can be checked by staining the chloroplast sample with lipophilic fluorescent dyes. For example, adding BODIPY FL C12 in chloroplast sample preparation resulted in continuous green halos surrounding the red autofluorescence of intact chloroplasts and fragmented green halos and considerably stained thylakoid membranes of broken chloroplasts [97]. Confirming that the recovery of fluorescence within the bleached region in FRAP experiments is due to diffusion and not because of switching of fluorophores between dark and fluorescent states (blinking) is crucial for the interpretation of the recovery curves. In order to examine the possibility of reversible fluorescence quenching, Goral and colleagues bleached entire chloroplasts and did not observe recovery of fluorescence within the 8 minutes of experiment. Although the chloroplasts isolated from protoplasts that express GFP-tagged proteins exhibit high green fluorescence (see Figure 3.2), it is difficult to say with certainty that chloroplasts with lower green fluorescence are from protoplasts that failed to be transfected or simply express the GFP-fusion at lower levels. In order to estimate the portion of the observed green fluorescence that originates from GFP, chloroplasts from protoplasts that have not undergone DNA transfection (WT protoplasts) or from protoplasts transfected with a non-fluorescent construct should be imaged. The latter would be a better control as the protoplasts would have been subjected to an identical preparation.

There is no biological evidence to support the hypothesis that Hcf106 is immobile in stroma-thylakoids. Therefore its apparent slow diffusion in photobleaching experiments is probably due to the membrane's organisation and protein spatial segregation. Indeed, studies on the *E. coli* plasma membrane have shown the homologous TatB protein to be highly mobile [115]. In order to test the hypothesis that Hcf106 is mobile and able to diffuse throughout the thylakoid network, Particle Strength Exchange simulations were employed to simulate FRAP experiments. This method was successfully used to extract quantitative information on diffusion of solutes in ER lumen [104] and ER membrane [109] using a three dimensional reconstruction of the actual FRAP domain on the ER. Since producing a three dimensional model of the thylakoid membrane is not experimentally possible, the computer simulations were based on approximations of thylakoid

networks extracted from confocal images of autofluorescence. Using Monte Carlo the supposed grana areas are identified as the regions on the image with the brighter intensity. These grana are then connected to their nearest neighbours. The position of the bleached region matched the position of the experimental bleached region.

The hypothesis that Hcf106 is free to move throughout the network is supported by the simulation results and fits the experimental data better than the hypothesis of restricted motion in stroma exposed membranes. More specifically, the simulation of Hcf106 diffusing 100 times slower in grana than in stroma lamellae ($0.60\,\mu m^2/s$ in stromal lamellae) appears to explain the data better than diffusing 10 times slower in grana ($0.082\,\mu m^2/s$ in stromal lamellae) or even uniformly with constant ratio ($0.012\,\mu m^2/s$). Perhaps a case of even a bigger ratio of diffusion constants could explain the data much better. Indeed, grana membranes are highly crowded with PSII complexes tightly-packed in a semi-crystalline array. It would not be surprising if for example, the entropic effect of excluded volume creates non-accessible diffusion paths for molecules such as Hcf106, that are then forced to diffuse around the large complexes, resulting in a slow apparent diffusion. Interestingly, assuming uniform diffusion for chlorophyll-containing complexes fitted the autofluorescence data best, with mean diffusion coefficient $0.025\,\mu m^2$. Comparing with the diffusion coefficients for chlorophyll-containing complexes obtained experimentally by other methods (see Table A.4) indicates that the uniformly diffusing PSE-obtained D corresponds closely to the value obtained by single-particle tracking (SPT) for diffusion in stromal lamellae ($0.027\,\mu m^2/s$), but is about 5 times larger than the value obtained by FRAP on grana patches ($0.0046\,\mu m^2/s$). However, the PSE result when assuming granal diffusion is 100 times slower than in stromal lamellae (ratio 100) roughly agrees with the FRAP on grana patches with mean diffusion coefficient $0.0082\,\mu m^2/s$, but significantly overestimates the stromal lamellae diffusion rate. To put these values into context, the diffusion of TatA-GFP in *E. coli* plasma membrane is around five times faster than the uniformly-diffusing PSE result for autofluorescent complexes, while GFP in *E. coli* cytoplasm and in aqueous buffer is about 300 and 3000 times faster, respectively.

PSE offers significant advantages over other simulation methods. It is order of magnitude more accurate when compared to Monte Carlo simulations of the same number of particles and also avoids the geometric limitations of finite differences method. Although finite element methods can be promising for problems with complex geometries it is also very challenging to program, very time-inefficient in trying to produce an accurate mesh and solving very large matrices [109]. The model thylakoid network is very simplistic, being two-dimensional and con-

structed from rectangles and circles. However, the experimental data is derived from two-dimensional images of chloroplasts, in which grana circles are often clearly visible. Due to the actual three-dimensional nature of the membranes it is likely that the diffusion coefficients reported here are under-estimated, particularly for grana stacks. Furthermore, biological membranes are not rigid planes as they undulate, tending to also cause an under-estimation. On the other hand, membrane proteins are diffusing on a two-dimensional surface, so it may not be order-of-magnitudes different to the two-dimensional model. The particular networks used for the simulation were fitted objectively to the fluorescence images. Based on this reasoning, the two-dimensional thylakoid model is a reasonable first approximation.

While the thylakoid membrane of higher plants assumes a highly-organised conformation, the outer and inner membranes of the chloroplast envelope are smooth spherical shells. The mobility of the membrane protein Toc159, a component of the chloroplast outer membrane translocon, was chosen as a comparison with the thylakoid-bound Hcf106 translocon. In order to draw meaningful conclusions on the relevance of mobility for translocon complexes and components, it is necessary to gather mobility data from a range of translocons situated in different membrane environments. Toc159 mobility was observed by FRAP both directly in a leaf and in isolated chloroplasts.

There is evidence to suggest that Toc159 also exists as a soluble fraction [60]. GFP-Toc159GM in intact leaves shows as a bright GFP halo. Endogenous full length Toc159 is also expressed. Intriguingly, the isolated chloroplasts show incomplete halos, containing gaps in fluorescence. This may indicate that the cytosol contains a reservoir of Toc159 that cycles in and out of the membrane. Once the cytosol is removed, as in the isolation procedure, this reservoir is lost and a new equilibrium concentration of Toc159 in the membrane is established. It is not *a priori* obvious that at the new concentration the Toc159 should necessarily be evenly distributed. Moreover, the fact that the halo becomes incomplete rather than merely darker suggests that the two Toc159 variants cluster together. An alternative explanation for the patchy halo is that a cofactor exists in the cytosol that acts to keep Toc159 within the membrane. Again, when the cytosol is lost, so is the prefactor, and consequently Toc159.

The mobility of a construct expressing only the truncated version of Toc159 was also examined. The diffusion coefficient of Toc159GM was found to be ten-fold higher when the endogenous full-length protein was not expressed. This result could suggest an antagonistic behaviour between the full length and the truncated protein with respect to complex incorporation. However, this result could be an artifact of comparing FRAP experiments performed in chloroplasts

and in leaves. Furthermore, in the absence of full length protein, Toc159GM and Toc159GM D946N demonstrated very similar mobility behaviour. Surprisingly, mutating the interaction site of Toc159 with Toc33 had no significant effect in the apparent diffusion. In all cases, Toc159GM was found to diffuse ten times slower than OEP7 which was not surprising if we take into account the large difference in size between the Toc159GM and OEP7. The fact that Toc159 is part of a large multiprotein complex spanning the chloroplast envelope could also be regarded as a source of mobility constraint.

In these studies we have considered homogenous populations where the diffusion may have a spatial dependence. It is also possible to argue for the existence of two populations with different mobilities. A steep initial gradient followed by a less steep gradient in a FRAP recovery curve can be indicative of the existence of two populations with different mobilities. The faster population recovers almost instantaneously while the mobility of the slower population explains the almost flat part of the curve. In the case of Hcf106, there is no biological evidence to date to support the existence of two mobility populations. However, when Hcf106-GFP is overexpressed, the dynamics inside the thylakoid membranes may be perturbed with the possibility of some GFP-tagged protein not associating with the native translocon but moving inside the membrane with a different diffusion coefficient. For the case of LHCII and PSII, previous studies have suggested the existence of a fast and a much slower diffusing population [97, 99]. Here, however, we have demonstrated that the autofluorescence recovery profile can be fitted with a uniformly diffusing homogenous population. It can also be argued, based on the recovery curve, that two populations with different mobilities exist in the Toc159 Construct 1 samples (endogenous Toc159 with GFP-Toc159GM). FRAP experiments are not sufficiently powerful to discriminate between heterogenously diffusing populations and spatially dependent diffusion. More sophisicated single-molecule experiments would help to resolve this issue.

7

Conclusions and future directions

The work presented in this thesis has improved our understanding on how the protein Hcf106, a core component of the plant TAT translocon, diffuses in the thylakoid membrane. A thorough computational investigation using Particle Strength Exchange simulations suggested that the three dimenional organisation of the thylakoid membrane imposes mobility constraints on its resident proteins. Moreover, proteins were found to laterally diffuse in the chloroplast outer envelope with diffusion constants typical for membrane proteins.

The FRAP and FLIP studies should be extended to investigate the mobility of cpTatC and Tha4, subunits of the ΔpH translocon in plants. For example, the putative function of Tha4 is transient association with the Hcf106-cpTatC to form the translocation pore in the presence of a substrate. Based on biological function, Tha4 is anticipated to undergo fast diffusion compared to the diffusion of Hcf106 in an unstacked thylakoid membrane. Transgenic plants should be created for studying mobility of proteins in the presence of native stoichiometries. Also mutations should be introduced to disrupt translocon formation and follow the mobility of individual protein components.

For more accurate characterisation of molecular diffusions, studies should evolve from ensemble average behaviours towards single-molecule imaging experiments using total internal reflection fluorescence microscopy (TIRF) or single particle tracking (SPT). Techniques such as the above can take into account the membrane heterogeneity and provide specific information on the nature of the motion at the molecular level. Molecular recognition using atomic force microscopy (AFM) could be used as a complementary approach to define the exact localisation of the transocon apparatus. AFM is typically used to measure the topography by raster scanning a sharp probe across a surface. It is also an important tool for specific ligand-receptor interactions at the piconewton-nanometer scale [116]. Anti-GFP could be attached to the AFM tip and scanned across transfected thylakoids. The translocation apparatus components would be engineered such that a GFP tag is exposed to the stroma. Thus topography information will be combined with direct localisation of the translocation complexes.

Grana and stroma-exposed thylakoid membranes could potentially have different elastic properties. A possible variable elasticity could assist in the folding of the single thylakoid bilayer to form stacks of grana. Using AFM, intact thylakoids should be imaged in solution under physiological conditions and the AFM images processed to obtain mechanical data. The spatial data may be collected by force curve mapping, which involves collecting force profiles on a grid of points covering the specimen and processing to produce a map of elasticity, or phase imaging which involves oscillating the the AFM cantilever and using the phase difference between driving and response to measure viscoelasticity.

The current PSE simulations do not take into account the three dimensional structure of the membrane. As a first extension step, PSE simulations should be repeated using cylinders to represent stroma-exposed membranes and superimposed discs to depict stacks of grana in three dimensions.

This work provides a platform for future directions towards a thorough understanding of the protein dynamics in chloroplast membranes. It is clear that this field will continue to benefit from multidisciplinary approaches combining fluorescent imaging and computer simulations.

Bibliography

[1] K. Jacobson, A. Ishihara, and R. Inman. Lateral diffusion of proteins in membranes. *Annu. Rev. Physiol.* 49:163–175, 1987.

[2] S. J. Singer and G. L. Nicolson. The fluid mosaic model of the structure of cell membranes. *Science* 175(4023):720–731, 1972.

[3] S. Ramadurai, A. Holt, V. Krasnikov, G. van den Bogaart, J. A. Killian, and B. Poolman. Lateral diffusion of membrane proteins. *J. Am. Chem. Soc.* 131(35):12650–12656, 2009.

[4] S. Asakura and F. Oosawa. Interaction between particles suspended in solutions of macromolecules. *J. Polym. Sci.* 33(126):183–192, 1958.

[5] D. W. Tank, E. S. Wu, and W. W. Webb. Enhanced molecular diffusibility in muscle membrane blebs: Release of lateral constraints. *J. Cell Biol.* 92(1):207–212, 1982.

[6] T. Fujiwara, K. Ritchie, H. Murakoshi, K. Jacobson, and A. Kusumi. Phospholipids undergo hop diffusion in compartmentalized cell membrane. *J. Cell Biol.* 157(6):1071–81, 2002.

[7] N. Destainville, F. Dumas, and L. Salom. What do diffusion measurements tell us about membrane compartmentalisation? Emergence of the role of interprotein interactions. *J. Chem. Biol.* 1(1):37–48, 2008.

[8] E. Ikonen. Roles of lipid rafts in membrane transport. *Curr. Opin. Cell Biol.* 13(4):470–477, 2001.

[9] D. A. Brown and E. London. Structure and function of sphingolipid- and cholesterol-rich membrane rafts. *J. Biol. Chem.* 275(23):17221–17224, 2000.

[10] D. Lingwood and K. Simons. Lipid rafts as a membrane-organizing principle. *Science* 327(5961):46–50, 2010.

[11] B. M. Aizenbud and N. D. Gershon. Diffusion of molecules on biological membranes of nonplanar form II. Diffusion anisotropy. *Biophys. J.* 48:543–546, 1985.

[12] B. A. Smith, W. R. Clark, and H. M. Mcconnell. Anisotropic molecular motion on cell surfaces. *Proc. Natl. Acad. Sci. U. S. A.* 76:5641–5644, 1979.

[13] H. Krobath, G. J. Schütz, R. Lipowsky, and T. R. Weikl. Lateral diffusion of receptor-ligand bonds in membrane adhesion zones: Effect of thermal membrane roughness. *Europhys. Lett.* 78(3):38003, 2007.

[14] R. Parthasarathy and J. T. Groves. Curvature and spatial organization in biological membranes. *Soft Matter* 3(1):24–33, 2007.

[15] S. M. Leitenberger, E. Reister-Gottfried, and U. Seifert. Curvature coupling dependence of membrane protein diffusion coefficients. *Langmuir* 24(4):1254–1261, 2008.

[16] Y. Shibata, C. Voss, J. M. Rist, J. Hu, T. A. Rapoport, W. A. Prinz, and G. K. Voeltz. The reticulon and Dp1/Yop1p proteins form immobile oligomers in the tubular endoplasmic reticulum. *J. Biol. Chem.* 283(27):18892–18904, 2008.

[17] K. Keegstra and K. Cline. Protein import and routing systems of chloroplasts. *Plant Cell* 11(4):557–570, 1999.

[18] S. Curtis and M. Clegg. Molecular evolution of chloroplast DNA sequences. *Mol. Biol. Evol.* 1(4):291–301, 1984.

[19] C. Aldridge, P. Cain, and C. Robinson. Protein transport in organelles: Protein transport into and across the thylakoid membrane. *FEBS J.* 276(5):1177–1186, 2009.

[20] Y. Asakura, T. Hirohashi, S. Kikuchi, S. Belcher, E. Osborne, S. Yano, I. Terashima, A. Barkan, and M. Nakai. Maize mutants lacking chloroplast FtsY exhibit pleiotropic defects in the biogenesis of thylakoid membranes. *Plant Cell* 16(1):201–214, 2004.

[21] B. Essigmann, S. Guler, R. A. Narang, D. Linke, and C. Benning. Phosphate availability affects the thylakoid lipid composition and the expression of SQD1, a gene required for sulfolipid biosynthesis in Arabidopsis thaliana. *Proc. Natl. Acad. Sci. U. S. A.* 95(4):1950–1955, 1998.

[22] M. S. Webb and B. R. Green. Biochemical and biophysical properties of thylakoid acyl lipids. *Biochim. Biophys. Acta* 1060(2):133–158, 1991.

[23] B. D. Bruce. The role of lipids in plastid protein transport. *Plant Mol. Biol.* 38(1-2):223–246, 1998.

[24] L. A. Staehelin. Chloroplast structure: from chlorophyll granules to supramolecular architecture of thylakoid membranes. *Photosynth. Res.* 76(1-3):185–196, 2003.

[25] P. Dey, M. Brownleader, and J.B.Harborne. The plant, the cell and its molecular components. *Plant Biochemistry*, pp. 1–47. Academic Press, 1997.

[26] J. Paolillo, D. J. The three-dimensional arrangement of intergranal lamellae in chloroplasts. *J. Cell Sci.* 6(1):243–253, 1970.

[27] J. Brangeon and L. Mustardy. The ontogenetic assembly of intrachloroplastic lamellae viewed in 3-dimensions. *Biol. Cell* 36:71–80, 1979.

[28] L. Mustrdy, K. Buttle, G. Steinbach, and G. Garab. The three-dimensional network of the thylakoid membranes in plants: quasihelical model of the granum-stroma assembly. *Plant Cell* 20:2552–2557, 2008.

[29] B. Andersson and J. Anderson. Lateral heterogeneity in the distribution of chlorophyll-protein complexes of the thylakoid membranes of spinach chloroplasts. *Biochim. Biophys. Acta* 593:427–440, 1980.

[30] P. Arvidsson and C. Sundby. A model for the topology of the chloroplast thylakoid membrane. *Aust. J. Plant Physiol.* 26:687–694, 1999.

[31] K. R. Miller and L. A. Staehelin. Analysis of thylakoid outer surface - coupling factor is limited to unstacked membrane regions. *J. Cell Biol.* 68(1):30–47, 1976.

[32] H. Kirchhoff, W. Haase, S. Haferkamp, T. Schott, M. Borinski, U. Kubitscheck, and M. Rogner. Structural and functional self-organization of photosystem II in grana thylakoids. *BBA-Bioenergetics* 1767:1180–1188, 2007.

[33] J. M. Anderson. Photoregulation of the composition, function, and structure of thylakoid membranes. *Annu. Rev. Plant Phys.* 37:93–136, 1986.

[34] E. Shimoni, O. Rav-Hon, I. Ohad, V. Brumfeld, and Z. Reich. Three-dimensional organization of higher-plant chloroplast thylakoid membranes revealed by electron tomography. *Plant Cell* 17(9):2580–2586, 2005.

[35] J. M. Anderson. Changing concepts about the distribution of photosystems I and II between grana-appressed and stroma-exposed thylakoid membranes. *Photosynth. Res.* 73(1-3):157–164, 2002.

[36] H. Kirchhoff, I. Tremmel, W. Haase, and U. Kubitscheck. Supramolecular photosystem II organization in grana thylakoid membranes:¢ evidence for a structured arrangement¢. *Biochem.* 43(28):9204–9213, 2004.

[37] J. F. Allen and J. Forsberg. Molecular recognition in thylakoid structure and function. *Trends Plant Sci.* 6(7):317–326, 2001.

[38] M. Tikkanen, M. Nurmi, S. Kangasjärvi, and E.-M. Aro. Core protein phosphorylation facilitates the repair of photodamaged photosystem ii at high light. *BBA-Bioenergetics* 1777:1432–1437, 2008.

[39] U. K. Larsson, B. Jergil, and B. Andersson. Changes in the lateral distribution of the light-harvesting chlorophyll-a/b protein complex induced by its phosphorylation. *Eur. J. Biochem.* 136(1):25–29, 1983.

[40] O. Vallon, L. Bulte, P. Dainese, J. Olive, R. Bassi, and F. A. Wollman. Lateral redistribution of cytochrome b6/f complexes along thylakoid membranes upon state transitions. *Proc. Natl. Acad. Sci. U. S. A.* 88(18):8262–8266, 1991.

[41] Y. Munekage, M. Hashimoto, C. Miyake, K.-I. Tomizawa, T. Endo, M. Tasaka, and T. Shikanai. Cyclic electron flow around photosystem I is essential for photosynthesis. *Nature* 429(6991):579–582, 2004.

[42] J. Olive, O. Vallon, F. A. Wollman, M. Recouvreur, and P. Bennoun. Studies on the cytochrome b6/f complex .II. Localization of the complex in the thylakoid membranes from spinach and chlamydomonas-reinhardtii by immunocytochemistry and freeze-fracture analysis of b6/f mutants. *Biochim. Biophys. Acta* 851(2):239–248, 1986.

[43] K. Cline and C. Dabney-Smith. Plastid protein import and sorting: different paths to the same compartments. *Curr. Opin. Plant Biol.* 11(6):585–592, 2008.

[44] B. Agne and F. Kessler. Protein transport in organelles: The Toc complex way of preprotein import. *FEBS J.* 276(5):1156–1165, 2009.

[45] M. Oreb, I. Tews, and E. Schleiff. Policing Tic n Toc, the doorway to chloroplasts. *Trends Cell Biol.* 18(1):19 – 27, 2008.

[46] F. Kessler and D. Schnell. Chloroplast biogenesis: diversity and regulation of the protein import apparatus. *Curr. Opin. Cell Biol.* 21(4):494–500, 2009.

[47] K. Inoue, A. J. Baldwin, R. L. Shipman, K. Matsui, S. M. Theg, and M. Ohme-Takagi. Complete maturation of the plastid protein translocation channel requires a type I signal peptidase. *J. Cell Biol.* 171(3):425–430, 2005.

[48] J. Bédard and P. Jarvis. Recognition and envelope translocation of chloroplast preproteins. *J. Exp. Bot.* 56(419):2287–2320, 2005.

[49] S. Hirsch, E. Muckel, F. Heemeyer, G. von Heijne, and J. Soll. A receptor component of the chloroplast protein translocation machinery. *Science* 266(5193):1989–1992, 1994.

[50] P. Jarvis. Targeting of nucleus-encoded proteins to chloroplasts in plants. *New Phytol.* 179(2):257–285, 2008.

[51] K. H. Chen, X. J. Chen, and D. J. Schnell. Initial binding of preproteins involving the Toc159 receptor can be bypassed during protein import into chloroplasts. *Plant Physiol.* 122(3):813–822, 2000.

[52] B. Bölter, T. May, and J. Soll. A protein import receptor in pea chloroplasts, Toc86, is only a proteolytic fragment of a larger polypeptides. *FEBS Lett.* 441(1):59 – 62, 1998.

[53] F. Kessler and D. J. Schnell. A GTPase gate for protein import into chloroplasts. *Nature Struct. Biol.* 9(2):81–83, 2002.

[54] E. Schleiff, J. Soll, M. Kuchler, W. Kuhlbrandt, and R. Harrer. Characterization of the translocon of the outer envelope of chloroplasts. *J. Cell Biol.* 160(4):541–551, 2003.

[55] S. Qbadou, T. Becker, O. Mirus, I. Tews, J. Soll, and E. Schleiff. The molecular chaperone Hsp90 delivers precursor proteins to the chloroplast import receptor Toc64. *EMBO J.* 25(9):1836–1847, 2006.

[56] T. May and J. Soll. 14-3-3 proteins form a guidance complex with chloroplast precursor proteins in plants. *Plant Cell* 12(1):53–64, 2000.

[57] J. Soll and E. Schleiff. Protein import into chloroplasts. *Nat. Rev. Mol. Cell Biol.* 5(3):198–208, 2004.

[58] T. Becker, M. Jelic, A. Vojta, A. Radunz, J. Soll, and E. Schleiff. Preprotein recognition by the toc complex. *EMBO J.* 23(3):520–530, 2004.

[59] A. Hiltbrunner, J. Bauer, P. A. Vidi, S. Infanger, P. Weibel, M. Hohwy, and F. Kessler. Targeting of an abundant cytosolic form of the protein import receptor at Toc159 to the outer chloroplast membranes. *J. Cell Biol.* 154(2):309–316, 2001.

[60] J. Bauer, A. Hiltbrunner, P. Weibel, P. A. Vidi, M. Alvarez-Huerta, M. D. Smith, D. J. Schnell, and F. Kessler. Essential role of the G-domain in targeting of the protein import receptor atToc159 to the chloroplast outer membranes. *J. Cell Biol.* 159(5):845–854, 2002.

[61] B. Agne, S. Infanger, F. Wang, V. Hofstetter, G. Rahim, M. Martin, D. W. Lee, I. Hwang, D. Schnell, and F. Kessler. A Toc159 import receptor mutant, defective in hydrolysis of GTP, supports preprotein import into chloroplasts. *J. Biol. Chem.* 284(13):8661–8670, 2009.

[62] Y.-S. Teng, Y.-s. Su, L.-J. Chen, Y. J. Lee, I. Hwang, and H.-m. Li. Tic21 is an essential translocon component for protein translocation across the chloroplast inner envelope membranes. *Plant Cell* 18(9):2247–2257, 2006.

[63] B. Alberts, A. Johnson, J. Lewis, M. Raff, K. Roberts, and P. Walter. *Molecular biology of the cell*. Garland Science, New York, fourth edition, 2002.

[64] W. Wickner and R. Schekman. Protein translocation across biological membranes. *Science* 310(5753):1452–1456, 2005.

[65] M. Gutensohn, E. Fan, S. Frielingsdorf, P. Hanner, B. Hou, B. Hust, and R. B. Klosgen. Toc, Tic, Tat et al.: Structure and function of protein transport machineries in chloroplasts. *J. Plant Physiol.* 163(3):333–347, 2006.

[66] H. Mori and K. Cline. Post-translational protein translocation into thylakoids by the Sec and Δph-dependent pathways. *BBA-Mol. Cell. Res.* 1541(1-2):80–90, 2001.

[67] H. Mori and K. Ito. The Sec protein-translocation pathways. *Trends Microbiol.* 9(10):494–500, 2001.

[68] K. Cline and H. Mori. Thylakoid Δph-dependent precursor proteins bind to a cpTatC-Hcf106 complex before Tha4-dependent transport. *J. Cell Biol.* 154(4):719–730, 2001.

[69] U. Gohlke, L. Pullan, C. A. McDevitt, I. Porcelli, E. de Leeuw, T. Palmer, H. R. Saibil, and B. C. Berks. The TatA component of the twin-arginine protein transport system forms channel complexes of variable diameter. *Proc. Natl. Acad. Sci. U. S. A.* 102(30):10482–10486, 2005.

[70] D. J. Schnell and D. N. Hebert. Protein translocons: Multifunctional mediators of protein translocation across membranes. *Cell* 112(4):491–505, 2003.

[71] M. C. Leake, N. P. Greene, R. M. Godun, T. Granjon, G. Buchanan, S. Chen, R. M. Berry, T. Palmer, and B. C. Berks. Variable stoichiometry of the tata component of the twin-arginine protein transport system observed by in vivo single-molecule imaging. *Proc. Natl. Acad. Sci. U. S. A.* 105(40):15376–81, 2008.

[72] I. A. Sparkes, J. Runions, A. Kearns, and C. Hawes. Rapid, transient expression of fluorescent fusion proteins in tobacco plants and generation of stably transformed plants. *Nature Protoc.* 1:2019–2025, 2006.

[73] L. Pena, editor. *Transgenic plants: methods and protocols*. Humana Press, 2005.

[74] H. Morise, O. Shimomura, F. H. Johnson, and J. Winant. Intermolecular energy transfer in the bioluminescent system of aequorea. *Biochem.* 13(12):2656–2662, 1974.

[75] O. Shimomura, F. H. Johnson, and Y. Saiga. Extraction, purification and properties of aequorin, a bioluminescent protein from the luminous hydromedusan, *Aequorea*. *J. Cell. Compar. Physl.* 59(3):223–239, 1962.

[76] M. Orm, A. B. Cubitt, K. Kallio, L. A. Gross, R. Y. Tsien, and S. J. Remington. Crystal structure of the aequorea victoria green fluorescent proteins. *Science* 273(5280):1392–1395, 1996.

[77] D. P. Barondeau, C. J. Kassmann, J. A. Tainer, and E. D. Getzoff. Understanding GFP chromophore biosynthesis: Controlling backbone cyclization and modifying post-translational chemistry. *Biochem.* 44(6):1960–1970, 2005.

[78] K. R. Siemering, R. Golbik, R. Sever, and J. Haseloff. Mutations that suppress the thermosensitivity of green fluorescent protein. *Curr. Biol.* 6(12):1653–1663, 1996.

[79] J. Haseloff, K. R. Siemering, D. C. Prasher, and S. Hodge. Removal of a cryptic intron and subcellular localization of green fluorescent protein are required to mark transgenic Arabidopsis plants brightly. *Proc. Natl. Acad. Sci. U. S. A.* 94(6):2122–2127, 1997.

[80] G. Zhang, V. Gurtu, and S. R. Kain. An enhanced green fluorescent protein allows sensitive detection of gene transfer in mammalian cells. *Biochem. Biophys. Res. Commun.* 227(3):707–711, 1996.

[81] X. Li, G. Zhang, N. Ngo, X. Zhao, S. R. Kain, and C.-C. Huang. Deletions of the Aequorea victoria green fluorescent protein define the minimal domain required for fluorescence. *J. Biol. Chem.* 272::28545–28549., 1997.

[82] J. P. Marques, I. Dudeck, and R. B. Klosgen. Targeting of EGFP chimeras within chloroplasts. *Mol. Genet. Genomics* 269:381–387, 2003.

[83] H. Lodish, A. Berk, P. Matsudaira, C. A. Kaiser, M. Krieger, M. P. Scott, L. Zipursky, and J. Darnell. *Molecular cell biology*. New York : W. H. Freeman ; Basingstoke : Palgrave, 2003.

[84] A. Nenninger, G. Mastroianni, and C. W. Mullineaux. Size dependence of protein diffusion in the cytoplasm of Escherichia coli. *J. Bacteriol.* 192(18):4535–4540, 2010.

[85] B. Matsumoto, editor. *Methods in cell biology. Vol.38, Cell biological applications of confocal microscopy*. San Diego ; London : Academic Press, 1993.

[86] D. Axelrod, D. E. Koppel, J. Schlessinger, E. Elson, and W. W. Webb. Mobility measurement by analysis of fluorescence photobleaching recovery kinetics. *Biophys. J.* 16(9):1055–1069, 1976.

[87] D. M. Soumpasis. Theoretical analysis of fluorescence photobleaching recovery experiments. *Biophys. J.* 41(1):95–97, 1983.

[88] B. M. Aizenbud and N. D. Gershon. Diffusion of molecules on biological membranes of nonplanar form a theoretical study. *Biophys. J.* 38:287–293, 1982.

[89] J. Ellenberg, E. D. Siggia, J. E. Moreira, C. L. Smith, J. F. Presley, H. J. Worman, and J. Lippincott-Schwartz. Nuclear membrane dynamics and reassembly in living cells: Targeting of an inner nuclear membrane protein in interphase and mitosis. *J. Cell Biol.* 138:11931206, 1997.

[90] P. Degond and S. Mas-Gallic. The weighted particle method for convection-diffusion equations: Part 1: The case of an isotropic viscosity. *Math. Comput.* 53:485–507, 1989.

[91] P. Degond and S. Mas-Gallic. The weighted particle method for convection-diffusion equations: Part 2: The anisotropic case. *Math. Comput.* 53:509–525, 1989.

[92] S. A. Jobling and L. Gehrke. Enhanced translation of chimeric messenger-rnas containing a plant viral untranslated leader sequence. *Nature* 325(6105):622–625, 1987.

[93] L. M. Tabe, T. Wardleyrichardson, A. Ceriotti, A. Aryan, W. Mcnabb, A. Moore, and T. J. V. Higgins. A biotechnological approach to improving the nutritive-value of alfalfa. *J. Anim. Sci.* 73(9):2752–2759, 1995.

[94] D. O. Hall and K. Rao. *Photosynthesis*. Cambridge University Press, 1994.

[95] C. Koncz, N.-H. Chua, and J. Schell, editors. *Methods in Arabidopsis research*. World Scientific, Singapore, 1992.

[96] Y. Asakura, S. Kikuchi, and M. Nakai. Non-identical contributions of two membrane-bound cpSRP components, cpFtsY and Alb3, to thylakoid biogenesis. *Plant J.* 56:1007–1017, 2008.

[97] T. K. Goral, M. P. Johnson, A. P. Brain, H. Kirchhoff, A. V. Ruban, and C. W. Mullineaux. Visualizing the mobility and distribution of chlorophyll proteins in higher plant thylakoid membranes: effects of photoinhibition and protein phosphorylation. *Plant J.* 62(6):948–959, 2010.

[98] E. Consoli, R. Croce, D. Dunlap, and L. Finzi. Diffusion of light-harvesting complex II in the thylakoid membranes. *EMBO Rep.* 6:782–786, 2005.

[99] H. Kirchhoff, S. Haferkamp, J. F. Allen, D. B. Epstein, and C. W. Mullineaux. Protein diffusion and macromolecular crowding in thylakoid membranes. *Plant Physiol.* 146(4):1571–1578, 2008.

[100] F.-J. Kao, Y.-M. Wang, J.-C. Chen, P.-C. Cheng, R.-W. Chen, and B.-L. Lin. Micro-spectroscopy of chloroplasts in protoplasts from Arabidopsis thaliana under single- and multi-photon excitations. *J. Lumin.* 98(1-4):107–114, 2002.

[101] A. Di Cola and C. Robinson. Large-scale translocation reversal within the thylakoid Tat system in vivo. *J. Cell Biol.* 171(2):281–289, 2005.

[102] E. Vladimirou, M. Li, C. P. Aldridge, L. Frigerio, M. Kirkilionis, and C. Robinson. Diffusion of a membrane protein, Tat subunit Hcf106, is highly restricted within the chloroplast thylakoid network. *FEBS Lett.* 583(22):3690–3696, 2009.

[103] C. W. Mullineaux. FRAP analysis of photosynthetic membranes. *J. Exp. Bot.* 55(400):1207–1211, 2004.

[104] I. F. Sbalzarini, A. Mezzacasa, A. Helenius, and P. Koumoutsakos. Effects of organelle shape on fluorescence recovery after photobleaching. *Biophys. J.* 89(3):1482–1492, 2005.

[105] F. Drepper, I. Carlberg, B. Andersson, and W. Haehnel. Lateral diffusion of an integral membrane protein: Monte Carlo analysis of the migration of phosphorylated light-harvesting complex II in the thylakoid membranes. *Biochem.* 32(44):11915–11922, 1993.

[106] M. J. Saxton. Lateral diffusion in an archipelago: The effect of mobile obstacles. *Biophys. J.* 52:989–997, 1987.

[107] H. Kirchhoff, S. Lenhert, C. Buchel, L. Chi, and J. Nield. Probing the organization of photosystem II in photosynthetic membranes by atomic force microscopy. *Biochem.* 47(1):431–440, 2008.

[108] H. R. Munro, Sean; Pelham. A C-terminal signal prevents secretion of luminal ER proteins. *Cell* 48:899 – 907, 1987.

[109] I. F. Sbalzarini, A. Hayer, A. Helenius, and P. Koumoutsakos. Simulations of (an)isotropic diffusion on curved biological surfaces. *Biophys. J.* 90(3):878–885, 2006.

[110] Y. J. Lee, D. H. Kim, Y.-W. Kim, and I. Hwang. Identification of a signal that distinguishes between the chloroplast outer envelope membrane and the endomembrane system in vivo. *Plant Cell* 13(10):2175–2190, 2001.

[111] J. Kiessling, S. Kruse, S. A. Rensing, K. Harter, E. L. Decker, and R. Reski. Visualization of a cytoskeleton-like FtsZ network in chloroplasts. *J. Cell Biol.* 151(4):945–950, 2000.

[112] A. Martin, D. Lang, S. T. Hanke, S. J. X. Mueller, E. Sarnighausen, M. Vervliet-Scheebaum, and R. Reski. Targeted gene knockouts reveal overlapping functions of the five *Physcomitrella patens* FtsZ isoforms in chloroplast division, chloroplast shaping, cell patterning, plant development, and gravity sensing. *Mol. Plant* 2(6):1359–1372, 2009.

[113] P. A. Millner, R. A. C. Mitchell, D. J. Chapman, and J. Barber. Fluidity properties of isolated chloroplast thylakoid lipids. *Photosynth. Res.* 5(1):63–76, 1984.

[114] E. Lam. Nucleic acids and proteins. *Plant Biochemistry*, pp. 315–350. Academic Press, 1997.

[115] N. Ray, A. Nenninger, C. Mullineaux, and C. Robinson. Location and mobility of twin-arginine translocase subunits in the Escherichia coli plasma membranes. *Biol. Chem.* 280:17961–17968, 2005.

[116] P. Hinterdorfer and Y. F. Dufrene. Detection and localization of single molecular recognition events using atomic force microscopy. *Nat. Methods* 3(5):347–355, 2006.

[117] R. Swaminathan, C. P. Hoang, and A. S. Verkman. Photobleaching recovery and anisotropy decay of green fluorescent protein GFP-S65T in solution and cells: cytoplasmic viscosity probed by green protein translation and rotational diffusion. *Biophys. J.* 72:1900–1907, 1997.

[118] M. B. Elowitz, M. G. Surette, P. E. Wolf, J. B. Stock, and S. Leibler. Protein mobility in the cytoplasm of Escherichia coli. *J. Bacteriol.* 181(1):197–203, 1999.

[119] C. W. Mullineaux, A. Nenninger, N. Ray, and C. Robinson. Diffusion of green fluorescent protein in three cell environments in Escherichia coli. *J. Bacteriol.* 188(10):3442–3448, 2006.

[120] B. L. Sprague, R. L. Pego, D. A. Stavreva, and J. G. McNally. Analysis of binding reactions by fluorescence recovery after photobleaching. *Biophys. J.* 86(6):3473–3495, 2004.

[121] B. L. Sprague and J. G. McNally. FRAP analysis of binding: proper and fitting. *Trends Cell Biol.* 15(2):84–91, 2005.

[122] T. J. Feder, I. BrustMascher, J. P. Slattery, B. Baird, and W. W. Webb. Constrained diffusion or immobile fraction on cell surfaces: A new interpretation. *Biophys. J.* 70(6):2767–2773, 1996.

[123] N. Periasamy and A. S. Verkman. Analysis of fluorophore diffusion by continuous distributions of diffusion coefficients: Application to photobleaching measurements of multicomponent and anomalous diffusion. *Biophys. J.* 75(1):557–567, 1998.

[124] K. Braeckmans, L. Peeters, N. N. Sanders, S. C. De Smedt, and J. Demeester. Three-dimensional fluorescence recovery after photobleaching with the confocal scanning laser microscope. *Biophys. J.* 85(4):2240–2252, 2003.

A

Model fitting results to experimental FRAP data

The following tables are the result of fitting analytical models to the data from FRAP experiments from Chapters 3 and 5. Note that the Soumpasis model fits for the Hcf106-GFP and autofluorescence FRAP data on thylakoids are for comparison only because the thylakoid membrane does not satisfy the assumptions of the model.

	Construct	D ($\mu m^2/s$)	s.e.	p	s.e.
endogenous Toc159 with GFP-Toc159GM	1	0.26	0.25	0.25	0.081
ppi2 mutation with GFP-Toc159GM	2	0.022	0.0060	0.89	0.043
ppi2 mutation with GFP-Toc159GM D946N	3	0.027	0.0081	0.86	0.038

Table A.1: Diffusion coefficient D and asymptotic recovery p for Toc159 constructs from Ellenberg model fits, with standard errors.

	D ($\mu m^2/s$)	s.e.	p	s.e.
Hcf106-GFP	0.0022	5.4×10^{-4}	0.37	0.017
Autofluorescence	8.1×10^{-4}	4.4×10^{-5}	0.51	0.046

Table A.2: Diffusion coefficient D and asymptotic recovery p for Hcf106-GFP and autofluorescence from Soumpasis model fits, with standard errors.

	τ (s^{-1})	s.e.	p	s.e.
Hcf106-GFP	0.20	0.041	0.12	0.019
Autofluorescence	0.088	0.013	0.17	0.048

Table A.3: Timescale τ and asymptotic recovery p for Hcf106-GFP and autofluorescence from exponential model fits, with standard errors.

Experiment	D ($\mu m^2/s$)	Reference
FRAP of GFP in aqueous buffer	87	[117]
FRAP of GFP in cytoplasm of *E. coli*	7.7	[118]
FRAP of TatA-GFP in plasma membrane	0.13	[119]
Single-particle tracking of phosphorylated LHCII in stromal lamellae of thylakoid membrane	0.027	[98]
FRAP of chlorophyll-containing protein complexes in grana patches	0.0046	[99]

Table A.4: A selection of experimentally obtained diffusion coefficients D relevant to this study.

B

PSE diffusion results

In this appendix the result of fitting PSE simulations to experimental data are presented for both Hcf106 and autofluorescence.

B.1 Hcf106

The following are diffusion coefficients resulting from PSE simulation fits to Hcf106 FRAP data, with residual sum of square errors (RSS).

Experiment	D $\mu m^2/s$	RSS
A	0.00475	0.184
B	0.00707	0.279
C	0.0148	0.124
D	0.0416	0.056
E	0.00926	0.241
F	0.00603	0.155
G	0.00504	0.174
H	0.00594	0.123
I	0.0132	0.305

Table B.1: Fitted diffusion coefficients for PSE Hcf106 FRAP simulations with uniform diffusion (3 s.f.). The mean is $\bar{D} = 0.012 \pm 0.004\,\mu m^2/s$ ($n = 9$, $\pm$ is standard error).

Experiment	D_l μm^2/s	RSS
A	1.97	2.09
B	1.92	3.18
C	0.228	0.0752
D	1.95	2.85
E	1.98	2.88
F	0.0109	0.0230
G	1.97	0.0434
H	1.99	0.954
I	1.99	0.602

Table B.2: Fitted diffusion coefficients for PSE Hcf106 FRAP simulations with diffusion restricted to the stromal lamellae (3 s.f.). The mean is $\bar{D}_l = 1.6 \pm 0.2$ μm^2/s ($n = 9$, ± is standard error).

Experiment	D_l (μm^2/s)	D_g (μm^2/s)	RSS
A	0.0408	0.00408	0.180
B	0.0522	0.00522	0.237
C	0.162	0.0162	0.132
D	0.208	0.0208	0.0538
E	0.0720	0.00720	0.250
F	0.0659	0.00659	0.165
G	0.0315	0.00315	0.137
H	0.0272	0.00272	0.115
I	0.0765	0.00765	0.237

Table B.3: Fitted diffusion coefficients for PSE Hcf106 FRAP simulations with ten-fold slower diffusion in grana (ratio 10) (3 s.f.). The mean is $\bar{D}_l = 0.082 \pm 0.020$ μm^2/s ($n = 9$, ± is standard error).

Experiment	D_l (μm^2/s)	D_g (μm^2/s)	RSS
A	0.399	0.00399	0.176
B	0.499	0.00499	0.220
C	0.940	0.00940	0.321
D	0.926	0.00926	0.279
E	0.697	0.00697	0.245
F	0.667	0.00667	0.166
G	0.293	0.00293	0.131
H	0.230	0.00230	0.0896
I	0.727	0.00727	0.228

Table B.4: Fitted diffusion coefficients for PSE Hcf106 FRAP simulations with hundred-fold slower diffusion in grana (ratio 100) (3 s.f.). The mean is $\bar{D}_l = 0.60 \pm 0.09$ μm^2/s ($n = 9$, ± is standard error).

B.2 Autofluorescence

The following are diffusion coefficients resulting from PSE simulation fits to autofluorescence FRAP data, with residual sum of square errors (RSS).

Experiment	D $\mu m^2/s$	RSS
A	0.00966	0.0250
B	0.0471	0.316
C	0.0200	0.0636
D	0.0125	0.0337
E	0.0291	0.101
F	0.0370	0.0468
G	0.0174	0.0467

Table B.5: Fitted diffusion coefficients for PSE autofluorescence FRAP simulations with uniform diffusion (3 s.f.). The mean is $\bar{D} = 0.025 \pm 0.005\,\mu m^2/s$ ($n = 9$, $\pm$ is standard error).

Experiment	D_l $\mu m^2/s$	RSS
A	3.82	3.91
B	4.99	2.05
C	4.99	6.20
D	3.82	0.198
E	4.96	2.41
F	4.72	0.284
G	1.97	1.41

Table B.6: Fitted diffusion coefficients for PSE autofluorescence FRAP simulations with diffusion restricted to stroma-exposed lamellae (3 s.f.). Note, due to a very poor fit, these simulations did not finish optimising. The mean is $\bar{D}_l = 3.1 \pm 0.4\,\mu m^2/s$ ($n = 9$, $\pm$ is standard error).

Experiment	D_g μm^2/s	RSS
A	3.09	0.989
B	3.82	4.88
C	3.09	4.54
D	1.18	1.91
E	3.82	3.25
F	1.37	0.278
G	4.55	4.08

Table B.7: Fitted diffusion coefficients for PSE autofluorescence FRAP simulations with diffusion restricted to grana (3 s.f.). Note, due to a very poor fit, these simulations did not finish optimising. The mean is $\bar{D_g} = 3.0 \pm 0.5$ μm^2/s ($n = 9$, ± is standard error).

Experiment	D_l (μm^2/s)	D_g (μm^2/s)	RSS
A	0.236	0.0236	0.750
B	0.236	0.0236	0.296
C	0.165	0.0165	0.0592
D	0.135	0.0135	0.0376
E	0.190	0.0190	0.0694
F	0.0169	0.00169	0.0445
G	0.127	0.0127	0.0400

Table B.8: Fitted diffusion coefficients for PSE autofluorescence FRAP simulations with ten-fold slower diffusion in grana (ratio 10) (3 s.f.). The mean is $\bar{D_l} = 0.16 \pm 0.03$ μm^2/s ($n = 9$, ± is standard error).

Experiment	D_l (μm^2/s)	D_g (μm^2/s)	RSS
A	0.818	0.00818	0.0269
B	0.982	0.00982	0.616
C	0.915	0.00915	0.370
D	0.966	0.00966	0.130
E	0.137	0.00137	0.0349
F	0.977	0.00977	0.0874

Table B.9: Fitted diffusion coefficients for PSE autofluorescence FRAP simulations with hundred-fold slower diffusion in grana (ratio 100) (3 s.f.). The mean is $\bar{D_l} = 0.82 \pm 0.11$ μm^2/s ($n = 9$, ± is standard error).

C

Extended FRAP models

C.1 FRAP analysis of diffusion plus binding

FRAP is also used to investigate dynamic molecular interactions that take place in cellular processes. Sprague and colleagues [120] have derived a general model for the case where diffusion and single binding reactions co-exist.

C.1.1 The general model

The reversible binding of protein to vacant binding sites can be expressed as

$$F + S \underset{k_{\text{off}}}{\overset{k_{\text{on}}}{\rightleftharpoons}} C \tag{C.1}$$

where F is the free protein, S are the vacant binding sites, C are the bound complexes and k_{off} and k_{on} the on- and off- rates respectively.

Taking the amount of free protein F to be f, of vacant binding sites S to be s and of bound complexes C to be c then the three coupled reaction-diffusion equations are

$$\frac{\partial f}{\partial t} = D_f \nabla^2 f - k_{\text{on}} f s + k_{\text{off}} c \tag{C.2a}$$

$$\frac{\partial s}{\partial t} = D_s \nabla^2 s - k_{\text{on}} f s + k_{\text{off}} c \tag{C.2b}$$

$$\frac{\partial c}{\partial t} = D_c D_c \nabla^2 c + k_{\text{on}} f s - k_{\text{off}} c \tag{C.2c}$$

Using the assumption that the biological system has reached equilibrium before photobleaching, F, S and C become F_{eq}, S_{eq} and C_{eq} representing the respective equilibrium concentrations. Although bleaching changes the number of free and

complexed molecules, the number of free binding sites stays constant $s = S_{eq}$ and $\partial s/\partial t = 0$. It is also assumed that the complexes are immobile on the time and length scale of the FRAP measurement, i.e. $D_c = 0$.

Hence, the three equation reaction-diffusion system reduces to

$$\frac{\partial f}{\partial t} = D_f \nabla^2 f - k^*_{on} f + k_{off} c \tag{C.3a}$$

$$\frac{\partial c}{\partial t} = k^*_{on} f - k_{off} c \tag{C.3b}$$

where $k_{on} S_{eq} = k^*_{on}$ is defined as a pseudo-first order rate constant.

C.1.2 Solving the reaction-diffusion system

Using a Laplace transform, the solution to the reaction-diffusion system is calculated for the case of a circular bleach. The bleached area is small compared to the size of fluorescent compartment and the fluorescent molecules are homogeneously distributed.

The average of the Laplace transform of the fluorescent intensity within the bleach spot is given by

$$\hat{f}(p) = \frac{1}{p} - \frac{F_{eq}}{p}[1 - 2K_1(qw)I_1(qw)]\left(1 + \frac{k^*_{on}}{p + k_{off}}\right) - \frac{C_{eq}}{p + k_{off}} \tag{C.4}$$

where q depends on k^*_{on}, k_{off} and D_f, w is the radius of the bleach spot, I_1 and K_1 are modified Bessel functions of the first and second kind and p is the Laplace variable that inverts to yield time. The predicted FRAP recovery can be computed numerically by inversion. This model can also be extended for the case of multiple binding sites [120].

C.1.3 Single binding state: Diffusion-uncoupled case

When the diffusion is very fast compared to binding at the timescale of the FRAP measurement, the fluorescence recovery can be separated into two phases. Free molecules instantly equilibrate after the bleach during a very rapid diffusive phase (typically less than 1 s) whereas recovery due to exchange at binding sites occurs over a slower period of seconds or minutes.

The total fluorescence recovery over time depends on C_{eq} and k_{off} and is given by the relation

$$f(t) = 1 - C_{eq} \exp^{-k_{off} t} \tag{C.5}$$

The values for C_{eq} and k_{off} can be extracted from fitting C.5 to the data which

can then be used to calculate the association constant k_{on}.

C.1.4 Effective diffsuion: Diffusion-coupled case

When the association time with the binding site is much faster than the time required to diffuse across the bleach spot, then fitting the pure diffusion model (1.19) is suitable. Inevitably, the diffusion rate, determined by the strength of binding, will be slower than the diffusion constant of unconjugated molecules.

The effective diffusion representing the slowed diffusion due to binding is given by

$$D_{\text{eff}} = \frac{D_f}{1 + k^*_{\text{on}}/k_{\text{off}}} \tag{C.6}$$

where D_f is the measured diffusion constant of the molecule in the absence of binding and k^*_{on} and k_{off} are, respectively, the off and pseudo-on rates as defined previously.

If the pure diffusion model is fitted to the data then the D_{eff} can be extracted from

$$t_D = \frac{w^2}{4D_{\text{eff}}} \tag{C.7}$$

Using C.6 the ratio $k^*_{\text{on}}/k_{\text{off}}$ can then be obtained.

The effective diffusion model does not allow independent estimates of the association and dissociation rates but only their ratio. Moreover, the existence of more than one binding state can be hindered as long as the sum of ratios of the individual association to dissociation rates equals the association dissociation rate of a single binding state. In other words, in the effective diffusion regime, the FRAP fit yields a predicted ratio of association rates to off rates that might reflect either a single binding state or the sum of several binding states [120, 121].

C.2 Modelling anomalous diffusion

The conventional FRAP recovery curve analysis assumes free random motion and the existence of an immobile diffusing species. However, FRAP is an ensemble method, i.e. looking at the average motions of thousands of particles thus masking the details of individual motions. Single particle tracking studies have revealed restricted, time-dependent motions which suggests the need for re-appraisal of FRAP data interpretation. Instead of assuming random diffusion with an immobile fraction, the motion might be better explained by complete but restricted mobility, or anomalous subdiffusion [122].

Anomalous diffusion is random lateral motion with potential energy traps. Molecules may remain stranded for short periods while diffusing. In cell mem-

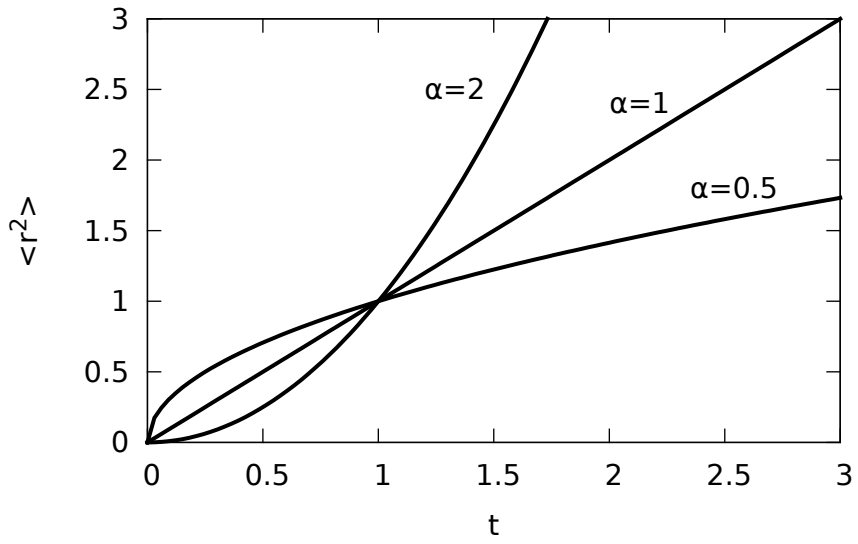

Figure C.1: Normal ($\alpha = 1$), sub-anomalous ($\alpha < 1$) and super-anomalous ($\alpha > 1$) diffusion.

branes, anomalous diffusion may be a result of both obstacles to diffusion, such as membrane heterogeneities or rafts, and binding traps with a distribution of binding energies or escape times [106].

In anomalous diffusion, the mean square displacement follows power law in time, instead of proportional in time like the normal diffusion case i.e.

$$< r^2 > \propto \Gamma t^{\alpha} = 4D(t)t \quad \text{with} \quad D(t) = \frac{1}{4}\Gamma t^{\alpha-1} \tag{C.8}$$

where Γ is the transport coefficient. Anomalous diffusion can be classified as subdiffusive when $\alpha < 1$ and superdiffusive when $\alpha > 1$ [123].

In order to test the hypothesis of anomalous diffusion Feder and colleagues solved the diffusion equation for a Gaussian beam following the approach summarised in [86]. They incorporated the time dependence relation C.8 and an immobile fraction.

$$F(t) = \left[F^0 \sum_{n=1}^{\infty} \frac{(-k)^n}{n!} \frac{1}{1 + n(1 + 2(t/\tau)^{\alpha})} \right] R + (1 - R)F_0 \tag{C.9}$$

where F^0 denotes the fluorescence intenisty before bleaching and F_0 is the fluorescence intensity immediately after bleaching, k is related to the bleach depth, R is the mobile fraction and τ is the characteristic time defined in terms of the transport coefficient Γ and beam radius w such as $\tau = (w^2/\Gamma)^{1/\alpha}$.

Feder et al. [122] measured the motion of fluorescently labeled immunoglobulin E complexed to high affinity receptors (FcERI) on rat basophilic leukemia cells

using both FRAP and single particle tracking. The latter revealed that 56% exhibit anomalous subdiffusion, 10% Brownian motion and 27% are immobile, while fitting both free diffusion with an immobile fraction and anomalous subdiffusion models to FRAP showed equally good fits. Periasamy and colleagues have developed and experimentally validated a method for detecting anomalous diffusion in FRAP data. The methods introduces the idea that fluorescence recovery data, $F(t)$, can be modeled as a continuous distribution of diffusion coefficients, $\alpha(D)$ by utilizing the maximum entropy method (MEM) [123]. While, with an appropriate analysis, FRAP data can reveal anomalous diffusion, single molecule techniques are needed to resolve this behaviour more effectively.

C.3 Three-dimensional FRAP

The models presented in the preceeding sections assume a two-dimensional motion in the lipid bilayer. However molecules may exhibit motion along the axial direction and therefore, 2D models could yield inaccurate diffusion coefficients. This issue may be addressed by the development of models incorporating the three-dimensional nature of cellular compartments. The fluorophore concentration distribution at time t can be calculated by solving the diffusion equation in cylindrical coordinates

$$\frac{\partial C(r,z,t)}{\partial t} = D\left[\left(\frac{\partial^2}{\partial r^2} + \frac{1}{r}\frac{\partial}{\partial r}\right)C(r,z,t) + \frac{\partial^2 C(r,z,t)}{\partial z^2}\right] \tag{C.10}$$

Braeckmans and colleagues used this approach to derive an equation for $F(t)$ for cylindrical disk and were able to fit the model to FRAP data for FITC-dextrans in the vitreous body of a bovine eye [124].

D

PSE code

In this Appendix MATLAB code listings are provided for the software used to generate thylakoid networks, perform particle strength exchange (PSE) simulations, and fit simulations to data.

D.1 Simulation fitting

Use nonlinear least-squares to find the diffusion constant D which minimises the error between the PSE simulation results, from `pse_simulation_integration.m`, and experimental data.

Listing D.1: `minimise_lsq.m`

```
1  function minD=minimise_lsq(bracket,datafile,location,exp_name,
       sim_type)
2  % bracket : [minD maxD] to search within
3  % datafile : name within setup_dir of experimental data file
4  % location : machine simulation is running
5  % exp_name : name of experiment, e.g. FRAP_002
6  % sim_type : simulation type (uniform,restricted,grestricted,
       ratio10,ratio100)
7  % Returns : best fitting D
8
9  % Data directory
10 setup_dir = setup_path(location);
11
12 % Experimental data file
13 exp=load([setup_dir datafile]);
14
```

```
15 % Setup simulation
16 setup_file = [setup_dir exp_name '_setup.mat'];
17 S=load(setup_file);
18 mkdir(setup_dir,sim_type);
19 result_dir = [setup_dir sim_type '/']; % must end with slash
20 sim_dir = [S.sim_name '_bisect/']; % must end with slash
21 mkdir(result_dir,sim_dir); % Make output directory
22 network_file=[setup_dir 'network_' S.sim_name '.mat']; % Network
       data file
23
24 % Check simulation type
25 if strcmp(sim_type,'restricted')
26   restriction=1;
27 elseif strcmp(sim_type,'grestricted');
28   restriction=2;
29 else
30   restriction=0;
31 end
32
33 n=200; % Particle grid dimension
34 Tstart=exp.time(1); % Simulation start time
35 Tend=exp.time(end); % Simulation end time
36 num_images=40; % Number of snapshot images to form
37 j=1; % Iteration count
38
39 % Setup PSE
40 pse_struct=pse_simulation_setup(n,network_file,S,restriction);
41
42 % Draw network
43 figure(1)
44 clf
45 network=load(network_file);
46 plot_network_overlay(network,[setup_dir S.image_name],S.croprect
      ,[S.x_c S.y_c S.r_c]);
47 saveas(gcf,[result_dir sim_dir 'network.pdf'],'pdf');
48
49 % Store current D bracket in case of restart
50 checkfilename=[result_dir sim_dir 'bisectcheckpoint.mat'];
51 if exist(checkfilename,'file')==2
52     checkpoint=load(checkfilename);
53     if size(checkpoint.flist,2)>=3 % need at least three points
```

```
        to bracket
54          flist=checkpoint.flist;
55          Dlist=checkpoint.Dlist;
56          j=checkpoint.j+1;
57          % Use previous results to pick bracket
58          [c,i]=min(flist); % index of min flist value
59          if i==1
60              bracket=[Dlist(1) Dlist(2)]; % Minimum at left edge
61          elseif i==size(flist,2)
62              bracket=[Dlist(i-1) Dlist(i)]; % Minimum at right
                    edge
63          else
64              % Pick smallest neighbouring flist value to bracket
                    with
65              if flist(i+1)>flist(i-1)
66                  bracket=[Dlist(i-1) Dlist(i)];
67              else
68                  bracket=[Dlist(i) Dlist(i+1)];
69              end
70          end
71          fprintf('Checkpoint found. Using bracket [%f,%f] and
                starting iteration %d\n',bracket(1),bracket(2),j);
72      else
73          fprintf('Checkpoint found, but not enough values to
                constrain bracket\n');
74      end
75  else
76      fprintf('Checkpoint not found. Using bracket [%f,%f]\n',
            bracket(1),bracket(2));
77  end
78
79  if bracket(1)>bracket(2)
80      error('bracket(1) must be less than bracket(2)');
81  end
82
83  % Setup optimisation algorithm
84  max_sims=40; % Maximum simulation evaluation count
85  minopts=optimset('OutputFcn',@checkpointfn,'MaxFunEval',max_sims
        ,'Display','iter','TolX',1e-4);
86
87  % Run optimisation algorithm
```

```
88 [minD,lsqerr,exitflag,output]=fminbnd(@run_sim,bracket(1),
       bracket(2),minopts);
89 if exitflag<0
90     error('fminbnd error %d occurred\n',exitflag);
91 end
92
93 fprintf('Closest fitting D: %f\n',minD);
94 fprintf('Least-squared error: %f\n',lsqerr);
95 fprintf('Number of iterations: %d\n',output.iterations);
96 fprintf('Number of simulations run: %d\n',output.funcCount);
97
98 % Nested simulation running function
99 % Returns the least-squared residual error against the
       experimental data
100 function lsqerr=run_sim(D2)
101     % Choose grana diffusion constant
102     if strcmp(sim_type,'ratio10')
103         D=0.1*D2;
104     elseif strcmp(sim_type,'ratio100')
105         D=0.01*D2;
106     else
107         D=D2;
108     end
109
110     % Run simulation
111     fprintf('Running %s simulation for D=%f\n',sim_type,D2);
112     [t,frap]=pse_simulation_integration(pse_struct,Tstart,Tend,D
           ,D2,result_dir,sim_dir,num_images);
113     fprintf('Simulation completed.\n');
114
115     % Plot recovery curve
116     plot(t,frap,'k-',exp.time,exp.normalised_intensities,'xr')
117     xlabel('Time','fontsize',18)
118     ylabel('Relative intensity','fontsize',18)
119     set(gca,'tickdir','out','fontsize',18)
120     set(gca, 'Box', 'off' );
121     saveas(gcf,[result_dir sim_dir 'recovery.pdf']);
122
123     % Least-squares error
124     lsqerr=lsq([t frap],[exp.time exp.normalised_intensities]);
125     fprintf('Iteration %d least-squared error: %f\n',j,lsqerr);
```

```
126
127     % Increment iteration counter
128     j=j+1;
129 end
130
131 % Nested checkpointing function
132 % Saves a mat-file with the current results and iteration number
133 function stop=checkpointfn(D, optimValues, state)
134     stop=false;
135     switch state
136         case 'iter'
137             [Dlist, si]=sort([Dlist D]); % keep D in right order
138             flist=[flist optimValues.fval]; % store current
                    residual
139             flist=flist(si); % use sort indices from Dlist to
                    sort flist
140             save(checkfilename,'j','Dlist','flist');
141         otherwise
142     end
143 end
144
145 end
```

D.2 PSE simulation

Integrates the PSE equations to perform a simulation, using the PSE structures created by `pse_simulation_setup.m`. Generates an image of the current simulation state at regular intervals and uses this to calculate the intensity within the ROI.

Listing D.2: `pse_simulation_integration.m`

```
1 function [t,frap,err]=pse_simulation_integration(ps,Tstart,Tend,
      D,D2,result_dir,sim_dir,number_of_images)
2 % ps : PSE simulation structure provided by pse_simulation_setup
      .m
3 % Tstart : initial time of simulation
4 % Tend : final time of simulation
5 % D : diffusion constant in lamellae
6 % D2 : diffusion constant in grana
7 % result_dir : main output directory
8 % sim_dir : simulation results subdirectory
```

```
% number_of_images : # of snapshot images to make
if nargin==7
    number_of_images=50; % default # snapshot images and data points for simulation output
end
NP=ps.NP; % # particles
NM=ps.NM; % # mirror particles
NC=ps.NC; % # cells
deltaT=0.1*ps.h^2/(4*max(D,D2)); % timestep
if Tstart>0 && deltaT>Tstart
    deltaT=Tstart;
end

% Set up image output pixel matrix
image_data=zeros(ps.image_pixels);
image_num=0;

% Normalisation constants
a=4/(ps.epsilon^2*pi);
c1=a*(ps.h^2*D*deltaT)/ps.epsilon^2;
c2=a*(ps.h^2*D2*deltaT)/ps.epsilon^2;

% Sum total strength for conservation check
current_strengths=ps.current_strength;
total_strength_before=sum(current_strengths);
new_strengths=zeros(NP+NM,1); % Vector of particle strengths

number_of_steps=ceil((Tend-Tstart)/deltaT); % # integration steps
snapshot_step=max(1,floor(number_of_steps/(number_of_images-1))); % how many integration steps per snapshot
number_of_steps=number_of_steps+snapshot_step; % Make sure to take snapshot at t>=Tend (otherwise interpolation with experiment data doesn't work)
assert(number_of_steps>0);
frap=zeros(min(number_of_steps,number_of_images),1);
t=zeros(min(number_of_steps,number_of_images),1);
fprintf('simulating %d steps with deltaT=%f...\n',number_of_steps,deltaT);

% Loop over time
```

```
44 current_time=Tstart;
45 for i=1:number_of_steps
46         if mod(i,100000)==0
47             fprintf('%d steps\n',i)
48         end
49         % At this point to write to output file:
50         %   image data for current strength
51         %   frap intensity of ROI
52         if mod(i-1,snapshot_step)==0
53             image_num=image_num+1;
54
55             % Build image pixel by pixel
56             fprintf('Forming image %d...',image_num);
57             for ii=1:length(ps.image_x)
58                 for jj=1:length(ps.image_y)
59                     % Sum pixel strength contributions for each
                          particle
60                     pixel_strength=0;
61                     for p=1:NP
62                         s_p=current_strengths(p);
63                         d_p=(ps.image_x(ii)-ps.particles(p,1))
                              ^2+(ps.image_y(jj)-ps.particles(p,2))
                              ^2; % Pixel-particle distance
64                         pixel_strength=pixel_strength+exp(-d_p*
                              ps.ib)*s_p; % Gaussian distance
                              weighting
65                     end
66                     % Store pixel value in image
67                    image_data(jj,ii)=pixel_strength;
68                 end
69             end
70             fprintf('done\n');
71
72             if image_num==1
73                 % Fix the intensity colour scale on first image
74                 intensity_scale=1/max(max(image_data));
75             end
76
77             % Display image
78             figure(1)
79             colormap(jet(256));
```

```
80          imagesc([ps.sim_dim(1) ps.sim_dim(2)],[ps.sim_dim(3)
                ps.sim_dim(4)],image_data*intensity_scale);
81          set(gca,'YDir','normal'); % Flip image to correct y-
                axis
82          colorbar;
83          xlabel('x (\mum)');
84          ylabel('y (\mum)');
85          hold on
86          draw_circle(ps.setup.x_c,ps.setup.y_c,ps.setup.r_c,'
                k'); % Draw ROI
87          saveas(gcf,[result_dir sim_dir 'seq_' num2str(
                image_num,'%03d.png')]);
88          hold off
89
90          % Record ROI intensity
91          frap(image_num)=sum(sum(ps.roi_pixels.*image_data));
92          t(image_num)=current_time;
93      end
94
95      % Loop over cells
96      for j=1:NC
97          particles_in_cell=ps.cell_lists{j};
98          cell_neighbours=ps.neighbours{j};
99          % Loop over particles in current cell
100         for k=1:size(particles_in_cell,1)
101             p=particles_in_cell(k);
102             s_p=current_strengths(p);
103             sum_of_strengths=0;
104             p_d=ps.distances{p};
105             % Loop over particles in neighbouring cells
106             for kk=1:size(cell_neighbours,1)
107                 d_n=p_d(kk); % exponential of square of
                        euclidean distance over constant b
108                 p_n=cell_neighbours(kk); % particle from
                        neighbouring cell
109                 s=current_strengths(p_n); % strength of the
                        particle
110                 f=(s-s_p)*d_n;
111                 sum_of_strengths=sum_of_strengths+f;
112             end
113             % Pick integration function depending on
```

```
                    location
114                 if p<=NP % only integrate real particles
115                     if ps.location_of_particles(p)==1
116                         new_strengths(p)=current_strengths(p)+c1
                                *sum_of_strengths; % grana
117                     else
118                         new_strengths(p)=current_strengths(p)+c2
                                *sum_of_strengths; % lamellae
119                     end
120                 end
121             end
122         end
123
124         % Update mirror particle strengths
125         new_strengths(NP+1:NP+NM)=new_strengths(ps.particle_type
                (NP+1:NP+NM));
126
127         % Update particle strengths vector
128         current_strengths=new_strengths;
129         current_time=current_time+deltaT; % Increment time
130
131
132 end
133
134 % Normalize FRAP
135 frap=(frap-ps.postbleach_intensity)/(ps.prebleach_intensity-ps.
        postbleach_intensity);
136 fprintf('simulation done\n');
137 % Check strength conservation
138 total_strength_after=sum(current_strengths);
139 err=100*(total_strength_after-total_strength_before)/
        total_strength_before;
140 fprintf('conservation error %.3f%%\n',err);
141
142 % Save FRAP data
143 save([result_dir sim_dir 'simulation.mat'],'t','frap');
```

D.3 PSE structure initialisation

Setup necessary structures for performing a PSE simulation on a thylakoid network. Places particles inside network, generates particle cell lists, and pre-calculates the exponential of the distance between nearby particles. Identifies pixels inside bleaching ROI and calculates pre- and post-bleach ROI intensity.

Listing D.3: `pse_simulation_setup.m`

```
function pse_struct=pse_simulation_setup(n,network_file,setup,
    restricted)
initial_strength=1;

NP=n^2; % Initial number of particles
% Load network
network=load(network_file);
% Simulation dimensions
sim_dim=[0 network.x_chloro 0 network.y_chloro];
% Generate particles on a grid
grid_particles=generate_grid_points(sim_dim(1),sim_dim(2),
    sim_dim(3),sim_dim(4),n);
h=(sim_dim(2)-sim_dim(1))/n; % Particle spacing
epsilon=1.0*h; % Width parameter
radius=3*epsilon; % Interaction radius
point_radius=floor(radius/h); % in particles

fprintf('Setting up PSE simulation for %s\n',setup.sim_name);
fprintf('n^2=%d h=%f h/epsilon=%f radius=%f\n',NP,h,h/epsilon,
    radius);
fprintf('point_radius=%.0f max_neighbours=%.0f\n',point_radius
    ,(2*point_radius)^2);

% Particle types:
%    0 : in network and not a boundary particle
%    >0 : in network and is a boundary particle, type number
    indicates mirror particle index

% Check whether particles are inside the thylakoid network
fprintf('Finding particles inside network...');
[inside_indexes,location_of_particles]=check_inside_network(
    grid_particles,network,restricted);
fprintf('%d found\n',length(inside_indexes));

```

```
29 % Set 'particles' to coordinates of particles inside network
30 particles=grid_particles(inside_indexes,:);
31 NP=size(particles,1); % NP is now reduced to particles inside
       network
32 location_of_particles=location_of_particles(inside_indexes);
33
34 % Find boundary particles by shrinking network by epsilon
35 fprintf('Finding boundary particles\n');
36 small_network=network;
37 small_network.radius_of_grana=small_network.radius_of_grana -
       epsilon;
38 small_network.lamellae_width=small_network.lamellae_width -
       epsilon;
39 small_indexes=check_inside_network(particles,small_network,
       restricted);
40
41 % Find the indices that are in the big network but not the small
        one
42 boundary_indexes=setdiff(1:NP,small_indexes);
43
44 % Create mirror particles for the boundary particles
45 [particles particle_type]=create_mirror_particles(
       boundary_indexes,particles,network);
46 NM=size(particles,1)-NP;
47
48 % Create cell lists by dividing simulation space into squares
49 [cell_lists,particle_cells,cells_size]=create_cell_lists(
       particles,sim_dim(2),sim_dim(4),radius);
50 NC=prod(cells_size);
51 num_particles_in_cells=cellfun('size',cell_lists,1); % #
       particles in each cell
52 fprintf('Number of cells: %d Particles per cell: %.2f, %d, %d (
       avg,min,max)\n',NC,NP/NC,min(num_particles_in_cells),max(
       num_particles_in_cells));
53
54 % Find nearest neighbours and calculate Eucliden distance to
       them
55 fprintf('Building nearest neighbour list and calculating
       Euclidean distances...\n');
56 neighbours=cell(NC,1);
57 distances=cell(NP+NM,1);
```

```
58 b=epsilon^2; % constant
59
60 % Loop over cells
61 for i=1:NC
62     if mod(i,1000)==0
63         fprintf('%d cells\n',i);
64     end
65
66     % Find indexes of neighbouring cells
67     [c_i,c_j]=ind2sub(cells_size,i);
68     indexes=cartprod(max(1,c_i-1):min(cells_size(1),c_i+1), max
       (1,c_j-1):min(cells_size(2),c_j+1));
69     cell_indexes=sub2ind(cells_size,indexes(:,1),indexes(:,2));
70
71     % Make list of particles in those neighbouring cells, plus
       the this cell
72     neighbours{i}=vertcat(cell_lists{cell_indexes});
73
74     % Calculate the (squared) distance between each particle
75     d=dist(particles(neighbours{i},:)').^2; % squares of
       euclidean distances
76
77     % Optimization: pre-calculate exponentials to save time in
       integration step
78     d=exp(-d/b);
79
80     % Store the list of exp(-d/b) for each particle in this cell
81     particles_in_this_cell=cell_lists{i};
82     for j=1:size(particles_in_this_cell,1)
83         p=particles_in_this_cell(j);
84         distances{p}=d(p==neighbours{i},:);
85     end
86 end
87
88
89 % PSF is approximated by Gaussian with variance 1/ib
90 diffraction_radius=0.212; % 212 nm (for 488nm excitation with NA
     =1.4)
91 ib=1/(2*diffraction_radius^2);
92
93 % Check which particles are in the bleach ROI
```

```
94  fprintf('Identifying ROI particles and assigning strengths...\n');
95  factor=check_circle(setup.x_c,setup.y_c,setup.r_c,particles(:,1),particles(:,2));
96  roi_particles=(factor==1);
97
98  % Assign initial strength of one to each particle (arbitrary choice)
99  current_strength=initial_strength*ones(NP+NM,1);
100
101 % Find the image pixels in bleach ROI
102 image_pixels=512;
103 image_x=linspace(sim_dim(1),sim_dim(2),image_pixels);
104 image_y=linspace(sim_dim(3),sim_dim(4),image_pixels);
105 img_width=sim_dim(2)-sim_dim(1);
106 img_height=sim_dim(4)-sim_dim(3);
107 roi=[floor(image_pixels*setup.x_c/img_width)+1;
108      floor(image_pixels*setup.y_c/img_height)+1;
109      floor(image_pixels*setup.r_c/sqrt(img_width^2+img_height^2))+1];
110 [x,y]=meshgrid(1:image_pixels,1:image_pixels);
111 roi_pixels=check_circle(roi(1),roi(2),roi(3),x,y);
112 [roi_j,roi_i]=find(roi_pixels); % rows are y and columns are x
113
114 % Calculate pre-bleach intensity of ROI
115 prebleach_intensity=0;
116 for i=1:length(roi_i)
117     for p=1:NP
118         d_p=(image_x(roi_i(i))-particles(p,1))^2+(image_y(roi_j(i))-particles(p,2))^2; % Pixel-particle distance
119         prebleach_intensity=prebleach_intensity+exp(-d_p*ib)*current_strength(p); % Gaussian distance weighting
120     end
121 end
122
123 % Bleach ROI to zero
124 current_strength(roi_particles)=0;
125 % Bleach nearby ROI with Gaussian weighting
126 roi_particles_ind=find(roi_particles);
127 nonroi_particles=setdiff(1:NP,roi_particles_ind);
128 for i=1:length(nonroi_particles)
```

```
129      p=nonroi_particles(i);
130      % Distance from edge of ROI circle
131      d_r=sqrt((setup.x_c-particles(p,1))^2+(setup.y_c-particles(p
             ,2))^2)-setup.r_c;
132      current_strength(p)=initial_strength*(1-exp(-d_r*ib));
133  end
134
135  % Calculate post-bleach intensity of ROI
136  postbleach_intensity=0;
137  for i=1:length(roi_i)
138      for p=1:NP
139          d_p=(image_x(roi_i(i))-particles(p,1))^2+(image_y(roi_j(i
                 ))-particles(p,2))^2; % Pixel-particle distance
140          postbleach_intensity=postbleach_intensity+exp(-d_p*ib)*
                 current_strength(p); % Gaussian distance weighting
141      end
142  end
143
144  % Package everything into a structure
145  pse_struct=struct('n',n,'NP',NP,'NM',NM,'NC',NC,'h',h,...
146      'sim_dim',sim_dim,'current_strength',current_strength,...
147      'particle_type',particle_type,'setup',setup,'cell_lists',...
148      {cell_lists},'neighbours',{neighbours},'distances',...
149      {distances},'epsilon',epsilon,'location_of_particles',...
150      location_of_particles,'particles',particles,...
151      'prebleach_intensity',prebleach_intensity,...
152      'postbleach_intensity',postbleach_intensity,'ib',ib,...
153      'image_pixels',image_pixels,'image_x',image_x,'image_y',...
154      image_y,'roi_pixels',roi_pixels);
```

Check whether given particles are inside grana, lamellae or out of the network. `restricted` option enables either grana or lamellae to be ignored as part of the network.

Listing D.4: `check_inside_network.m`

```
1  function [inside_indexes,location_of_particles]=
       check_inside_network(particles,network,restricted)
2  % restricted: 1 indicates grana do not count as network
3  %             2 indicates lamellae do not count as network
4  % Returns:-
5  % inside_indexes: index into particles for particles inside
       network
```

```
6  % location_of_particles: 1=grana, 2=lamellae, 0=outside
7
8  grana=network.grana;
9  lamellae=network.lamellae;
10 width=network.lamellae_width;
11 radius_of_grana=network.radius_of_grana;
12 NP=size(particles,1);
13 location_of_particles=zeros(NP,1);
14 inside_network=zeros(NP,1);
15
16 for i=1:NP
17     % Is particle inside any grana?
18     in_grana=0;
19     if restricted~=1
20         for k=1:size(grana,1)
21             in_grana = in_grana | check_circle(grana(k,1),grana(
                   k,2),radius_of_grana,particles(i,1),particles(i
                   ,2));
22         end
23     end
24
25     % Is particle inside any lamellae?
26     in_lamellae=0;
27     if restricted~=2
28         for k=1:size(lamellae,1)
29             in_lamellae = in_lamellae | check_rectangle(lamellae
                   (k,1),lamellae(k,2),lamellae(k,3),lamellae(k,4),
                   particles(i,1),particles(i,2),width,
                   radius_of_grana);
30         end
31     end
32
33     % Inside network if inside grana or lamellae
34     inside_network(i)=in_grana |in_lamellae ;
35
36     % Note which object the particle was inside, if any
37     if in_grana
38         location_of_particles(i)=1;
39     else if in_lamellae
40             location_of_particles(i)=2;
41         end
```

```
42      end
43
44  end
45
46  % Find indexes of the particles inside network
47  inside_indexes=find(inside_network);
```

Sort particles into cell lists, by dividing area into squares and assigning a cell list to each square. This procedure is purely to increase the efficiency of the simulation by ignoring the interaction between far away particles.

Listing D.5: `create_cell_lists.m`

```
1  function [cell_lists,particle_cells,cells_size]=
       create_cell_lists(particles,x_max,y_max,radius)
2  % cell_lists : list of particles for each cell
3  % particles_cells: which cell each particle is in
4  % cells_size : number of cells in x and y
5
6  NP=size(particles,1);
7  num_cell_x=floor(x_max/radius);
8  num_cell_y=floor(y_max/radius);
9  cells_size=[num_cell_x num_cell_y];
10 num_cells=num_cell_x*num_cell_y;
11 cell_lists=cell(num_cells,1);
12 particle_cells=zeros(NP,1);
13
14 % Loop over particles
15 for i=1:NP
16     % Which cell is particle i in?
17     xp=particles(i,1);
18     yp=particles(i,2);
19     cx=max(min(floor(xp/radius) + 1, num_cell_x),1);
20     cy=max(min(floor(yp/radius) + 1, num_cell_y),1);
21     particle_cells(i)=sub2ind([num_cell_x num_cell_y],cx,cy);
22 end
23
24 % Loop over cells
25 for i=1:num_cells
26     % Which particles are in cell i?
27     p_i=find(particle_cells==i);
28     cell_lists{i}=p_i;
29 end
```

In order to enforce boundary conditions, it is necessary to create particles that mirror the position of each of the boundary particles across the boundary. This procedure takes the coordinates of the boundary particles and generates a mirror particle for each. Each boundary particle must be identified with either a grana or a lamellae so that the correct reflection across the boundary can be used.

Listing D.6: `create_mirror_particles.m`

```
1  function [new_particles particle_type]=create_mirror_particles(
       boundary_indexes,particles,network)
2
3  width=network.lamellae_width;
4  radius_of_grana=network.radius_of_grana;
5  grana=network.grana;
6  lamellae=network.lamellae;
7  NP=size(particles,1);
8  NM=size(boundary_indexes,2);
9  new_particles=zeros(NP+NM,2);
10 new_particles(1:NP,:)=particles;
11 num_granas=size(grana,1);
12 particle_type=zeros(NP+NM,1);
13
14 % Loop over boundary particles
15 for i=1:size(boundary_indexes,2)
16     bi=boundary_indexes(i);
17     factor=0;
18     k=0;
19
20     % Check whether particle is in grana or lamellae
21     while factor==0 && k<num_granas
22         k=k+1;
23         factor = check_circle(grana(k,1),grana(k,2),grana(k,3),
               particles(bi,1),particles(bi,2));
24     end
25
26     if factor==1
27         % Boundary particle is in grana
28
29         % Calculate the direction of vector between the centre
               of the granum and the boundary particle
30         direction=[grana(k,1)-particles(bi,1) grana(k,2)-
               particles(bi,2)];
31         sum_squares=sum(direction.^2);
```

```
32          unit=(1/sqrt(sum_squares)).*direction;
33
34          % Calculate the euclidean distance between the centre of
                the granum and the boundary particle
35          euclidean_distance=sqrt(sum((grana(k,1:2)-particles(bi
                ,:)).^2));
36
37          % Calculate the indentation of the boundary particle i.e
                . how far inside the granum it is compared to the
                radius of granum
38          indent=grana(k,3)-euclidean_distance;
39
40          % Find the position of the mirror particle by following
                the direction vector for the radius of the granum and
                the indention
41          mirror=grana(k,1:2) - (grana(k,3)+indent).*unit;
42
43          % Add the mirror particle to the list of particles
44          new_particles(NP+i,:)=mirror;
45
46          % Set particle type of the new mirror particle to the
                boundary particle number
47          particle_type(NP+i)=bi;
48
49      else
50          % Boundary particle is not in grana
51          num_lam=size(lamellae,1);
52
53          % Check if boundary particle is in lamellae
54          factor=0;
55          k=0;
56          while factor==0 && k<num_lam
57              k=k+1;
58              factor = check_rectangle(lamellae(k,1),lamellae(k,2)
                    ,lamellae(k,3),lamellae(k,4),particles(bi,1),
                    particles(bi,2),width,radius_of_grana);
59          end
60
61          if factor==1
62              % Boundary particle is in lamellae
63
```

```
64              % Calculate the direction of vector between the
                    centres of the two grana that the lamallae joins,
                     and calculate the unit and the orthogonal vector
65              direction=[lamellae(k,1)-lamellae(k,3); lamellae(k
                    ,2)-lamellae(k,4)];
66              sum_squares=sum(direction.^2);
67              unit=(1/sqrt(sum_squares)).*direction;
68              orthogonal_vector=[0 -1;1 0]*unit;
69
70              % Calculate the distance of the boundary particle to
                     the line joining the two grana centres
71              v1 = [lamellae(k,1) lamellae(k,2)];
72              v2 = [lamellae(k,3) lamellae(k,4)];
73              p = [particles(bi,1) particles(bi,2)];
74              distance = (det([v2-v1;p-v1]))/norm(v2-v1);
75
76              % Calculate the indentation of the boundary particle
                    , i.e. how far inside the lamellae it is compared
                     to the width of lamellae
77              indent=width/2-abs(distance);
78
79              % Find the position of the mirror particle by adding
                     following the orthognal direction vector twice
                    the indentation length away from the boundary
                    particle
80              mirror = particles(bi,1:2) - sign(distance)*(2*
                    indent).*orthogonal_vector';
81
82              % Add the mirror particle to the list of particles
83              new_particles(NP+i,:)=mirror;
84
85              % Set new mirror particle type to the boundary
                    particle number
86              particle_type(NP+i)=bi;
87          else
88              % Particle is not in grana or lamellae. This should
                    never happen.
89              disp('Warning! This particle is an alien!')
90          end
91      end
92  end
```

D.4 Network generation

The procedures in this section are used to automatically generate an abstracted thylakoid network, consisting of circles representing grana and rectangles representing lamellae, from an autofluorescence image of a chloroplast.

This procedure randomly places grana (in two batches) over the chloroplast in the image and then uses a Monte Carlo algorithm to optimise their placement over the brightest parts of the image. The thylakoids in the image show as bright patches in the autofluorescence channel.

Listing D.7: `image_process_mc.m`

```
1  function grana_pos=image_process_mc(image_name,width,height,
       croprect,grana_radius,separation,show_figures)
2
3  placing_iterations=500000; % Maximum # of attempts for initial
       grana placement without overlap
4  grana_covering=0.85; % Fraction of chloroplast image that should
        be covered with grana
5  mc_iterations=10000; % # of Monte Carlo iterations
6  second_placing_iteration=500; % Iteration when second batch of
       grana is placed
7  intensity_trajectory_interval=10; % # iterations between
       recorded mean intensity
8
9  % Reading chloroplast image and crop if necessary
10 lorig = imread(image_name);
11 if ~isempty(croprect)
12     lorig=imcrop(lorig,croprect);
13 end
14
15 pixels_h=size(lorig,1);
16 pixels_w=size(lorig,2);
17 pixels=mean(size(lorig));
18 if size(lorig,3)==3
19     % Converting image from RGB to grey scale
20     lorig  = rgb2gray(lorig);
21 end
22
23 % Stretch constrast and median filter to smooth out noise
24 I=medfilt2(imadjust(lorig),[3 3]);
25
26 % Initial mean intensity
```

```
27 mean_intensity=mean2(I);
28
29 % Determine bounds of cell from image
30 BW=im2bw(I,min(1,1.6*graythresh(I))); % Threshold image to keep
       brightest parts in middle
31 [ptsY,ptsX]=find(BW==1); % Rows are Y, cols are X
32 DT=DelaunayTri(ptsX,ptsY); % Triagulation of all the cell pixels
33 [k A]=convexHull(DT); % Determine the convex hull
34 % Display progress if required
35 if show_figures
36     figure;
37     ptsX=(ptsX-1)*width/(pixels_w-1); % Convert pixels to
          microns
38     ptsY=(ptsY-1)*height/(pixels_h-1);
39     plot(ptsX,ptsY,'.k');
40     hold on
41     plot(ptsX(k),ptsY(k),'r');
42     hold off
43     xlabel('x (\mum)');
44     ylabel('y (\mum)');
45     if show_figures==2
46         saveas(gcf,'mc_convex_hull.pdf');
47     end
48     title('Convex hull');
49 end
50
51 grana_radius_pixels=floor((pixels-1)*grana_radius/mean([width
       height]));% Grana radius in pixels
52 separation=floor((pixels-1)*separation/mean([width height]));%
       Minimum grana separation in pixels
53 fprintf('Grana radius is %d pixels\n',grana_radius_pixels);
54 fprintf('Separation is %d pixels\n',separation);
55 pseudo_temp=mean_intensity; % Pseudo-temperature for Monte Carlo
       weighting
56
57 % Compute desired number of grana from the area of the convex
       hull
58 num_grana=floor(grana_covering*A/(pi*(grana_radius_pixels+
       separation)^2));
59 fprintf('Total is %d grana\n',num_grana);
60
```

```
61 % Randomly place first batch of grana
62 found=1;
63 i=0;
64 grana_pos=zeros(num_grana,2); % In pixels
65 placed_grana=floor(num_grana/3); % Place third of the grana
       first
66 fprintf('Placing %d grana\n',placed_grana);
67 % Keep trying to place until all are placed or max iterations
       exceeded
68 while found<=placed_grana && i<placing_iterations
69     P=floor(rand(1,2).*pixels)+1;
70     % Valid point if inside convex hull and not overlapping other
           grana
71     if ~isnan(pointLocation(DT,P)) && not_overlapping(grana_pos
          (1:found-1,:),P,grana_radius_pixels,3*separation)
72         grana_pos(found,:)=P;
73         found=found+1;
74     end
75     i=i+1;
76 end
77 if i>=placing_iterations
78     error('Exceeded maximum grana placing iterations');
79 end
80
81 % Calculate initial intensity within each grana
82 [x,y]=meshgrid(1:pixels_w,1:pixels_h);
83 grana_int=zeros(num_grana,1);
84 for i=1:placed_grana
85     gi=(x-grana_pos(i,1)).^2 + (y-grana_pos(i,2)).^2 <=
           grana_radius_pixels^2;
86     grana_int(i)=mean2(I(gi));
87 end
88
89 % First point of mean grana intensity trajectory
90 grana_int_series=zeros((mc_iterations/
       intensity_trajectory_interval)+1,1);
91 grana_int_series(1)=mean(grana_int(1:placed_grana));%/
       mean_intensity;
92 fprintf('Total grana intensity before: %.2f\n',grana_int_series
       (1));
93
```

```
94 % Plot grana if required
95 if show_figures
96     real_grana_pos=(grana_pos-1)*diag([width/(pixels_w-1) height
       /(pixels_h-1)]);
97     plot_grana_on_image(I,real_grana_pos(1:placed_grana,:),
       grana_radius,width,height);
98     if show_figures==2
99         saveas(gcf,'mc_initial_positions.pdf');
100    end
101    title('Initial positions');
102 end
103
104 % Move the grana according to Monte Carlo
105 % For the first time period move only the first batch of grana
106 % During the second time period, introduce the remaining grana
      and fix the positions of the previous batch
107 second_placing=0;
108 first_moving_index=1;
109 steps=0;
110 t=1;
111 % Loop over iterations
112 for i=1:mc_iterations
113    if mod(i,1000)==0
114        fprintf('Iteration %d\n',i);
115    end
116    % Loop over grana: only first batch in first period, only
       second batch in second period
117    for j=first_moving_index:placed_grana
118        % Generate a random move in pixel lattice
119        r=rand;
120        if r<0.25
121            % Move left
122            new_pos=grana_pos(j,:)+[-1 0];
123        elseif r<0.5
124            % Move right
125            new_pos=grana_pos(j,:)+[1 0];
126        elseif r<0.75
127            % Move up
128            new_pos=grana_pos(j,:)+[0 1];
129        elseif r<=1.0
130            % Move down
```

```
131             new_pos=grana_pos(j,:)+[0 -1];
132         else
133             error('This shouldn''t happen!');
134         end
135
136         % Accept or reject the move according to Monte Carlo
                rule
137         index=[1:j-1 j+1:placed_grana]; % Exclude the current
                grana when checking for overlap
138         % Reject move immediately if grana now overlaps another
139         if not_overlapping(grana_pos(index,:),new_pos,
                grana_radius_pixels,separation)
140             % Move not overlapping other grana, so check new
                    intensity
141             gi=(x-new_pos(1)).^2 + (y-new_pos(2)).^2 <=
                    grana_radius_pixels^2;
142             new_int=mean2(I(gi));
143
144             % Accept move if the intensity is higher or, if
                    lower, then with probability Boltzmann-like
                    probability
145             if new_int>=grana_int(j)
146                 % Intensity is higher, accept move
147                 grana_pos(j,:)=new_pos;
148                 grana_int(j)=new_int;
149             else if rand>(exp((new_int-grana_int(j))/pseudo_temp
                    ))
150                     % Intensity is lower, but move accepted by
                            chance
151                     grana_pos(j,:)=new_pos;
152                     grana_int(j)=new_int;
153                 end % Move rejected
154             end
155         end
156         steps=steps+1;
157     end
158
159     % If first time period has finished and second batch of
            grana haven't been placed, do so now
160     if second_placing==0 && i>second_placing_iteration
161         % Plot grana if required
```

```
162         if show_figures
163             real_grana_pos=(grana_pos-1)*diag([width/(pixels-1)
                    height/(pixels-1)]);
164             plot_grana_on_image(I,real_grana_pos(1:placed_grana
                    ,:),grana_radius,width,height);
165             if show_figures==2
166                 saveas(gcf,'mc_first_batch.pdf');
167             end
168             title('First batch positions')
169         end
170
171         % Place second batch of grana, using same algorithm has
                before
172         k=0;
173         fprintf('Placing another %d grana\n',num_grana-
                placed_grana);
174         while found<=num_grana && k<placing_iterations
175             P=floor(rand(1,2).*pixels)+1;
176             if ~isnan(pointLocation(DT,P)) && not_overlapping(
                    grana_pos(1:found-1,:),P,grana_radius_pixels,
                    separation)
177                 grana_pos(found,:)=P;
178                 found=found+1;
179             end
180             k=k+1;
181         end
182         if k>=placing_iterations
183             error('Exceeded maximum grana placing iterations');
184         end
185
186         % Plot grana if required
187         if show_figures
188             real_grana_pos=(grana_pos-1)*diag([width/(pixels-1)
                    height/(pixels-1)]);
189             plot_grana_on_image(I,real_grana_pos,grana_radius,
                    width,height);
190             if show_figures==2
191                 saveas(gcf,'mc_second_placing.pdf');
192             end
193             title('Second placing')
194         end
```

```
195
196         % Calculate initial intensity of newly placed grana
197         for k=placed_grana+1:num_grana
198             gi=(x-grana_pos(k,1)).^2 + (y-grana_pos(k,2)).^2 <=
                    grana_radius_pixels^2;
199             grana_int(k)=sum(sum(I(gi)));
200         end
201         second_placing=1;
202         first_moving_index=placed_grana+1;
203         placed_grana=num_grana;
204     end
205
206     % Record trajectory of mean grana intensity
207     if mod(i,intensity_trajectory_interval)==0
208         grana_int_series(t+1)=mean(grana_int(1:placed_grana));%/
                mean_intensity;
209         t=t+1;
210     end
211 end
212
213 fprintf('Total grana intensity after: %.2f\n',grana_int_series(
    end));
214
215 % Convert grana pixel coordinates to real coordinates
216 grana_pos=(grana_pos-1)*diag([width/(pixels_w-1) height/(
    pixels_h-1)]);
217
218 % Plot final positions if required
219 if show_figures
220     plot_grana_on_image(I,grana_pos,grana_radius,width,height);
221     if show_figures==2
222         saveas(gcf,'mc_final_pos.pdf');
223     end
224     title('Final positions')
225
226     figure;
227     plot([0 1:intensity_trajectory_interval:mc_iterations],
            grana_int_series);
228     xlabel('Iterations');
229     ylabel('Mean grana intensity');
230     if show_figures==2
```

```
231             saveas(gcf,'mc_trajectory.pdf');
232         end
233         title('Intensity trajectory');
234 end
```

Given a list of grana coordinates randomly connect with lamellae according to proscribed weightings.

Listing D.8: generate_network.m

```
1  function generate_network(x_chloro,y_chloro,grana_positions,
       radius_of_grana,lamellae_width,separation,network_file)
2
3  % Lamellae connection ratios
4  with_two=0.75; % ~75% with two connections
5  with_three=0.10; % ~10% with three connections
6  maxIters=50000; % Maximum number of connection attempts
7
8  % Calculate distances between given grana positions
9  A=dist(grana_positions');
10 A(A==0)=Inf; % Force distance to self to be ignored
11 number_of_grana=size(grana_positions,1);
12
13 % Calculate distances to first, second and third nearest granas
14 [fromCoord,toCoord,A,first_adj]=find_neighbouring_grana(A,
       grana_positions);
15 [fromCoord2,toCoord2,A,second_adj]=find_neighbouring_grana(A,
       grana_positions);
16 [fromCoord3,toCoord3,~,third_adj]=find_neighbouring_grana(A,
       grana_positions);
17
18 % Loop until the network is fully connected
19 connected=0;
20 iters=0;
21 while connected==0 && iters<maxIters
22     % All have a least one connection to nearest neighbour
23     lamellae=[fromCoord toCoord];
24     B=first_adj;
25
26     % Randomly connect grana to second nearest with probability
           with_two
27     r=rand(1,number_of_grana);
28     ind=find(r<with_two);
```

```
29
30      % Add entries in adjacency matrix for the newly connected
            grana
31      B(:,ind)=B(:,ind) | second_adj(:,ind);
32      lamellae=[lamellae; fromCoord2(ind,:) toCoord2(ind,:)];
33
34      % Randomly connect grana to third nearest with probabilty
            with_three
35      r=rand(1,number_of_grana);
36      ind2=find(r<with_three);
37      lamellae=[lamellae; fromCoord3(ind2,:) toCoord3(ind2,:)];
38
39      % Add entries in adjanceny matrix to for the newly connected
            grana
40      B(:,ind2)=B(:,ind2) | third_adj(:,ind2);
41
42      % Make sure adjacency matrix is symmetric
43      B=B | B' | diag(diag(ones(number_of_grana)));
44
45      % Check if network connected by summing adjacency matrix
            power series
46      S=zeros(number_of_grana);
47      for i=1:number_of_grana
48          S=S + B^i;
49      end
50
51      % Connected if matrix S has entirely nonzero elements
52      connected=(nnz(S)==number_of_grana^2);
53      iters=iters+1;
54  end
55  if iters>=maxIters
56      error('Maximum iterations exceeded attempting to connect
            network');
57  end
58
59  % Include grana radius with coordinates
60  radii = radius_of_grana*ones(number_of_grana,1);
61  grana = [grana_positions radii];
62
63  % Save network
64  save(network_file,'lamellae','grana','connected','
```

```
radius_of_grana','lamellae_width','x_chloro','y_chloro');
```

Given a list of grana positions and distances between them, find the nearest neighbouring grana, for each grana. Removes these entries from the distance matrix so that the function can easily be used to find the second nearest, and so on.

Listing D.9: `find_neighbouring_grana.m`

```
function [fromCoord,toCoord,A,adj]=find_neighbouring_grana(A,
    grana_positions)

% Find minimum distance from each grana
[C,I]=min(A);

% Store indexes of each pair
granum_one=[1:size(grana_positions,1)];
granum_two=I;

% Convert matrix indexes to linear index and set distances to
    infinity
idx=sub2ind(size(A), granum_two, granum_one);
A(idx)=Inf;

% Remove entries from adjacency matrix
adj=zeros(size(A));
adj(idx)=1;

% Store the start and end coordinates between nearest grana
[from,to]=find(adj);
fromCoord=grana_positions(from,:);
toCoord=grana_positions(to,:);
```

D.5 Utility functions

Check if the given point is inside a circle

Listing D.10: `check_circle.m`

```
function in=check_circle(x_c,y_c,r_c,p_x,p_y)

in=(p_x-x_c).^2+(p_y-y_c).^2<r_c^2;
```

Check if the given point is inside a rectangle.

Listing D.11: check_rectangle.m

```
function in=check_rectangle(x_a,y_a,x_b,y_b,c_x,c_y,width)

[v1 v2 v3 v4]=make_rectangle(x_a,y_a,x_b,y_b,width);
x_1=v1(1);
y_1=v1(2);
x_2=v2(1);
y_2=v2(2);
x_3=v3(1);
y_3=v3(2);
x_4=v4(1);
y_4=v4(2);

% Point is inside rectangle if on the inside-side of each
    constituent line
in=line_equation(x_1,y_1,x_2,y_2,c_x,c_y) & line_equation(x_2,
    y_2,x_3,y_3,c_x,c_y) & line_equation(x_3,y_3,x_4,y_4,c_x,c_y)
     & line_equation(x_4,y_4,x_1,y_1,c_x,c_y);
```

Check which side of a line a point is on.

Listing D.12: line_equation.m

```
function side=line_equation(x_1,y_1,x_2,y_2,c_x,c_y)
m=(y_2-y_1)/(x_2-x_1);
eq=c_y-y_1-m*(c_x-x_1);
side = sign(eq)==sign(x_2-x_1);
```

Check whether a grana placed at point P would overlap (with a given minimum separation) any previously placed grana.

Listing D.13: not_overlapping.m

```
function passed=not_overlapping(grana_positions, P, grana_radius
    ,separation)

passed=1;
for n=grana_positions'
    if sqrt( (n(1) - P(1))^2 + (n(2) - P(2))^2)<grana_radius*2+
       separation
        passed=0;
        return
    end
end
```

Generate the Cartesian product of two sets, that is, $X \times Y = \{(x, y) \mid x \in Y \text{ and } y \in Y\}$.

Listing D.14: `cartprod.m`

```
function C=cartprod(A,B)

C=zeros(length(A)*length(B),2);
n=1;
for i=1:length(A)
    for j=1:length(B)
        C(n,:)=[A(i) B(j)];
        n=n+1;
    end
end
```

E

FRAP and FLIP analysis code

In this appendix the main code for analysing FRAP and FLIP data is listed.

E.1 FRAP code

Front-end script for analysing FRAP data with a rectangular ROI

Listing E.1: `roi_rect.m`

```
1  function [data,fit]=roi_rect(roi,corr_roi,img_size,track,
       timedeltas,filter,pixels)
2  % roi : coordinates of bottom left and top right vertices of
       bleach rectangle
3  % corr_roi : coordinates of bottom left and top right vertices
       of correction rectangle
4  % img_size : image size in microns
5  % track : attempt to track cell movement, true or false
6  % timedeltas : list of one or more frame durations
7  % filter : image filename filter
8  % pixels : number of pixels per axis
9
10 % Convert ROI vectors to components
11 roicell=num2cell(roi);
12 [x1,y1,x2,y2,x3,y3,x4,y4]=deal(roicell{:});
13 roicell=num2cell(corr_roi);
14 [ex1,ey1,ex2,ey2,ex3,ey3,ex4,ey4]=deal(roicell{:});
15
16 % Default arguments
17 if nargin<4
```

```
18      track=false;
19  end
20  if nargin<5
21      timedeltas=0.65;
22  end
23  if nargin<6
24      filter='';
25  end
26  if nargin<7
27      pixels=512;
28  end
29
30  % Find pixels in bleach and correction ROIs
31  [x,y]=meshgrid(1:pixels,1:pixels);
32  z_bleach=frap_check_rectangle(x1,y1,x2,y2,x3,y3,x4,y4,x,y);
33  z_corr=~frap_check_rectangle(ex1,ey1,ex2,ey2,ex3,ey3,ex4,ey4,x,y
        );
34
35  % ROI strip width in microns
36  roi_rect=vertices_to_rect(roi);
37  w_um=(min(roi_rect(3:4))/pixels)*img_size;
38
39  % Analyse FRAP data
40  [data,fit]=analyse_frap(z_bleach,z_corr,timedeltas,filter,track
        ,[],w_um,@draw_roi_rect);
41
42      % Nested function for drawing rectangular ROIs, with
            optional shift
43      function draw_roi_rect(shift_x,shift_y)
44          if nargin==0
45              shift_x=0;
46              shift_y=0;
47          end
48          hold on
49          plot_rectangle(x1+shift_x,y1+shift_y,x2+shift_x,y2+
                shift_y,x3+shift_x,y3+shift_y,x4+shift_x,y4+shift_y)
50          plot_rectangle(ex1+shift_x,ey1+shift_y,ex2+shift_x,ey2+
                shift_y,ex3+shift_x,ey3+shift_y,ex4+shift_x,ey4+
                shift_y,'r')
51          hold off
52      end
```

```
53
54 end
```

Front-end script for analysing FRAP data with a circular ROI.

Listing E.2: `roi_circle.m`

```
1  function [data,fit]=roi_circle(roi,corr_roi,roi_um,track,
       timedeltas,filter)
2  % roi : x, y and radius of bleach circle
3  % corr_roi : x, y and radius of bleach circle
4  % roi_um : roi radius in microns
5  % track : attempt to track cell movement, true or false
6  % timedeltas : list of one or more frame durations
7  % filter : image filename filter
8
9  % Default parameters
10 if nargin<4
11     track=false;
12 end
13 if nargin<5
14     timedeltas=0.65;
15 end
16 if nargin<6
17     filter='';
18 end
19
20 % Find pixels in bleach and correction ROIs
21 [x,y]=meshgrid(1:512,1:512);
22 x_c=roi(1);
23 y_c=roi(2);
24 r_c=roi(3);
25 z_bleach=check_circle(x_c,y_c,r_c,x,y,0,0);
26 z_corr=check_circle(corr_roi(1),corr_roi(2),corr_roi(3),x,y,0,0)
       ;
27
28 % Analyse FRAP
29 [data,fit]=analyse_frap(z_bleach,z_corr,timedeltas,filter,track,
       roi,roi_um,@draw_roi_circle);
30
31     % Nested function for drawing circular ROIs, with optional
           shift
32     function draw_roi_circle(shift_x,shift_y)
```

```
33          if nargin==0
34              shift_x=0;
35              shift_y=0;
36          end
37          hold on
38          draw_circle(x_c+shift_x,y_c+shift_y,r_c);
39          draw_circle(corr_roi(1)+shift_x,corr_roi(2)+shift_y,
                corr_roi(3),'r');
40          hold off
41      end
42
43  end
```

From a sequence of images extract the intensity of the ROI, apply photobleaching correction and normalise. Called from `roi_rect.m` and `roi_circle.m`.

Listing E.3: `analyse_frap.m`

```
1  function [data,fit]=analyse_frap(z_bleach,z_corr,timedeltas,
       filter,track,roi,roi_um,draw_func)
2  % z_bleach : pixel mask for bleach ROI
3  % z_corr : pixel mask
4  % timedeltas : list of one or more frame durations
5  % filter : filename filter
6  % track : attempt to track cell movements, true or false
7  % roi : x, y and radius of ROI
8  % roi_um : roi radius in microns
9  % draw_func : function for drawing ROI
10
11 path='';
12 % Get prebleach intensity inside bleach ROI
13 [file,path]=uigetfile(['*' filter '*.tiff;*' filter '*.tif'],'
       Pick last prebleach',path);
14
15 % Load image
16 M=imread([path file]);
17 if size(M,3)==3
18     M=rgb2gray(M);
19 end
20
21 % Stretch contrast (linearly and without clipping)
22 ilim=stretchlim(M,0);
23 M=imadjust(M,ilim,[]);
```

```
24
25 if track
26     % Copy ROIs
27     z_bleach_orig=z_bleach;
28     z_corr_orig=z_corr;
29     pre_cm_x=-1;
30 end
31
32 % Calculate bleach ROI intensity prior to bleach
33 pre_bleach_roi_M=double(z_bleach).*double(M);
34 prebleach_intensity=sum(sum(pre_bleach_roi_M))
35 prebleach_corr_roi_M=double(z_corr).*double(M);
36 prebleach_corr=sum(sum(prebleach_corr_roi_M))
37
38 total_c=0;
39 time=[];
40 last_time=-timedeltas(1); % Set negative to start from zero
41
42 bleach_roi_list=[];
43 corr_roi_list=[];
44 corr_formula=[];
45
46 % Loop over frame durations (for each post bleach series)
47 for i=1:length(timedeltas)
48     % Ask for first post bleach image file
49     [file,path]=uigetfile(['*' filter '*.tiff;*' filter '*.tif'
         ],'Pick first postbleach',path);
50     % Extract filename components
51     n=regexp(file,'(?<prefix>.*)_(?<timeprefix>[Tt])(?<time>\d+)
         (?<suffix>.*)\.(?<ext>.*)','names');
52     time_chars=length(n.time); % Number of characters in time
         value
53     time_format=['%0' num2str(time_chars) 'd']; % Format string
         for time value
54     t=str2double(n.time); % Current time
55     imfile=[path file]; % Image filename
56
57     c=0;
58     % Do each frame, until run out of files
59     while exist(imfile,'file')
60         % Load image
```

```
61          M=imread(imfile);
62          if size(M,3)==3
63              M=rgb2gray(M);
64          end
65
66          % Adjust contrast with same parameters as prebleach
67          M=imadjust(M,ilim,[]);
68
69          if track
70              if pre_cm_x==-1
71                  % If this is first frame locate cell centre
72                  [pre_cm_x,pre_cm_y]=find_cell_centre(M,roi);
73                  shift_x=0;
74                  shift_y=0;
75                  cm_x=pre_cm_x;
76                  cm_y=pre_cm_y;
77              else
78                  % For subsequent frames, find cell centre
79                  [cm_x,cm_y]=find_cell_centre(M,roi);
80                  % Calculate translation required to align with
                        previous cell centre
81                  shift_x=-floor(pre_cm_x-cm_x);
82                  shift_y=-floor(pre_cm_y-cm_y);
83                  % Translate bleach and correction ROIs
84                  z_bleach=circshift(z_bleach_orig,[shift_x
                        shift_y]);
85                  z_corr=circshift(z_corr_orig,[shift_x shift_y]);
86              end
87          end
88
89          % Visualise
90          figure(1)
91          clf
92          imshow(M)
93          if track
94              % Draw ROIs
95              feval(draw_func,shift_x,shift_y);
96              hold on;
97              % Draw initial and current cell centres
98              plot(cm_x,cm_y,'gx',pre_cm_x,pre_cm_y,'yx');
99              hold off;
```

```
100             else
101                 % Draw ROIs
102                 feval(draw_func);
103             end
104
105             % Calculate bleach ROI intensity
106             bleach_roi_M=double(z_bleach).*double(M);
107             bleach_roi_list=[bleach_roi_list; sum(sum(bleach_roi_M))
                    ];
108
109             % Calculate correction ROI intensity
110             corr_roi_M=double(z_corr).*double(M);
111             corr_roi_sum=sum(sum(corr_roi_M));
112             corr_roi_list=[corr_roi_list; corr_roi_sum];
113             % Calculate factor required to compensate for
                    photobleaching
114             corr_factor=prebleach_corr/corr_roi_sum;
115             corr_formula=[corr_formula; corr_factor];
116
117             % Next filename
118             t=t+1;
119             c=c+1;
120             imfile=[path n.prefix '_' n.timeprefix num2str(t,
                    time_format) n.suffix '.' n.ext];
121         end
122         total_c=total_c+c;
123         % Add frame times for this series
124         time=[time; last_time+(1:c)'*timedeltas(i)];
125         last_time=time(end);
126 end
127
128
129 % Correct the intensities for photobleaching
130 corr_intensities=bleach_roi_list.*corr_formula;
131
132 % Normalise the data to fractional recovery between 0 and 1
133 normalised_intensities=(corr_intensities-corr_intensities(1))/(
        prebleach_intensity-corr_intensities(1))
134 % Store uncorrected intensities for comparison
135 uncorr_intensities=(bleach_roi_list-bleach_roi_list(1))/(
        prebleach_intensity-bleach_roi_list(1))
```

```
136
137 tfit=linspace(min(time),max(time),200);
138 % Fit Soumpasis recovery function to the data
139 try
140     [fitdata,model,goodness,D]=fit_soumpasis(time,
        normalised_intensities,roi_um);
141     yfit=feval(model,tfit);
142     % Soumpasis function is NaN for small t, so use power series
        approximation
143     nanind=find(isnan(yfit));
144     [~,powerapprox]=soumpasis(tfit(nanind),model.tau,model.p);
145     yfit(nanind)=powerapprox;
146     nanind=find(isnan(fitdata));
147     [~,powerapprox]=soumpasis(time(nanind),model.tau,model.p);
148     fitdata(nanind)=powerapprox;
149 catch e
150     fprintf('Soumpasis model fitting failed\n');
151     fitdata=zeros(size(time));
152     model=[];
153     goodness=[];
154     D=[];
155     yfit=zeros(fliplr(size(tfit)));
156 end
157
158 % Fit exponential recovery function
159 try
160     [expfitdata,expmodel,expgoodness]=fit_exponential(time,
        normalised_intensities);
161     expfit=feval(expmodel,tfit);
162 catch
163     expfit=zeros(fliplr(size(tfit)));
164 end
165
166 % Fit Ellenberg recovery function
167 [ellfitdata,ellmodel,ellgoodness]=fit_ellenberg(time,
    normalised_intensities,roi_um);
168 ellfit=feval(ellmodel,tfit);
169
170 % Save corrected intensities and times together
171 data = [time normalised_intensities fitdata bleach_roi_list
    corr_formula corr_intensities corr_roi_list
```

```
    uncorr_intensities];
% Package everything into a mat-file
save([path n.prefix n.suffix '_data.mat'],'time',...
  'normalised_intensities','fitdata','bleach_roi_list',...
  'corr_formula', 'corr_intensities','prebleach_intensity',...
  'goodness','D','model','tfit','yfit','expfitdata','expmodel'
      ,...
  'expgoodness','expfit','uncorr_intensities','ellfitdata',...
  'ellmodel','ellgoodness','ellfit');

% Plot data and fitted recovery curves
plot(time, normalised_intensities, 'k.', tfit, expfit,'g',tfit,
    ellfit,'r')
hold on
if ~isempty(yfit)
    plot(tfit,yfit,'b');
end
legend('Data','Exp','Ellenberg','Soumpasis');
xlabel('Time (s)','fontsize',14)
ylabel('Relative intensity','fontsize',14)
set(gca,'tickdir','out','fontsize',14)
ylim([0,1])
saveas(gcf,[path n.prefix n.suffix '_recovery.pdf'])

fprintf('Total frames: %d\n',total_c);
fit=[tfit' yfit];
```

E.2 FLIP code

Analyse FLIP image sequence by calculating intensity of whole image and correcting for photobleaching.

Listing E.4: `analyse_flip.m`

```
function data=analyse_flip(timedelta,photobleach_data,filter)
% timedelta : frame duration
% photobleach_data : photobleach ROI intensities corresponding
    to sequence
% filter : image filename filter

path='';
% Get prebleach image
```

```
8  [file,path]=uigetfile({'*' filter '*.tiff;*' filter '*.tif'},'
       Pick last prebleach',path);
9  M=imread([path file]);
10 if size(M,3)==3
11    M=rgb2gray(M);
12 end
13
14 % Stretch contrast (linearly and without clipping)
15 ilim=stretchlim(M,0);
16 M=imadjust(M,ilim,[]);
17
18 % Intensity before bleaching
19 prebleach_intensity=sum(sum(M));
20
21 intensity_list=[];
22
23 % Get first bleach frame image
24 [file,path]=uigetfile({'*' filter '*.tiff;*' filter '*.tif'},'
       Pick first postbleach',path);
25 % Extract filename components
26 n=regexp(file,'(?<prefix>.*)_(?<timeprefix>[Tt])(?<time>\d+)(?<
       suffix>.*)\.(?<ext>.*)','names');
27 time_chars=length(n.time); % Number of characters in time value
28 time_format=['%0' num2str(time_chars) 'd'];
29 t=str2double(n.time);
30 imfile=[path file];
31
32 c=0;
33 % Do each frame, until run out of files
34 while exist(imfile,'file')
35     % Load image
36     M=imread(imfile);
37     if size(M,3)==3
38         M=rgb2gray(M);
39     end
40     % Adjust the contrast using same parameters as prebleach
41     M=imadjust(M,ilim,[]);
42
43     % Visualise
44     figure(1)
45     clf
```

```
46      imshow(M)
47
48      % Calculate bleach ROI intensity
49      intensity=sum(sum(M));
50      intensity_list=[intensity_list; intensity];
51
52      % Next image filename
53      t=t+1;
54      c=c+1;
55      imfile=[path n.prefix '_' n.timeprefix num2str(t,time_format
            ) n.suffix '.' n.ext];
56  end
57  % Frame times
58  time=(0:(c-1))'*timedelta;
59
60  % Correct for photobleaching and normalise
61  normalised_intensities=intensity_list/prebleach_intensity
62  pb=load(photobleach_data);
63  corr_intensities=normalised_intensities./feval(pb.model,time);
64
65  % Save corrected intensities and times together
66  data = [time normalised_intensities intensity_list
        corr_intensities];
67  save([path n.prefix n.suffix '_flip_data.mat'],'time',...
68      'normalised_intensities','intensity_list',...
69      'prebleach_intensity','corr_intensities');
70
71  % Plot FLIP data
72  plot(time, normalised_intensities, 'k.',time,corr_intensities,'
        bx')
73  xlabel('Time (s)','fontsize',14)
74  ylabel('Fractional intensity','fontsize',14)
75  set(gca,'tickdir','out','fontsize',14)
76  ylim([0,1])
77  saveas(gcf,[path n.prefix n.suffix '_flip.pdf'])
78
79  fprintf('Total frames: %d\n',c);
```

F

Reprints

FEBS Letters 583 (2009) 3690–3696

journal homepage: www.FEBSLetters.org

Diffusion of a membrane protein, Tat subunit Hcf106, is highly restricted within the chloroplast thylakoid network

Elina Vladimirou [a,b,c], Michael Li [a,b,c], Cassie P. Aldridge [a], Lorenzo Frigerio [a], Markus Kirkilionis [c], Colin Robinson [a,*]

[a] Department of Biological Sciences, University of Warwick, Coventry CV4 7AL, United Kingdom
[b] MOAC Doctoral Training Centre, University of Warwick, Coventry CV4 7AL, United Kingdom
[c] Mathematics Institute, University of Warwick, Coventry CV4 7AL, United Kingdom

ARTICLE INFO

Article history:
Received 12 July 2009
Revised 16 October 2009
Accepted 19 October 2009
Available online 23 October 2009

Edited by Richard Cogdell

Keywords:
Thylakoid
Hcf106
Photobleaching
Tat system
Photosystem II

ABSTRACT

The thylakoid membrane forms stacked thylakoids interconnected by 'stromal' lamellae. Little is known about the mobility of proteins within this system. We studied a stromal lamellae protein, Hcf106, by targeting an Hcf106-GFP fusion protein to the thylakoids and photobleaching. We find that even small regions fail to recover Hcf106-GFP fluorescence over periods of up to 3 min after photobleaching. The protein is thus either immobile within the thylakoid membrane, or its diffusion is tightly restricted within distinct regions. Autofluorescence from the photosystem II light-harvesting complex in the granal stacks likewise fails to recover. Integral membrane proteins within both the stromal and granal membranes are therefore highly constrained, possibly forming 'microdomains' that are sharply separated.

1. Introduction

The thylakoid membrane carries out the critical processes of light capture, electron transport and photophosphorylation. In higher plant chloroplasts, it is commonly found as a highly organised network with a characteristic structure in which stacks of individual thylakoids ('grana') are connected by single 'stromal' thylakoids. Within this system, the appressed granal membranes are enriched in photosystem II (PSII) while the stromal lamellae contain the bulk of photosystem I (PSI) and the ATP synthase (reviewed in [1]). The thylakoid also has an unusual, galactolipid-rich lipid composition [2]).

While thylakoidal protein–pigment complexes have been studied in detail, much less is known about the physical nature of the thylakoid membrane and the consequences of its domain structure. It is commonly assumed that the lipids are highly fluid, as is the case with most biological membranes. Studies on a variety of other membrane systems have concluded that the lipids almost invariably undergo rapid diffusion in the plane of the bilayer and high rates of diffusion have been calculated in some cases [3,4]. Furthermore, it is generally accepted that chloroplasts evolved from endosymbiotic cyanobacteria, and studies on cyanobacterial thylakoid lipids have shown that they exhibit high rates of diffusion [5]. However, very few studies have analysed the mobility of the thylakoid membrane proteins, and those studies have focused almost exclusively on a single photosynthetic complex, the light-harvesting complex of PSII (LHCII), which itself exhibits aberrant behaviour. LHCII is mostly found in the appressed granal membranes and recent studies on isolated PSII particles suggest that the majority of LHCII complexes are relatively immobile, possibly due to macromolecular crowding effects that stem from the high protein concentration [6]. A proportion of the LHCII complexes are believed to be more mobile, consistent with the need for LHCII particles to migrate to PSI particles during state transitions (see below). In general, however, the PSII/LHCII complexes are exceptional membrane proteins and very little is known about the nature of the numerous membrane proteins in the non-appressed 'stromal' membranes.

In this report we have studied the mobility of a thylakoid membrane protein, Hcf106, which is a core component of the plant Tat protein translocase. Hcf106 is a single-span membrane protein that forms a complex with cpTatC in the non-appressed stromal thylakoids [7,8]. Bioimaging studies on the *Escherichia coli* homolog of Hcf106, TatB, have previously shown that this protein undergoes rapid diffusion within the *E. coli* plasma membrane [9]. In this

* Corresponding author. Fax: +44 2476 523568.
E-mail address: colin.robinson@warwick.ac.uk (C. Robinson).

0014-5793/$36.00
doi:10.1016/j.febslet.2009.10.057

report we have used a similar approach to study the mobility of Hcf106 within the thylakoids of transiently transfected protoplasts. We show that its diffusion is highly restricted, providing direct evidence for a strict compartmentation of membrane types within the continuous thylakoid membrane bilayer.

2. Materials and methods

2.1. Plasmid construction

A DNA fragment containing the *hcf106* gene was amplified with the forward primer F1 5′-TCATCATCTAGAATGGCCATGGCGTTACAGATTA-3′ and reverse primer R1 5′-TTCTCCTTTACTATCTTGCCTTGGAGGAGATGCAG-3′. mGFP5 was amplified with the forward primer F2 5′-CAAGGCAAGATAGTAAAGGAGAAGAACTTTTCACTG-3′ and reverse primer R2 5′-TGATGACTGCAGTTATTTGTATAGTTCATCCATGCC-3′. The amplified fragments were used to generate the fusion between Hcf106 and mGFP5 with the forward primer F1 and reverse primer R2. The resulting product was digested with XbaI and PstI and cloned into cauliflower mosaic virus 35S-promoter-driven expression vector pDHA. To generate the 'TP-GFP' construct, the coding region for the 23K-GFP fusion protein [10] was subjected to site-specific mutagenesis to remove the terminal 28 residues of the 23K transit peptide, generating a protein with a stroma-targeting peptide.

2.2. Transient transformation of leaf protoplasts

Protoplasts were prepared from 4 to 7 cm long axenic leaves of *Nicotiana tabacum* cv Petit Havana SR1. Protoplasts were subjected to polyethylene glycol-mediated transfection as described previously [11]. The transfected protoplasts were incubated overnight at 25 °C in the dark.

2.3. Chloroplast isolation and fractionation

Protoplast pellets were resuspended in 4 ml HS buffer (50 mM HEPES–KOH and 330 mM sorbitol, pH 8.0) and homogenised by repeated passage through a needle and a 20 μm pore mesh. The suspension was loaded on top of a 35% (v/v) Percoll pad and centrifuged at 1400×*g* for 8 min at 4 °C. Pellets (intact chloroplasts) were washed once in HS buffer, pelleted at 3000×*g* for 2 min, and resuspended in 200 μl HS. A sample of 20 μl of chloroplasts was transferred on a polylysine glass slide (Sigma–Aldrich).

2.4. Confocal microscopy and FRAP

The FRAP experiments were performed on a Leica TCS SP5 laser-scanning confocal microscope at room temperature. The 488 nm line of the argon laser was used in combination with a 63 × oil immersion objective (NA 1.4). A circular area of 1 μm diameter

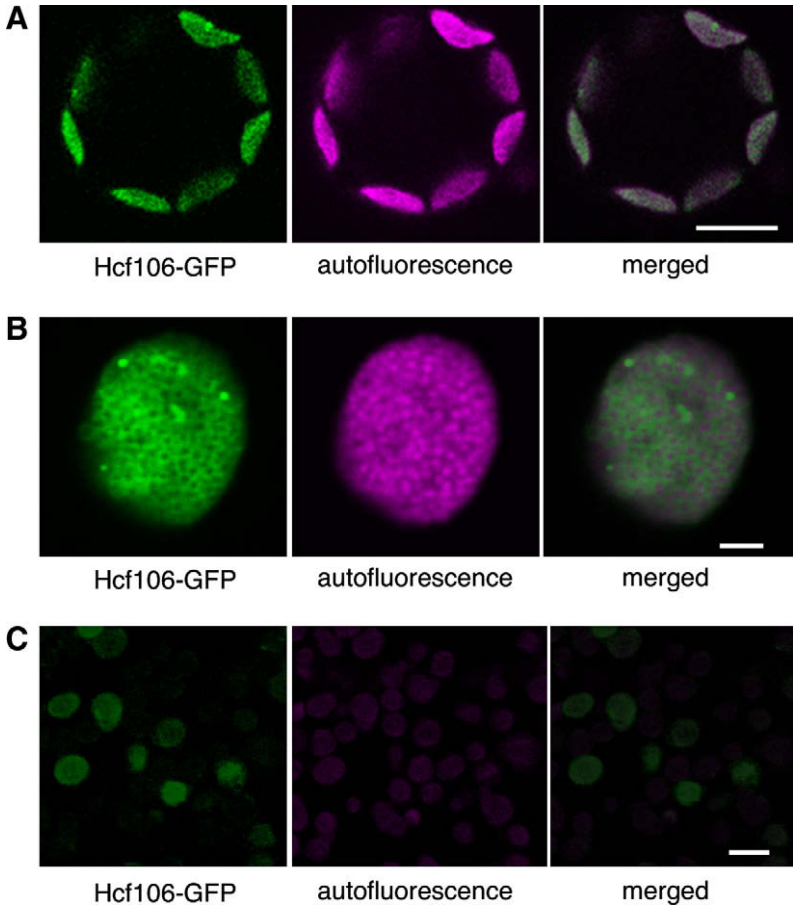

Fig. 1. Hcf106-GFP is targeted to stromal lamellae within the thylakoids of transfected tobacco protoplasts. (A) Tobacco leaf protoplasts were transfected with a plasmid encoding an Hcf106-GFP fusion protein. Eighteen hours after transfection, protoplasts were analysed by confocal microscopy with excitation at 488 nm and emission measured at 500–530 nm (GFP measurement settings; left panels) and emission detected at >650 nm to detect thylakoid autofluorescence due to LHCII (centre panels). Merged images are shown on the right. Scale bar: 10 μm. (B) Protoplasts were transfected with the Hcf106-GFP construct as in (A), and intact chloroplasts were isolated and analysed by confocal microscopy. Images were captured using 16-line averaging and the panel shows GFP fluorescence, autofluorescence (magenta) the merged image. Scale bar: 2 μm. (C) A mixed population of transfected and non-transfected chloroplasts was isolated from a preparation of transfected protoplasts. The transfected chloroplasts exhibit significantly higher green fluorescence than the non-transfected chloroplasts due to expression of Hcf106-GFP. Scale bar: 10 μm.

(Fig. 2A) was bleached for 3.3 s and the recovery of the green and autofluorescence within that area was followed with a fast post-bleach imaging and further slower post-bleach imaging (one image per 1.3 s and 10 s, respectively; Fig. 2A; one image per 0.66 s, 2 s and 5 s, respectively, Fig. 3A and B). Fluorescence intensities were corrected for imaging photobleaching. For the additional experiments, a circular area of 0.4 μm diameter (Figs. 2B and 4B) was repeatedly bleached and the recovery of the green fluorescence within that area was followed with very fast post-bleach imaging (one image per 0.75 s).

3. Results

3.1. Diffusion of Hcf106-GFP is highly constrained within the thylakoid membrane

Hcf106 is a single membrane span protein with the larger, C-terminal domain on the stromal face of the membrane. The *E. coli* homolog, TatB, has been visualised in intact bacterial cells after tagging with green fluorescent protein (GFP) at the C-terminus, and shown to be highly mobile within the plasma membrane [9]. TatB-GFP incorporates into TatABC complexes and we expect the majority of the Hcf106-GFP to assemble with cpTatC. However, by over-expressing the Hcf106-GFP relative to the indigenous cpTatC, the protein stoichiometry may be disturbed and a protein pool not involved in complex formation may therefore exist. Thus, we might expect to measure a component with high diffusion coefficient. According to Saffman–Delbruck theory, the diffusion of transmembrane protein is proportional to the natural logarithm of the reciprocal of the protein radius [12]. Therefore, even large Hcf106–cpTatC complexes of 700 kDa [8] should be highly mobile in a typically fluid bilayer, assuming a globular configuration.

In order to study Hcf106 within intact chloroplasts, we transfected tobacco protoplasts with a construct encoding *Arabidopsis* Hcf106 linked to GFP. The protoplast transfection system has been widely used to study the targeting of proteins into chloroplasts, and GFP-tagged proteins can be readily visualised using laser-scanning confocal microscopy (e.g. [10]). Fig. 1A shows a typical transfected protoplast 18 h after transfection. The magenta panel shows autofluorescence from thylakoid pigments, which serves as a chloroplast marker, and the green channel shows the presence of GFP fluorescence within the chloroplasts. This

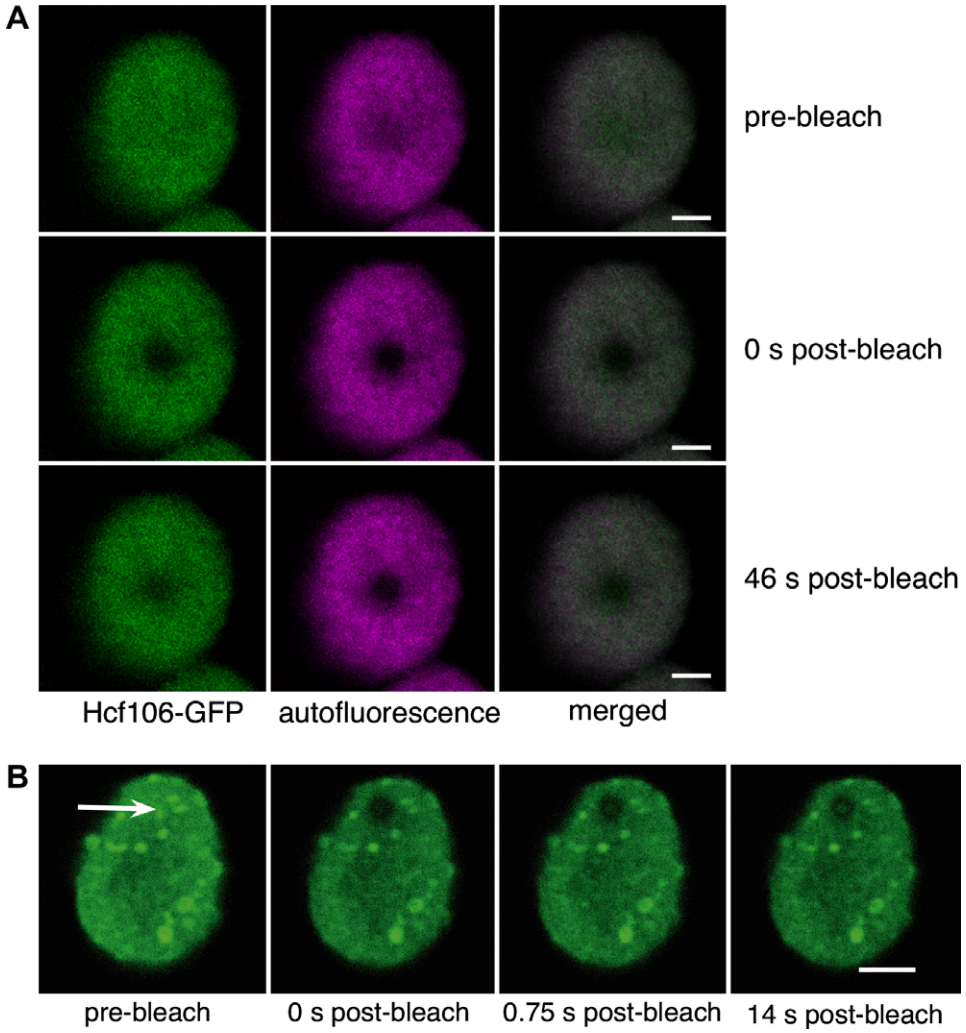

Fig. 2. Diffusion of Hcf106-GFP within the thylakoid network is highly constrained (A) protoplasts were transfected with the Hcf106-GFP construct as in 1A, and intact chloroplasts were isolated and analysed by confocal microscopy. The panel shows an individual chloroplast before and after photobleaching of a circular area of 1 μm in diameter. Images are shown prior to photobleaching (pre-bleach), immediately after bleaching (0 s post-bleach) and 46 s after the bleaching (lower row). Scale bar: 2 μm. (B) Protoplasts were transfected with Hcf106-GFP and chloroplasts were isolated. A region of 0.4 μm diameter was repeatedly photobleached with consecutive laser flashes and images were analysed before the bleaching ('pre-bleach'), immediately after the final photobleach (0 s post-bleach), 0.75 s after the final bleach and 14 s post-bleach. Scale bar: 2 μm.

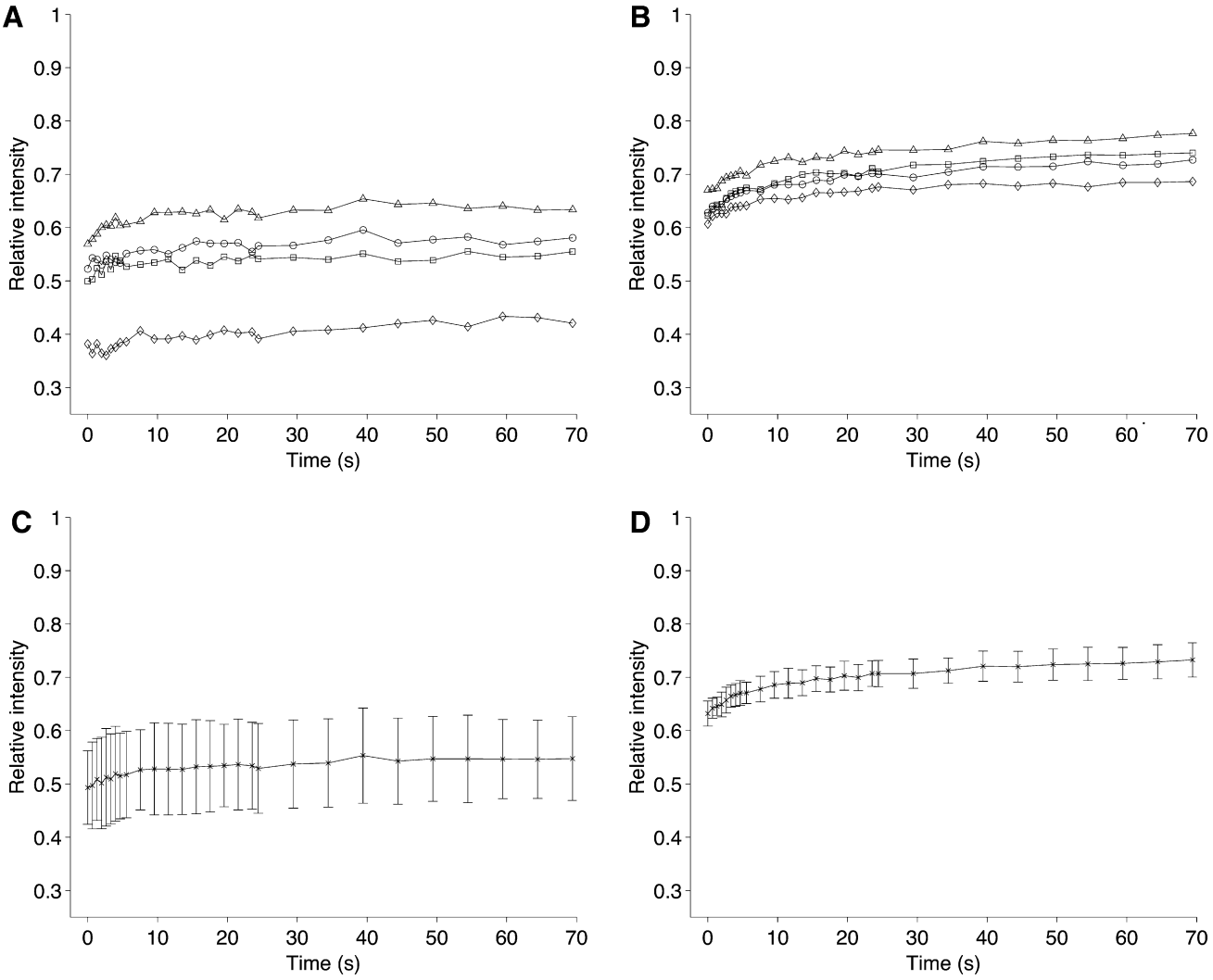

Fig. 3. Quantification of recovery rates for Hcf106-GFP and autofluorescence after photobleaching. Chloroplasts were isolated from protoplasts expressing Hcf106-GFP as in Fig. 2A and thylakoid regions were photobleached in the same manner. The graphs show the recovery data for four individual experiments. (A) Individual Hcf106-GFP fluorescence recovery curves after photobleaching of 1 μm diameter region. (B) Recovery data for autofluorescence from the same experiments. (C) and (D) show the averaged data for Hcf106-GFP and autofluorescence, respectively.

confirms that Hcf106-GFP is efficiently targeted to the chloroplasts.

Chloroplasts were isolated from transfected protoplasts, and a single chloroplast is shown at higher magnification in Fig. 1B. Both the GFP fluorescence and autofluorescence are widely distributed throughout the chloroplast and the merged image confirms that the fluorescence patterns overlap in general terms, which means that Hcf106-GFP is present in the thylakoid system and not the soluble stromal phase, as expected. Hcf106 is known to be located in the stromal lamellae, and close analysis of Fig. 1B shows that the Hcf106-GFP construct is likewise located primarily, if not exclusively, within these membranes. Most of the autofluorescence in the thylakoid network originates from the light-harvesting complexes of PSII (LHCII), which are primarily located in the granal lamellae [1]. Accordingly, the images in Fig. 1B, taken using line averaging for higher resolution, show the autofluorescence (magenta) to exhibit a punctate pattern, reflecting their presence in the grana. In contrast, Hcf106-GFP fluorescence originates primarily from regions where the magenta spots are absent. The merged image confirms that the GFP and autofluorescence signals do not overlap, clearly indicating that the Hcf106-GFP is present in the stromal lamellae.

As a further control in this experiment, we confirmed that the green fluorescence shown in transfected chloroplasts does indeed originate from Hcf106-GFP. Low-level green fluorescence can often be observed with non-transfected chloroplasts, and this is associated with multi-photon excitation artifacts [13]. Fig. 1C shows a mixed population of transfected and non-transfected chloroplasts, and it is clear that the transfected population exhibit a far higher level of green fluorescence than do the non-transfected examples.

We investigated the lateral mobility of membrane protein Hcf106 by means of fluorescence recovery after photobleaching (FRAP). In this technique, a region of GFP fluorescence is irreversibly bleached using the confocal laser and the recovery of fluorescence in the region, signifying diffusion of neighbouring molecules, is monitored. In order to avoid excessive photobleaching of GFP and increase imaging speed we cannot use line averaging, therefore granal and stromal lamellae are not well-resolved in confocal images associated with FRAP experiments. In the selected region (1 μm diameter), the GFP fluorescence intensity was bleached to about 30% of the initial value and images of the chloroplasts were taken immediately after the bleach and after additional times up to 46 s. The post-bleach images of Fig. 2A show that the region is effectively bleached (see 0 s post-bleach image taken immediately

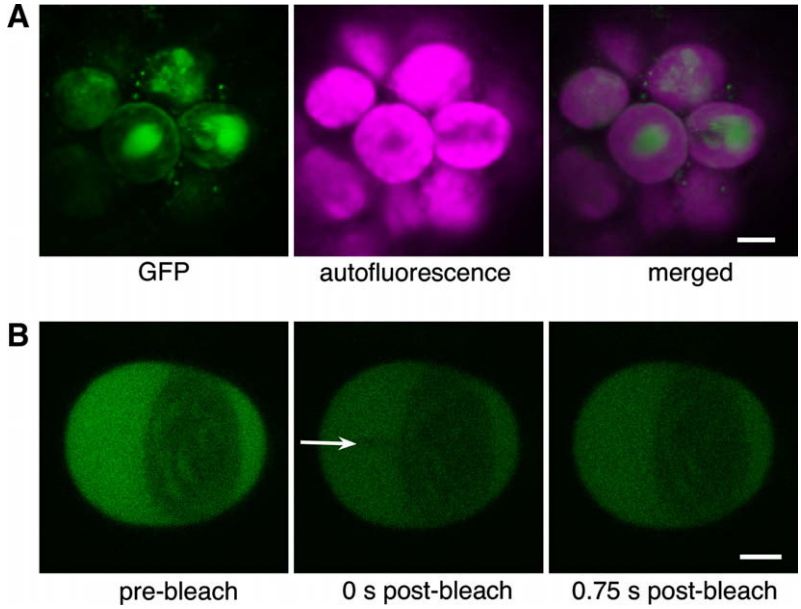

Fig. 4. GFP is highly mobile within the stroma. A construct encoding the transit peptide of Rubisco small subunit fused to GFP (TP-GFP) was used to transfect protoplasts, as carried out with the Hcf106-GFP construct. Panel A shows a confocal image of a single protoplast with the GFP fluorescence, autofluorescence and merged images indicated. Scale bar: 3 μm. Panel B shows a photobleaching experiment carried out on a single chloroplast after isolation, using the multiple-bleach protocol used in Fig. 2B. The figure shows a pre-bleach image, an image taken immediately after final bleach (bleach spot of 0.4 μm diameter indicated with an arrow), and a further image taken 0.75 s after the final bleach. Scale bar: 2 μm.

afterwards), and that this region remains substantially bleached over the subsequent 46 s recovery period. Data recorded for a further 2 min confirm that fluorescence within bleached regions fail to recover over extended periods of time (data not shown). This result indicates that the diffusion of this protein within this region is highly constrained. It is also notable that the thylakoid autofluorescence fails to recover substantially (see below).

Additional experiments were carried out using a smaller bleach region (circle of 0.4 μm diameter) with more intensive bleaching. Here, the region of interest was subjected to repeated short bleaches and the data in Fig. 2B show images taken before the bleaching process (pre-bleach), immediately after the final photobleach (0 s post-bleach), 0.75 s after the final bleach and after a further 14 s recovery period. The data show that the region remains clearly bleached even 14 s after the bleaching process, confirming that the diffusion of Hcf106-GFP is highly constrained over this time scale.

The GFP fluorescence recovery profiles from four separate FRAP experiments are shown in Fig. 3A. In these experiments, the photobleaching reduced Hcf106-GFP fluorescence to between 38% and 57% of the original level in the affected circular region of 1 μm diameter, and the recovery curves for Hcf106-GFP (A) confirm that the bleached regions recover very little fluorescence over a 70 s post-bleach period. The average recovery amounts to 6% of their original GFP fluorescence (Fig. 3C).

3.2. Thylakoid pigment autofluorescence exhibits a slow diffusion rate, but stromal GFP diffuses rapidly

The above data clearly show that the Hcf106-GFP fluorescence fails to recover substantially in the bleached regions of the thylakoids, but it is clear that the same applies to the chlorophyll fluorescence (shown in magenta). In Fig. 2A, the autofluorescence in the region of interest remained bleached over extended time scales and this again indicates that these protein–pigment complexes are highly constrained and unable to diffuse into this area with the kinetics normally associated with biological membranes. This autofluorescence stems primarily from LHCII [1], the bulk of which is located in the granal membranes (whereas Hcf106 is located in the stromal lamellae). The autofluorescence recovery data were also plotted for the experiments described in Fig. 3A, and the results again show a slow rate of recovery (average of 10% over the four experiments; Fig. 3B and D). These data confirm that the autofluorescence recovers to only a minor extent in the regions of interest, although it is notable that the recovery of the autofluorescence is slightly more pronounced than that of Hcf106-GFP.

Given that both Hcf106-GFP and the thylakoid autofluorescence exhibit such low levels of diffusion over these areas, at least at the level of resolution available with this approach (see below), we considered it important to confirm that GFP is in fact mobile in compartments that are known to favour rapid diffusion. We therefore targeted GFP into the stromal compartment by fusion to the first, stroma-targeting domain of transit peptide of a lumenal protein (the 23 kDa component of the oxygen-evolving complex), reasoning that the GFP should diffuse much more freely in the stroma and thus serve as a control to validate the FRAP conditions used in this study. Tobacco protoplasts were transfected with this transit peptide-GFP construct (TP-GFP) and allowed to express the protein overnight under the conditions used for Hcf106-GFP. Fig. 4A confirms that this fusion protein is targeted to the stroma. The image shows a group of chloroplasts within a transfected protoplast, and it is clear that the GFP is mainly concentrated in one region of the chloroplast. In this region, there is little overlap with the thylakoid autofluorescence present throughout the rest of the organelle. GFP is thus targeted primarily into the stroma as expected.

Chloroplasts were then isolated from transfected protoplasts and FRAP experiments were carried out exactly as described above for the HCF106-GFP construct. Fig. 4B shows images taken immediately before and after a photobleaching series, carried out exactly as in Fig. 2B for Hcf106-GFP studies. The bleach region is shown arrowed. Immediately after the final bleach, a very faint bleaching is apparent, but this has fully recovered by the 0.75 s post-bleach time point. We conclude that stromal GFP is far more mobile than

Hcf106-GFP, at least over the distances studied in this experimental setup.

4. Discussion

Biological membranes are generally regarded as highly dynamic entities, with both the lipid and protein constituents undergoing rapid diffusion unless tethered. Here, we have studied the diffusion of a thylakoid membrane protein in non-appressed membranes. This is the first such study of a non-photosynthetic thylakoid membrane protein, and the results show that even relatively small photobleached regions fail to recover fluorescence to any significant extent over timescales that are extended by the standards of biological systems. In a previous study on the *E. coli* plasma membrane [4], the diffusion coefficient for TatA-GFP was estimated to be 0.13 $\mu m^2\ s^{-1}$, which is similar to that calculated for a eukaryotic plasma membrane protein [3]. This corresponds to an average time to diffuse over 1 μm of about 7 s. In this study, we have shown that on average, a bleached region of 1 μm diameter recovers only about 6% of its lost fluorescence over a timescale of 70 s. Hcf106-GFP thus appears to diffuse extremely slowly throughout the thylakoid network, and these data thus reveal a key feature about the nature of the thylakoid network.

The actual structure of the thylakoid system is still a matter of debate. Some studies propose that granal stacks are connected by stromal lamellae that wind around the grana in a helical manner, with each granum connected to several stromal lamellae, while other data contradict this 'quasi-helical' model (discussed in [14]). However, the key point is that the thylakoid network is formed from one continuous membrane, which encloses a correspondingly continuous lumenal phase. In this context, our data provide clear evidence that this membrane system is highly compartmentalised such that diffusion of membrane proteins is constrained to a marked degree.

It is highly unlikely that the data reflect tethering of Hcf106-GFP by stromal or lumenal cytoskeleton-type elements. First, no such elements have been characterised as being associated with the thylakoid membrane, and secondly, there are no indications that this protein transport system should be tethered in any way. Indeed, studies on the *E. coli* plasma membrane have shown the homologous TatB protein to be highly mobile [9].

Other data have clearly shown that thylakoid membrane proteins must be mobile to some extent. First, there is ample evidence that a portion of the LHCII complex is mobile and able to move from PSII to PSI during so-called state transitions, in which the system attempts to achieve equal excitation of PSI and PSII [1]. Redistribution of excitation occurs over periods in the region of 30 min, although this could still imply a relatively slow rate of diffusion within the bilayer. Moreover, the PSII repair cycle is believed to involve a large-scale disassembly–reassembly process following damage to D1 protein, and much of this is believed to occur in the stromal lamellae [1].

One possible explanation is that thylakoid membrane proteins are simply immobile within the stromal lamellae, but this seems unlikely. An alternative explanation is that Hcf106 is in fact highly mobile, but only within distinct domains that are effectively constrained by boundaries. In this scenario, the stromal lamellae could be viewed as individual 'islands' of membrane that are separated by grana, through which diffusion to other stromal lamellae is blocked. Granal stacks are between 0.3 μm and 0.6 μm in diameter, which means that they, and the connecting stromal lamellae, would be in the same general size range as the smallest bleach regions used in this study (0.4 μm). The photobleaching data would thus be consistent with a mosaic model, in which individual regions of stromal membrane are largely isolated from each other. Equally, the same arrangement could explain the limited diffusion of LHCII in the granal membranes; our data show that the diffusion of this complex is similarly constrained and this finding is consistent with those of Kirchhoff et al. [6] who studied LHCII diffusion in isolated PSII particles. The mobility of LHCII in intact thylakoid membranes was also studied using single particle tracking (SPT) by linking LHCII with a fluorescent bead [15]. It is probable that only LHCII particles in the most superficial grana margins and in the top stroma lamellae were labelled due to steric hindrance. Both non-phosphorylated (LHCII) and phosphorylated (P-LHCII) conformations were found to exhibit average diffusion of $8.4 \times 10^{-11}\ cm^2\ s^{-1}$ and $2.7 \times 10^{-10}\ cm^2\ s^{-1}$, respectively, in fairly restricted corrals with only few complexes exploring larger domains of the membrane. These observations lend support to the hypothesis that Hcf106-GFP diffuses within limited domains. There is also evidence from other organelles that diffusion can be sensitive to 'bottlenecks' in the membrane. For example, overexpression of reticulons at the ER membrane induces constrictions, which create pockets of luminal material whose diffusion is severely hampered [16,17]. However, we have no clear information on the nature of any membrane properties that may serve to prevent diffusion so effectively. SPT studies on the thylakoid membrane protein Hcf106 may be able to shed further light on this.

In summary, the presence of distinct forms of thylakoid membrane is well-known and the compositions of the stromal and granal lamellae have been characterised in some detail. In this report we provide direct evidence that the stromal lamellae are effectively self-contained domains throughout the thylakoid network.

Acknowledgements

This work was funded by a grant from the Biotechnology and Biological Sciences Research Council to C.R., M.A.K. and L.R., and from Engineering and Physical Sciences Research Council PhD studentships to E.V. and M.L. We thank Ashley Goddard for his contributions to the work. We thank Conrad Mullineaux for extremely helpful comments during the course of this work.

References

[1] Andersson, B. and Anderson, J.M. (1980) Lateral heterogeneity in the distribution of chlorophyll-protein complexes of the thylakoid membranes of spinach chloroplasts. Biochim. Biophys. Acta 593, 427–440.
[2] Bruce, B.D. (1998) The role of lipids in plastid protein transport. Plant Mol. Biol. 38, 223–246.
[3] Zhang, F., Lee, G.M. and Jacobson, K. (1993) Protein lateral mobility as a reflection of membrane microstructure. BioEssays 15, 579–588.
[4] Mullineaux, C.W., Nenninger, A., Ray, N. and Robinson, C. (2006) Diffusion of green fluorescent protein in three cell environments in *Escherichia coli*. J. Bacteriol. 188, 3442–3448.
[5] Sarcina, M., Murata, N., Tobin, M.J. and Mullineaux, C.W. (2003) Lipid diffusion in the thylakoid membranes of the cyanobacterium Synechococcus sp.: effect of fatty acid desaturation. FEBS Lett. 553, 295–298.
[6] Kirchhoff, H., Haferkamp, S., Allen, J.F., Epstein, D.B.A. and Mullineaux, C.W. (2008) Protein diffusion and macromolecular crowding in thylakoid membranes. Plant. Physiol. 146, 1571–1578.
[7] Asakura, Y., Kikuchi, S. and Nakai, M. (2008) Non-identical contributions of two membrane-bound cpSRP components, cpFtsY and Alb3, to thylakoid biogenesis. Plant J. 56, 1007–1017.
[8] Cline, K. and Mori, H. (2001) Thylakoid ΔpH-dependent precursor proteins bind to a cpTatC–Hcf106 complex before Tha4-dependent transport. J. Cell Biol. 154, 719–729.
[9] Ray, N., Nenninger, A., Mullineaux, C.W. and Robinson, C. (2005) Location and mobility of twin-arginine translocase subunits in the *Escherichia coli* plasma membrane. J. Biol. Chem. 280, 17961–17968.
[10] Di Cola, A. and Robinson, C. (2005) Large-scale translocation reversal within the thylakoid Tat system in vivo. J. Cell Biol. 171, 281–289.
[11] Pedrazzini, E.A.G., Bollini, R., Ceriotti, A. and Vitale, A. (1994) Binding of BiP to an assembly-defective protein in plant cells. Plant J. 5, 103–110.
[12] Saffman, P.G. and Delbrück, M. (1975) Brownian motion in biological membranes. Proc. Nat. Acad. Sci. USA 72, 3111–3113.

[13] Kao, F.-J., Wang, Y.-M., Chen, J.-C., Cheng, P.-C., Chen, R.-W. and Lin, B.-L. (2002) Micro-spectroscopy of chloroplasts in protoplasts from Arabidopsis thaliana under single- and multi-photon excitations. J. Lumin. 98, 107–114.
[14] Mustárdy, L., Buttle, K., Steinbach, G. and Garab, G. (2008) The three-dimensional network of the thylakoid membranes in plants: quasihelical model of the granum-stroma assembly. Plant Cell 20, 2552–2557.
[15] Consoli, E., Croce, R., Dunlap, D.D. and Finzi, L. (2005) Diffusion of light-harvesting complex II in the thylakoid membranes. EMBO Rep. 6, 782–786.
[16] Shibata, Y., Voss, C., Rist, J.M., Hu, J., Rapoport, T.A., Prinz, W.A. and Voeltz, G.K. (2008) The reticulon and DP1/Yop1p proteins form immobile oligomers in the tubular endoplasmic reticulum. J. Biol. Chem. 283, 18892–18904.
[17] Tolley, N., Sparkes, I.A., Hunter, P.R., Craddock, C.P., Nuttall, J., Roberts, L.M., Hawes, C., Pedrazzini, E. and Frigerio, L. (2008) Overexpression of a plant reticulon remodels the lumen of the cortical endoplasmic reticulum but does not perturb protein transport. Traffic 9, 94–102.